UTRECHT UNIVERSITY
MSC THESIS

The tectonometamorphic evolution of a garnet peridotite lens, N. Jämtland, Sweden

From Sub-Continental Lithospheric Mantle to Orogenic Garnet Peridotite exposed at the surface,

Jacob Verbaas

8/23/2011

Abstract

The Friningen Peridotite Lens, found in N. Jämtland, Central Sweden is a tectonically emplaced garnet peridotite lens located in the Seve Nappe Complex (SNC) of the Scandinavian Caledonides. The peridotite records older protolith mineral assemblages than the host gneisses and is crosscut by a basic garnet pyroxenite dike. Metamorphism in the SNC due to an early Caledonian event is dated at 500 ± 50 Ma. Microstructural analyses indicate the proposed collision of the Virisen island arc cannot be responsible for this event as the garnet peridotite originates from Sub-Continental lithospheric mantle. The most likely conceptual model for the origin of the SNC is a collision of Baltica with an unknown microcontinent. Geochemical analyses of the dike indicate extensive metasomatism during the residence time of the peridotite lens in the mantle wedge. Micro- and mesostructural evidence indicates the dike behaves as a low viscosity layer during deformation.

Table of Contents

5. Discussion

1. Introduction

The Scandinavian Caledonides form part of a mountain range that was formed by the accretion of multiple terranes. An Early Caledonian orogeny (500 ± 50 Ma) involved Baltica and a microcontinent and/or perhaps Siberia. The second, the Scandian main phase involves closure of the Iapetus ocean resulting in a collision between the two adjacent continental blocks Baltica and Laurentia (430 – 400 Ma) *(Spengler, 2006)*. The final collisional event resulted in an east vergent nappe stack of different metamorphic grades. This nappe stack is subdivided from top to bottom in the Uppermost, Upper, Middle and Lower allochton, which are all superposed on the Autochton, the Baltic shield *(Gee, 1975)*.

In the Scandinavian Caledonides the Seve Nappe Complex (SNC) belongs to the upper part of the middle allochthon *(Gee, 2008)*. In northern Jämtland and southern Västerbotten, central Sweden, the SNC forms one of the major thrust complexes interpreted to be derived from the outermost western edge of Baltica and/or transitional domains related to the Iapetus ocean. The SNC consists from top to bottom of a western, eastern and central belt *(Zwart, 1974)*. The eastern and western belts contain mineral assemblages of low-middle amphibolite facies, the central belt of upper amphibolite to granulite facies (including locally eclogites). The Central belt is thus a high grade belt over and underlain by lower grade belts. The SNC is riddled with orogenic mantle peridotites *(Calon, 1979; Bucher, 1991)*. The high pressure peridotite bodies in the central belt are interpreted to have been emplaced during an Early Caledonian event approximately 500 ± 50 Ma *(Gademan et al., 2011)*. Other peridotites in the Seve Nappe show lower grade assemblages due to their position in the Caledonian front during the main Scandian phase of metamorphism. The associated country rocks in which the high grade peridotites are emplaced are isofacial eclogite bearing high pressure gneisses of contrasting affinity.

One of these mantle peridotites, here called the Friningen peridotite lens, located in the central belt of the SNC, is the subject of the present study. This mantle peridotite is a garnet-bearing dunite/lherzolite and possibly records a tectono-metamorphic evolution from the Archean untill the mid-Paleozoic *(van Roermund, 1989; Brueckner et al., 2004)* and thus may contain a wealth of geological information concerning the evolution of lithospheric mantle with Baltic affinity. This tectonically emplaced lithospheric mantle fragment contains evidence of a multi-stage metamorphic history. In addition basic dikes, consisting of garnet and pyroxenes (whithout plagioclase or olivine) cut through the peridotite outcrops. In this MSc thesis the tectonometamorphic evolution of the Friningen garnet peridotite is re-evaluated. Using the analyses of macro, meso- and microstructural evidence, EMP geothermobarometry and bulk rock geochemical analyses, the tectonometamorphic evolution of the Friningen garnet peridotite lens is evaluated. Emphasis lies on the relationship between basic dikes which crosscut the garnet peridotite.

2. Geological setting

2.1. **Paleogeographical history of Scandinavia/Baltica**

Baltica is defined here as the terrane that existed from the break-up of Rhodinia to the assembly of Pangea. Protobaltica is the terrane that existed prior to the assembly of Rhodinia. Protobaltica amalgamated from three separate terranes termed Volgo-Uralia, Sarmatia and Fennoscandia. The Proterozoic crust of Fennoscandia was created soon after 1.9 Ga in a series of events called the Svecofennian Orogeny *(Bogdanova et al., 2001)*. Subsequent collisions with Volgo-Uralia and Sarmatia occurred giving rise to the Fennoscandian terrane. The main thrust nappes of the Scandinavian Caledonides are emplaced on top of the Fennoscandian part of the Baltic shield and its late Vendian sedimentary record. Protobaltica eventually accreted with Laurentia creating Rhodinia around ~900 Ma.
During the break-up of Rhodinia, which started at 800 Ma, Protobaltica remained attached to Laurentia *(Torsvik 2002)*. The inauguration of plate spreading forming the Northern Iapetus Ocean separated the two terranes *(Torsvik & Cocks, 2005)*. Around 450 Ma, convergence between Avalonia and Baltica culminated in the closure of the Tornquist sea and 'soft docking' of Avalonia against Baltica.
This is based on paleomagnetics and the correlation of Avalonian derived mid-Caradoc ashfalls of Baltica. *(Torsvik, 2002)*. The Scandinan phase of the Caledonian orogeny which closed the Iapetus Ocean only took place in the Late Siluran – Early Devonian (430 - 400 Ma) and marked the suturing of Laurussia. Around 130 Ma later, during the Mid-Carboniferous all large continents but Siberia formed part of the Supercontinent Pangea (*Torsvik, 2006)*.
The plate reconstructions illustrated in figure 2.1.1 are from *Roberts (2003),* and are reconstructions which give a conceptual model for the movement of Baltica and adjacent terranes during the Caledonian orogeny, but predating the Scandian phase. Proterozoic movements of Baltica and the possible controversial anticlockwise rotation of this continent are beyond the scope of this thesis. The plate reconstructions of *Roberts (2003)* in figure 2.1.1 do show a rotation of ~90 ° of –baltica.

2.2. Allochtons and Autochton

Apart from Eastern America, the Northern Caledonides formed as a result of the convergence and collision between Baltica and Laurentia, after closure of the Iapetus ocean *(Torsvik et al., 1992; 1996)*. The remnants of the Caledonian orogenic event can however also be observed in the UK, Ireland and along the east coast of North America which must have involved other tectonic blocks. The Scandinavian Caledonides are classically divided into a number of allochtons separated by tectonic contacts, overlying a parautochton. These are from top to bottom the uppermost, upper, middle and lower allochthons which overlie the Baltic shield *(Figure 2.2.1)*. These comprise thin skinned thrust nappes which have been carried eastwards over low angle thrust faults *(Törnebohm, 1888)*.
The uppermost allochthon is correlated to Laurentia on the basis of sedimentary data *(Stephens & Gee, 1985)*, chemostratigraphic data *(Melezhik et al., 2002; Roberts et al., 2002)*, and early NW thrust faulting *(Roberts et al., 2001)*.
The upper allochthon was in Sweden originally divided in the Seve and Köli nappes, although correlations with similar rocks in the middle Allochton of Norway now place the Seve nappe in the middle allochton *(Gee, 2008)*. The Köli nappes are subdivided into different nappes, all with felsic igneous basements intercalated with turbidites, limestones and volcanic rocks *(Lutro, 1979; Stephens and Gee, 1985)*. The Köli Nappes are oceanic in origin and have been interpreted to have been derived from or very near to the margin of Baltica on the basis of stratigraphic similarity. In addition to this turbidites of the Köli Nappes are derived from the Baltic margin in the east.

The lower part of the middle Allochthon consists mainly of crystalline and sedimentary rocks interpreted to be derived from relatively outboard Baltica. Sandstones (Särv, Leksdal, and Saetra nappes) are locally intruded by mafic dikes of Proterozoic and/or Iapetus age *(Gee et al., 1985; Roberts, 1988; Greiling, 1989).*

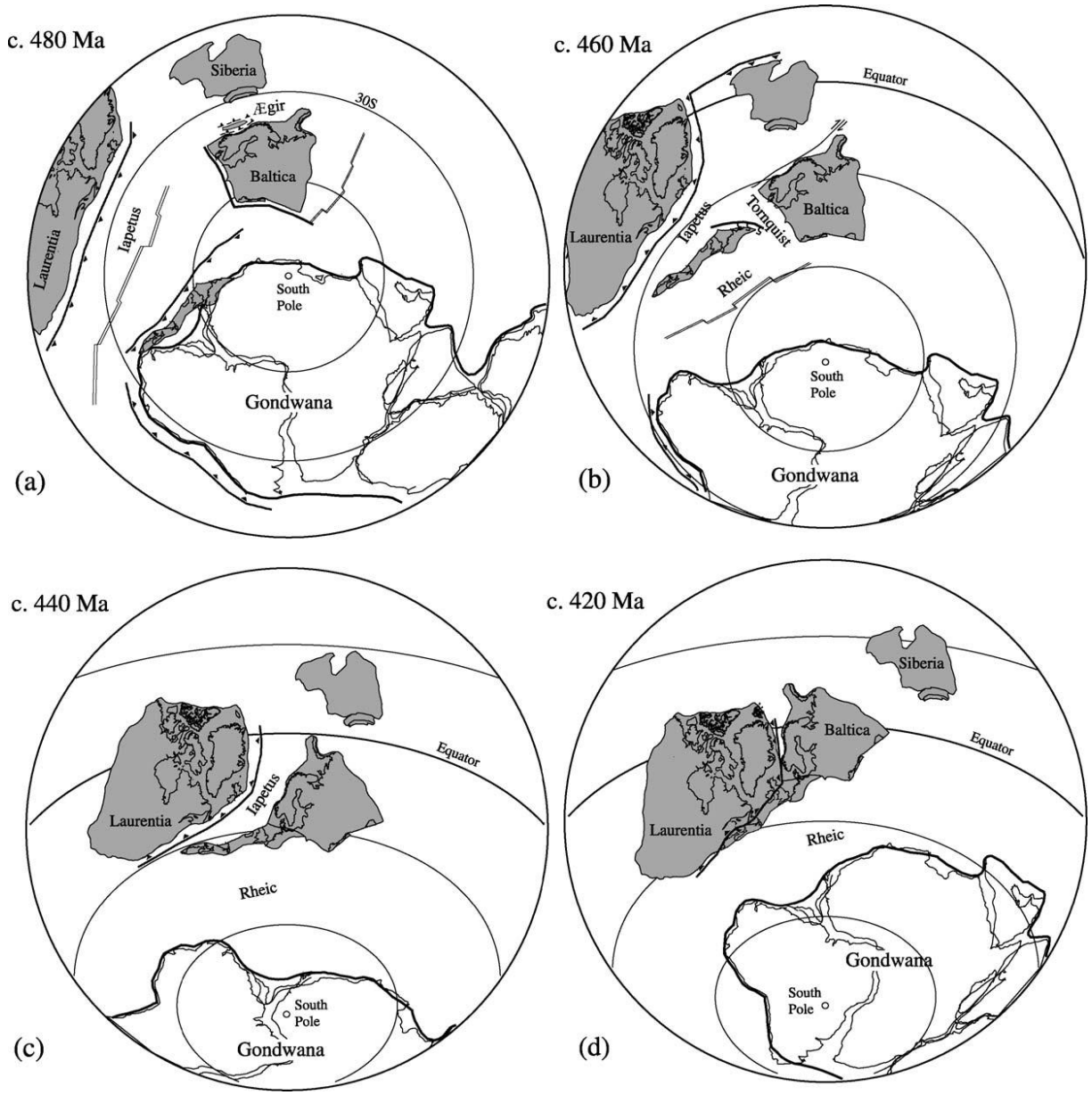

Figure 2.1.1; Plate reconstructions adopted from Roberts et al., 2003

The crystalline host rock has been dated with zircon U-Pb geochronology at 1776 Ma. In contrast, zircons in dikes are dated 1026 Ma *(Greiling et al., 2002)*. They are believed to correlate to the Scandinavian dolerite group even though this was dated at 1.26 Ga *(Söderlund et al., 2005; Greiling et al., 2007).*

The lower allochthon is of weak metamorphic grade *(Andreasson,1980; Arnbom, 1980)* and composed of crystalline and sedimentary rocks. This allochthon has a baltican affinity and was transported east-southeastward over the autochthon *(Roberts & Gee, 1985)*. Mafic dikes cut across granitoid and syenitic country rock *(Greiling, 1982; Greiling et al., 1993).*

According to *Greiling et al., (2007)* these dikes, including those of the middle allochthon can be correlated to the Scandinavian dolerite group on the basis of chemical signatures.
The Fennoscandian crystalline basement of the Baltic shield is overlain by a number of greywackes and sandstones of Vendian to lower Wenlock age *(Basset, 1985; Gayer & Greiling, 1989).*

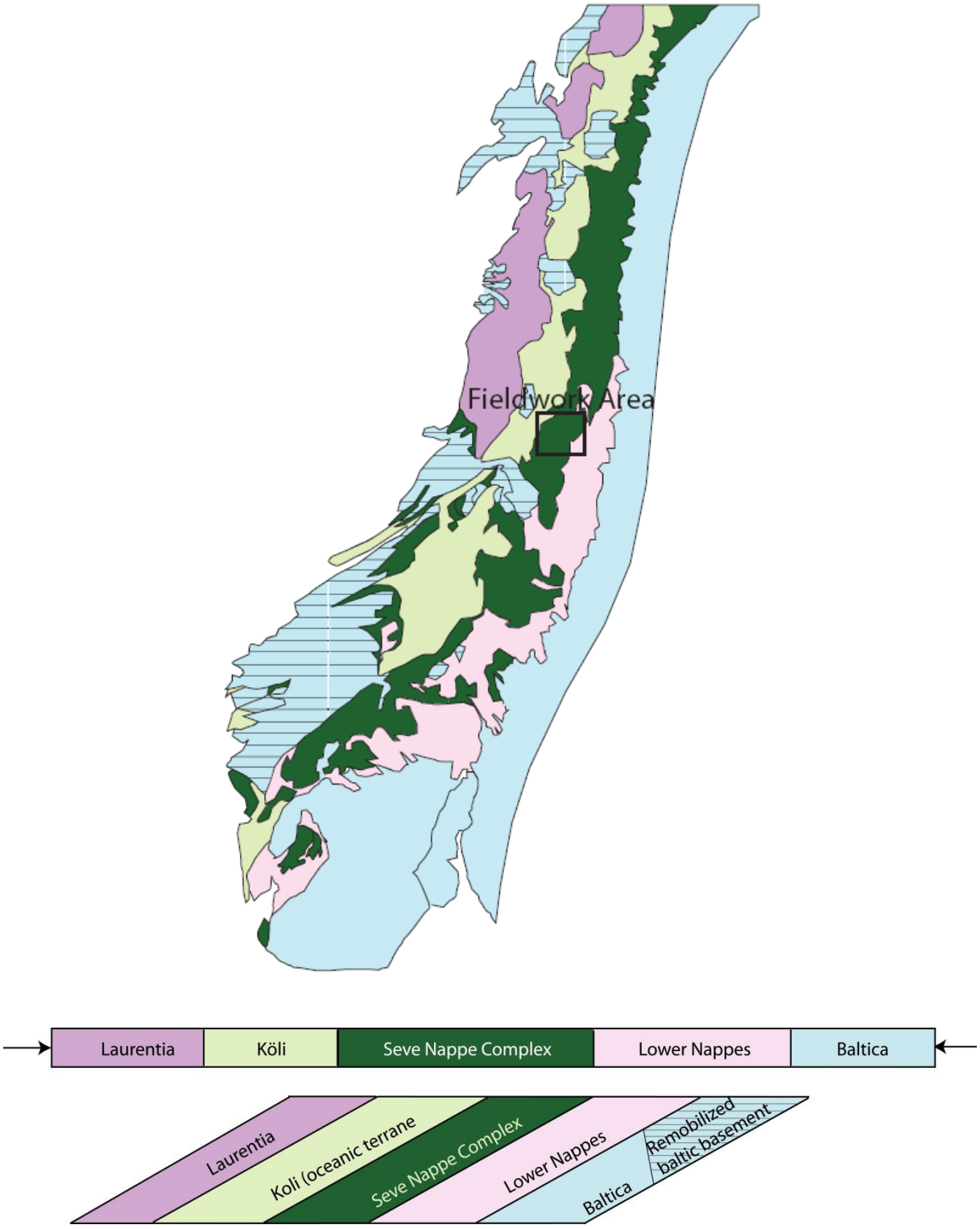

Figure 2.2.1; Terrane map of the Scandinavian Caledonides. Below is the legend including the oversimplified nappe stack geometry of the Scandinavian Caledonides *(Modified after Gademan et al., 2011)*

2.3. The Seve Nappe Complex

The upper part of the Middle Allochton called the Seve Nappe Complex (SNC) is subdivided in three belts. The western, central and eastern belts of the SNC comprise different lithologies and different metamorphic grades. The SNC wedges out to the west, where the Köli Nappes overlie the lower structural units directly *(Zachrisson, 1973)*. In terms of structural position, the Western belt overlies the Central belt which in turn overlies the Eastern belt. The Western belt consists of quartzitic and garnet bearing micaschist with locally lenses of amphibolite, termed the Svärtsjobacken schist. The contact between the Western belt and the Köli Nappe is tectonic; the nature of the contact between the Western belt and the Central belt is not determined due to bad exposures *(Trouw, 1974)*. The Central belt consists of high grade migmatites, gneisses with locally eclogites and orogenic mantle peridotite bodies, quartzo-feldspathic gneiss and amphibolites. Eclogites and mantle slices normally occur as isofacial (with respect to the host rock) lenses from m-scale to km-scale *(Bucher, 1991)*. The metamorphic grade of peridotite bodies in the central belt of the SNC does not fit the metamorphic field gradient of the Scandian Seve rocks *(Bucher, 1991)*. The whole central gneiss zone might be up to 5 km thick. The contact between the central gneiss zone and the underlying belt is mylonitic *(Zachrisson, 1969; Trouw, 1973; Zwart, 1974)*.
The Eastern belt contains mainly meta-arkoses to feldspar bearing quartzites, and garnet micaschist with occasional marble layers and amphibolites. The contact with the underlying Särv nappe (of the lower allochthon) is tectonic. Eclogites also occur in the Eastern belt of the SNC *(van Roermund, 1985)*.
The three belts always have the same superposition but are not very continuous in thickness. From one locality to another, one belt might have wedged out to reappear in another area, however always in the same structural level *(Zwart, 1974)*.

2.4. Metamorphism and age dating in the SNC

The Seve Nappe Complex hosts metamorphic rocks which have reached their peak metamorphic grade prior to the Scandian phase of the Caledonian orogenic cycle *(Mork et al., 1988; Brueckner et al., 2004; Root & Corfu, in review; Gademan et al., 2011)*. To the north of Jämtland, the Sarek and Kalak nappes are the equivalent of the Seve Nappes. A number of studies have attempted to date the metamorphism in the SNC, all coming to ages of 500-445 Ma *(Mork et al., 1988; Brueckner et al., 2004; Root & Corfu, in review; Gademan et al., 2011)*. UHP bodies, such as the Friningen garnet peridotite lens was dated at 445 Ma *(Brueckner et al., 2004)* and eclogite bodies in Jämtland and Norbotten record ages of 482 and 446 Ma, respectively *(Root & Corfu, in review)*. An eclogite body in the Tjeliken lens, in the Eastern Belt of the SNC, demonstrates inheritance ages of 1700 Ma *(Root & Corfu, in review)*. Although the Norbotten eclogite ages (derived from the Vaimok and Tsäkkok) are significantly older, all ages indicate a pre-Scandian age for a (U)HP event. *Root & Corfu (in review)* argue that Sm-Nd ages on eclogites are generally older than U-Pb ages. This is based on the Sm-Nd and U-Pb ages derived from the Vaikmok, Tjeliken and Tsäkkok lens. However, U-Pb dating of the Tjeliken eclogite at 446 ± 1 Ma *(Root & Corfu, in review)* does correspond with Sm-Nd age dating on the basic dikes of the Friningen garnet peridotite at ~450 Ma *(Brueckner & van Roermund, 2004)*. The relation between these sometimes contrasting (between eclogites of Tjeliken, Tsäkkok & Vaikmok) and sometimes corroborating (Tjeliken eclogite and Friningen garnet peridotite) ages has yet to be determined. Monazite ages *(Gademan et al., 2011)* using the chemical EMP age dating technique define an age for the SNC of 500 ± 50 Ma. This data is based on 750 analyses which were taken from quartzo feldspathic lithologies of the central belt. These monazite ages

cannot be related to the subduction of the Baltoscandian margin underneath Laurentia during Scandian times. Recently, workers have hypothesized about the origin of the Seve and Kalak Nappes as being derived from peri-Gondwanan or Avalonian margins *(Roberts et al., 2010),* Baltica *(Brueckner & van Roermund, 2004; Gademan et al., 2011)* and Laurentia *(Kirkland, 2011).* During convergence of Baltica and Laurentia these terranes were squeezed between the cratons and translated along large strike slip faults to the Baltican margin *(Root & Corfu, in review).* This draws similarities with the existence of terranes like Svalbard, of which the origin and translation during the Caledonian orogenic cycle remains unclear. This is consistent with the observation of *Corfu et al., (2007)* that alkali and gabbroic complexes in the Kalak nappe are not found in nappes with Baltic affinity. Also Root & *Corfu (2011, in review),* emphasize that an external provenance of the SNC is more likely considering that early Caledonian eclogites in the SNC might formed anywhere in Iapetus. *Andreasson et al., (1998)* termed all rocks recording evidence of Baltoscandian rift infill as the Seve-Kalak superterrane. This has its advances but it should be remembered that prior to Early Caledonian docking of the terrane a shared history is not yet proven. As such, *Corfu (2007)* found alkali and gabbroic complexes in the Kalak and thus interprets both the Seve and the Kalak as external. The complexes exposed in the Kalak have not been found in the Seve Nappe Complex.

The Seve Nappe Complex shows an inverted metamorphic grade, with granulite to eclogite facies in the Central Belt and low/middle amphibolite facies in the adjacent Eastern and Western Belts *(Figure 2.4.1A and B).* The metamorphic pressure of the Central Belt differs parallel to the axis of the Caledonian orogen. The highest pressures are in the Avardo gneiss > 18 Kb, medium pressures are found in the Marsfjallet gneiss 12,5-18 Kb and the lowest pressures occur in the Lillfjället gneiss < 12,5 Kb. The inverted metamorphic grade of the SNC, together with the north-south oriented pressure gradient in the Central Belt, requires an explanation in the context of the Caledonian orogeny. This forms part of the topic and problem investigated in this MSc thesis.

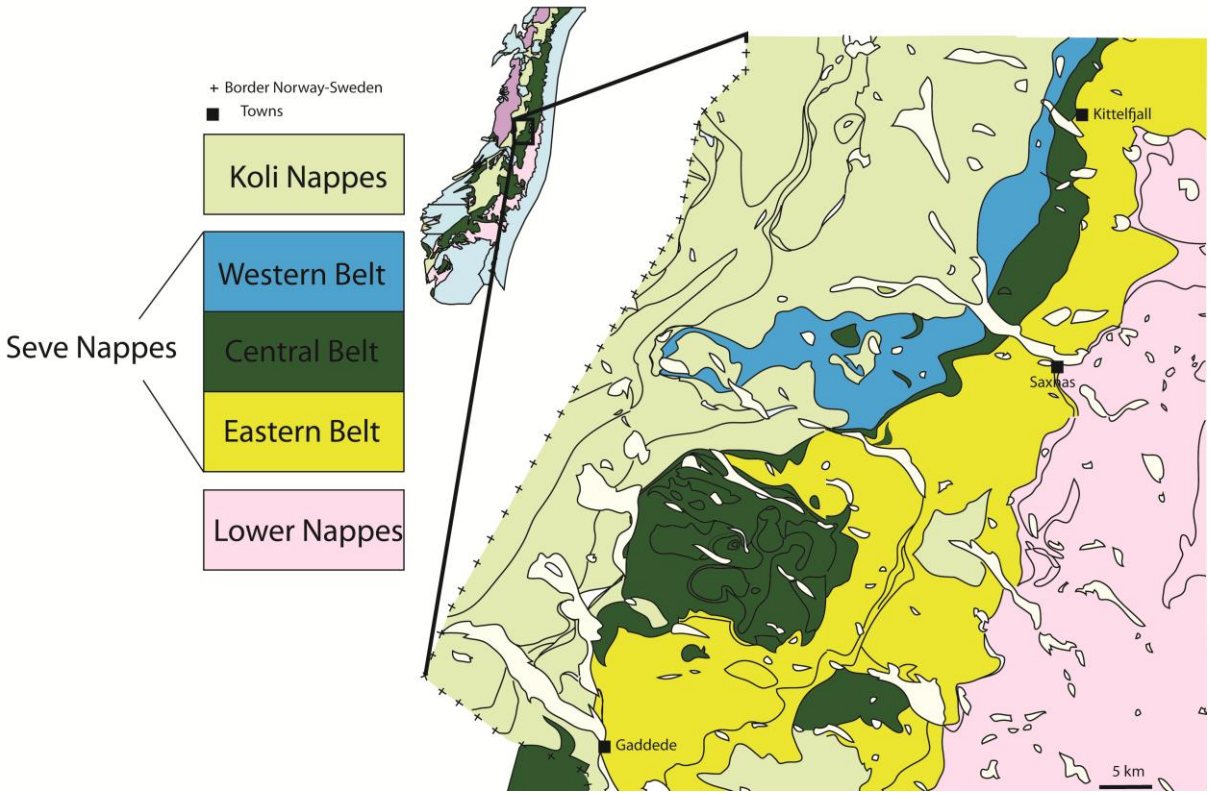

Figure 2.4.1A; Terrane map of the Scandinavian Caledonides showing the different nappe Complexes. (*Modified after Gademan et al., 2011)*

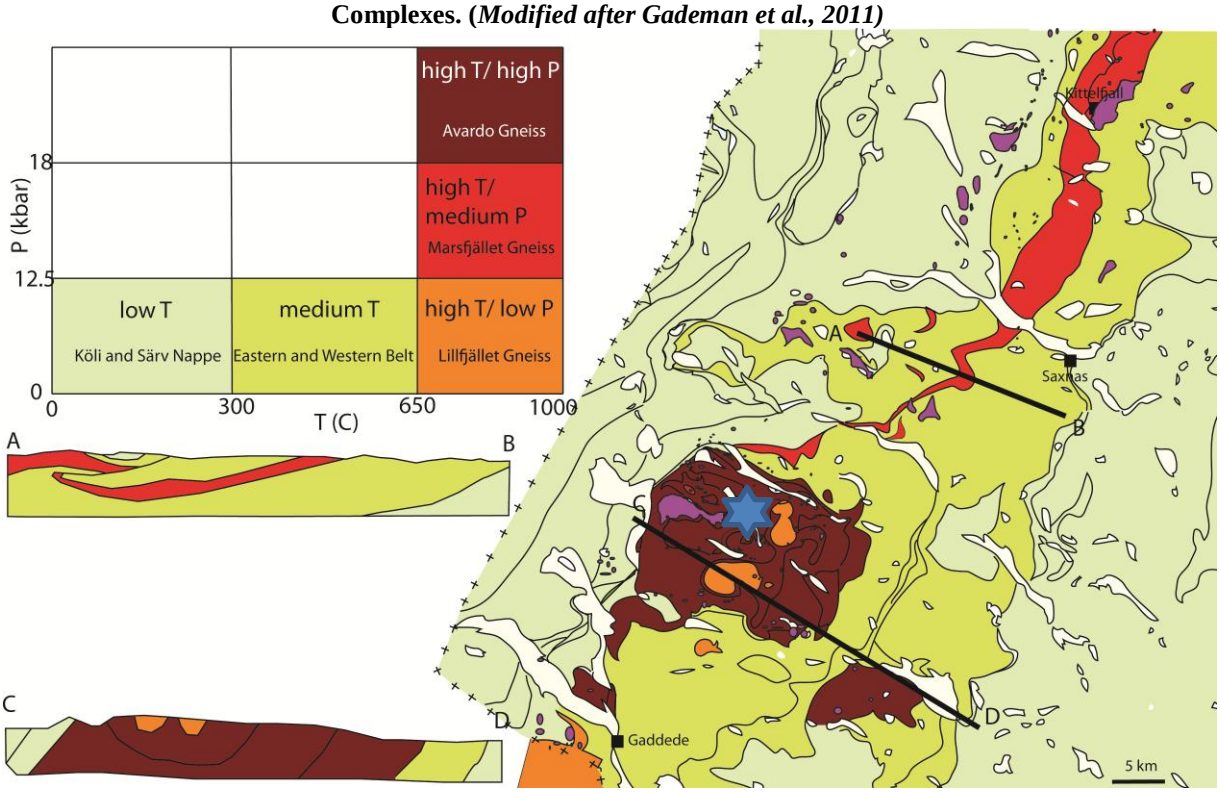

Figure 2.4.1B; Metamorphic map showing the temperature of the formation of the peak mineral assemblage. A roughly NS oriented pressure gradient occurs in the Central Belt of the SNC. The Friningen peridotite lens is indicated with a blue star and occurs in the Avardo HP gneiss. (*Modified after Gademan et al., 2011)*

2.5. Polyorogenic history of the Scandinavian Caledonides

The Caledonian orogeny cannot be explained just by the convergence and collision of Baltica with Laurentia. Multiple (U)HP metamorphic phases and multiple exotic terranes must also be accounted for. Paleogeographic reconstructions of the formation of the Scandinavian Caledonides are so far sparse, 2 models have been proposed.
One model *(Roberts, 2003)* has tried to explain the different terranes of the Scandinavian Caledonides. This model takes into account different Early Caledonian events called the Trondheim, Finnmarkian, and Taconian event. The Taconian event is an accretionary event of diverse arc complexes along the eastern Laurentian margin and has been recognized in the uppermost allochton *(Roberts, 2003).*

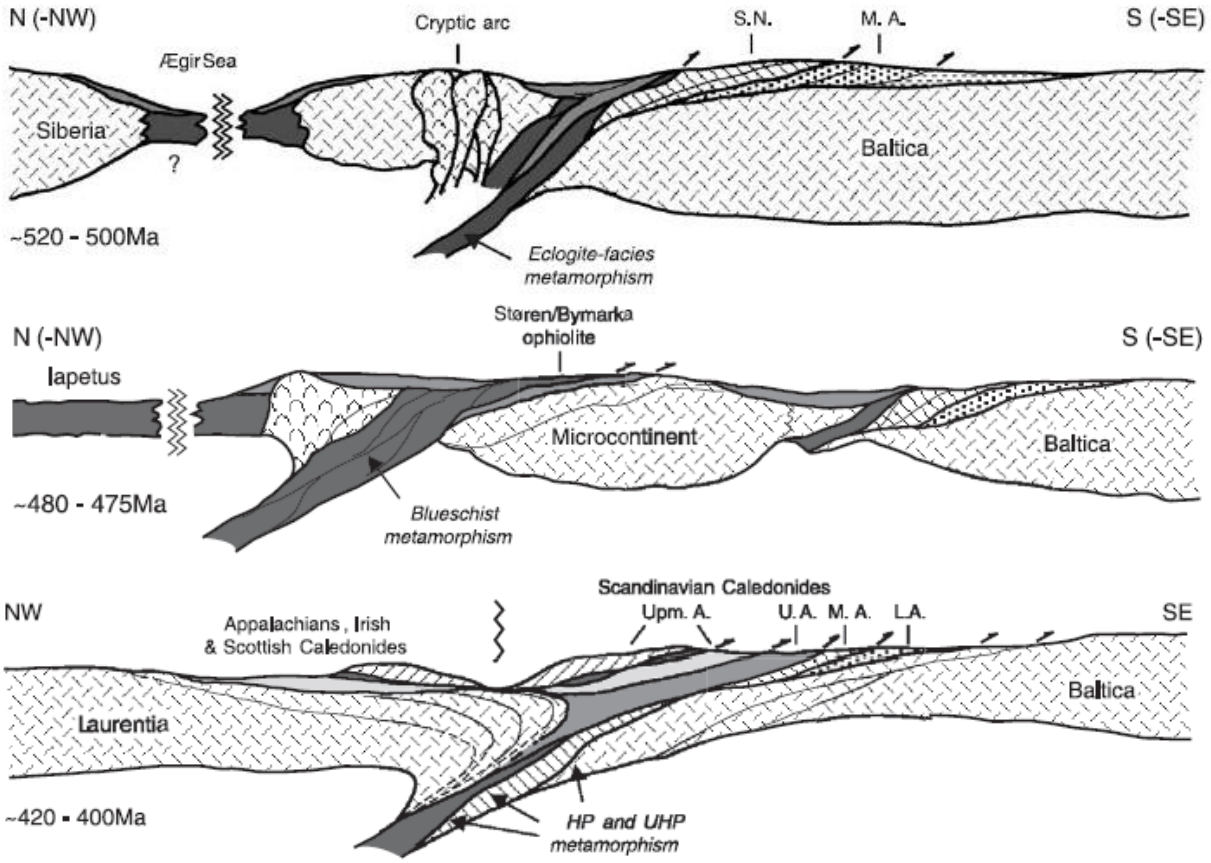

Figure 2.5.1; Conceptual geodynamic model. The upper transect shows the Finnmarkian orogeny, the middle transect shows the Trondheim event and the lower transect the Scandian orogeny. *(After Roberts, 2003)*

The Finnmarkian 520-500 Ma orogenic event emplaced the SNC and lower nappes on to the western edge of Baltica *(Figure 2.5.1).* This event involved eclogite facies metamorphism but does not give an explanation for the occurrence and emplacement of eclogites and mantle peridotites in the SNC. The Trondheim event, recognized only in the area around Trondheim occurred around 480-475 Ma between an unknown terrane and the microcontinent of which the SNC was derived. The Scandian main phase is shown with the allochtons emplaced and HP and UHP metamorphism occurring in deep subducted continental crust. For details of this paleogeographical model the reader is referred to *Roberts (2003).*

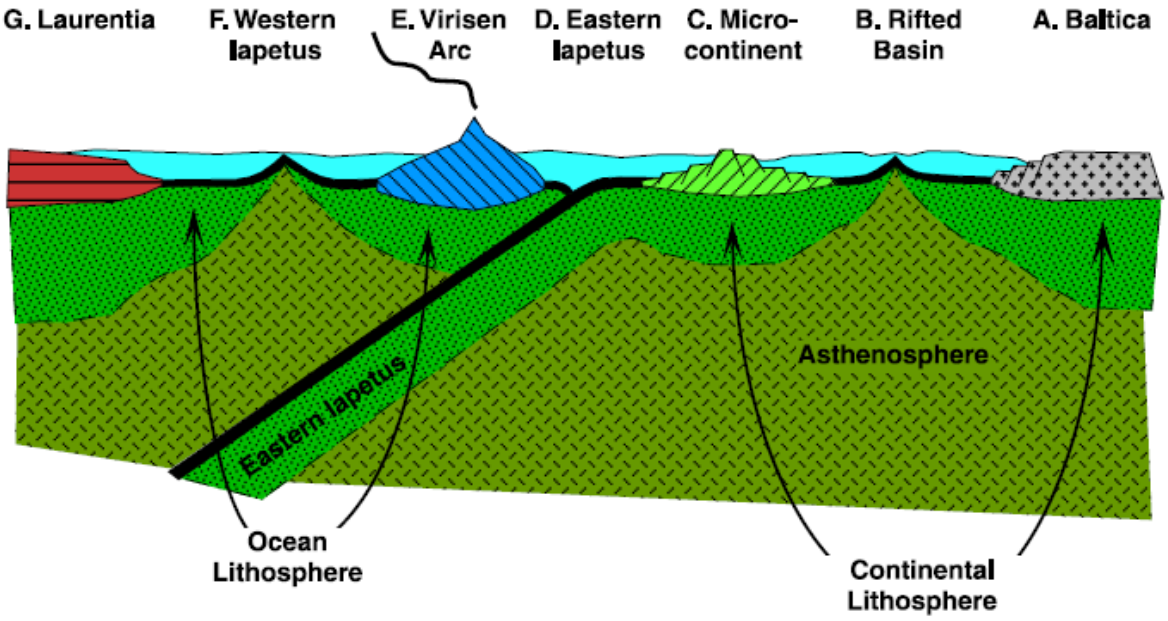

Figure 2.5.2; Starting configuration of the geodynamic model proposed by *Brueckner & van Roermund (2004)*

The second model *(Brueckner & van Roermund, 2004)*, takes into account all proposed ages for (U)HP metamorphism in the Scandian and Early Caledonian. The starting configuration can be seen in figure 2.5.2. In this paleogeographic reconstruction, the Virisen arc is accreted to a microcontinent of possible Baltic affinity. This occurred during what is known as the Finnmarkian orogeny (520-500 Ma). This allows for a period of continental subduction during which Norrbotten peridotite bodies were incorporated in the continental crust. Subsequently, Baltica underthrusts the composite terrane leading to deep continental subsduction and renewed incorporation of peridotites. The final Scandian collision of Baltica and Laurentia also involves deep continental subduction and the synchronous UHP metamorphism of the WGR *(Figure 2.5.3)*. For the details of the model the reader is referred to *Brueckner & van Roermund (2004)*.

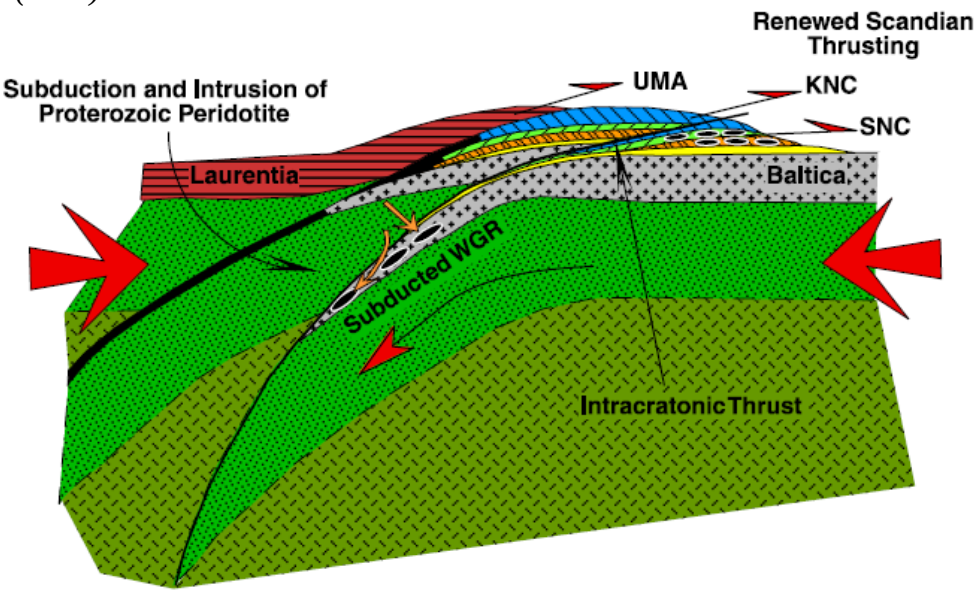

Figure 2.5.3; Final Scandian subduction of the WGR, and reactivation of the nappe stacks which were already in place. *(After Brueckner & van Roermund, 2004)*

Concerning Caledonian gravitational collapse and exhumation of subducted basement both authors are in favor of slightly different processes. *Roberts (2003)* infers extensional collapse of the mountain belt under the influence of a reduced stress field which creates large listric extensional faults. *Brueckner & van Roermund (2004)* infer slab breakoff as a result of the difference in buoyancy between subducted oceanic and continental crust. After slab breakoff, the briefly subducted continental crust is rapidly returned to the surface through some level of extensional faulting.

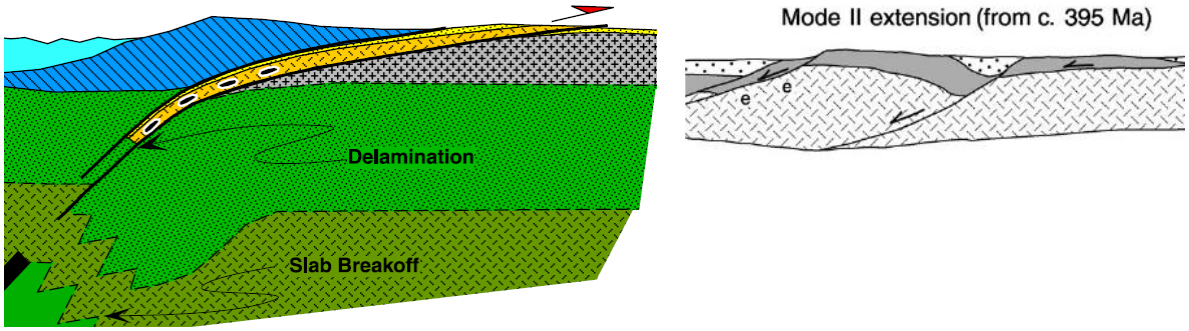

Figure 2.5.4; To the left, exhumation of UHP terranes *(After Brueckner & van Roermund, 2004)* and to the right, extensional collapse *(After Roberts, 2003)* Note that extensional collapse cannot explain the occurrence of eclogite facies rocks at the surface

Although both models are good first order attempts to explain the final geometry of the Caledonian orogeny, new data and insights ask for a revision of parts of these models. Roberts does not explain the occurrence of mantle peridotites (SNC or WGR), especially concerning the exhumation of these. *Brueckner & vam Roermund (2004)*, uses two events prior to the Scandian phase but the newly available monazite dating of the Central Belt of the SNC *(Gademan et al., 2011)* puts the necessity of a collision between Baltica and a microcontinent at 450 Ma in doubt. The Jämtlandian orogeny of 450 Ma has led to the incorporation of the SNC peridotite bodies during a period of continental subduction of Baltica. The SNC was exhumed ~430 Ma due to slab breakoff (of the rifted basin in *figure 2.5.2*). However also during the Scandian orogeny the western Baltic margin subducted and this led to the incorporation of the WGR peridotite bodies.

2.6. Mantle peridotites in collision zones

A number of mechanisms can operate in bringing mantle material in or on top of continental crust. These mechanisms include ophiolite obduction (for example in the Oman ophiolite) and deep ductile imbrication of the lower crust *(Medaris & Carswell, 1990)*. The latter process can incorporate spinel mantle peridotites but not garnet peridotites *(van Roermund, 2009)*.
Garnet peridotites can form from lower pressure protoliths when a low pressure mantle peridotite, entrained in continental crust, subducts with this crust to large depths and subsequently returns to the surface. These are prograde garnet peridotite which originates from lower pressure hydrated peridotites. Sub-Continental Lithospheric Mantle (SCLM) peridotite, lithospheric mantle material which is now exposed at the surface, originates as a high pressure protolith. SCLM can be distinguished from prograde peridotites since garnets and spinels in these peridotites are not hydrated and will not contain prograde textures. When garnets are not found in peridotites an origin as sub-oceanic lithosphere cannot be ruled out. The lithosphere underneath island arcs might reach thicknesses that allow for the stability of spinel in the sub-oceanic lithosphere.

A certain mechanism must operate in order to incorporate these mantle peridotites in the continental crust during deep continental subduction. Diamond in eclogite facies rocks shows that continental subduction can reach depths that allow it to be juxtaposed with garnet peridotite in the overlying mantle wedge *(Brueckner, 1998; Brueckner & Medaris et al., 2000; van Roermund et al., 2002; van Roermund, 2009).* Exhumation of subducting continental crust and its peridotite cargo, possibly after oceanic slab break off which terminates the effects of slab pull, exposes these rocks back to the surface by buoyancy.
A recent new classification diagram has been proposed by *Cong et al., (2011).* This classification-proposal directly links the type of SCLM and the thermobarometric data derived from it to the type of geodynamic setting during collision. The SCLM peridotites are subdivided into four types *(see also figure 2.6.1 and 2.6.2),* A, B, C & D. Type A and B correspond to old mantle wedges in which type A is static and type B is active. The term active here implies there is substantial flow and upwelling in the upper part of the asthenospheric wedge. Type C and D correspond to young mantle wedges, type C being static and type D being active *(see also figure 2.6.1 and 2.6.2).*
Thermobarometric data derived from EMP mineral chemistries of peridotites can thus give much geodynamical information on the nature of the collisional process. Further, the evolution of the SCLM before collision can also be addressed.

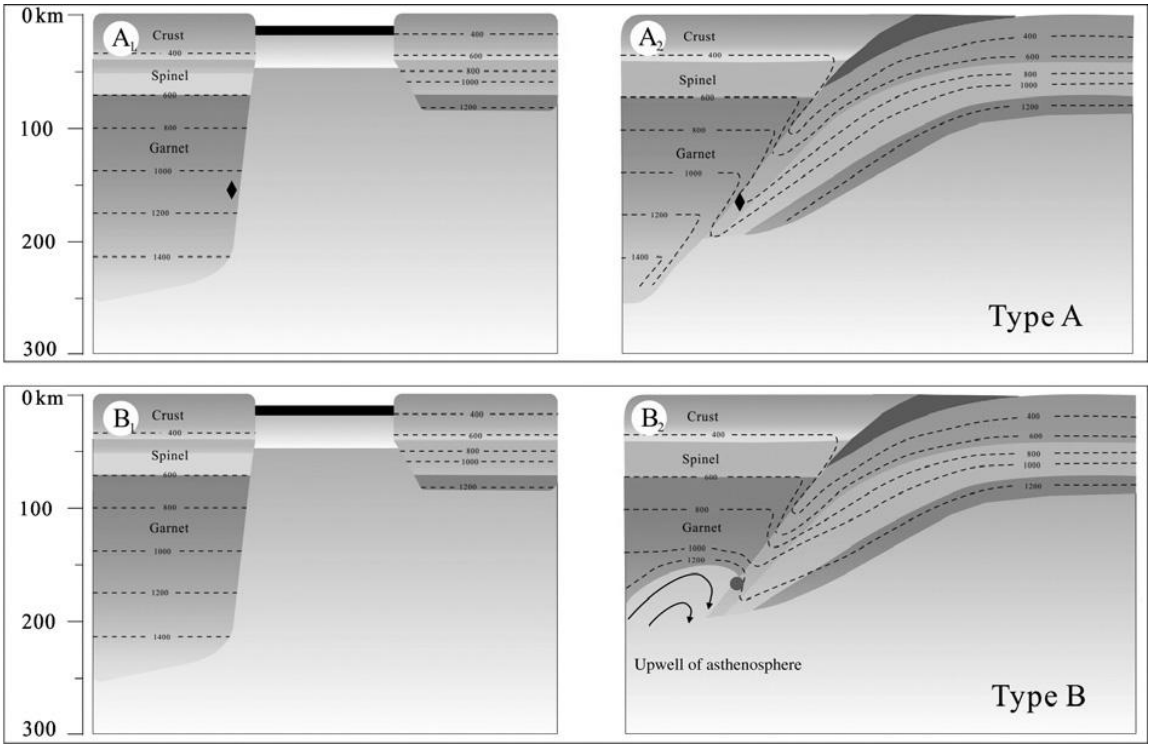

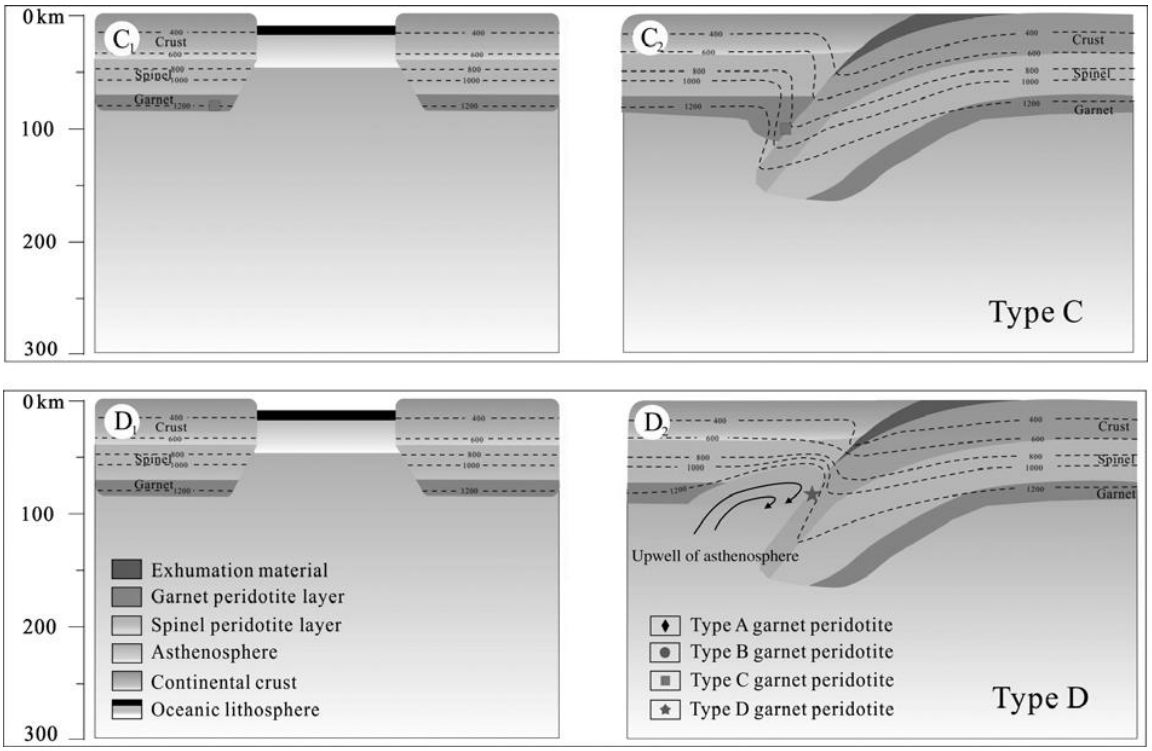

Figure 2.6.1; Different modes of collision depending on the PT conditions of the mantle wadge prior to collision *(After Zhang et al., 2011)*

The conceptual geodynamic collisions illustrated in figures 2.6.1 A-D have PT conditions of the SCLM which are depicted in figure 2.6.2. It is essential to have qualitative analyses on microstructures and quantitave analyses on mineral chemistry. This allows themobarometry to be applied and interpretated. Subsequently individual minerals and/or mineral pairs might be dated, for example different periods of garnet growth can be dated using the Sm-Nd age dating technique. This can constrain the evolution of the SCLM of the overriding terrain.

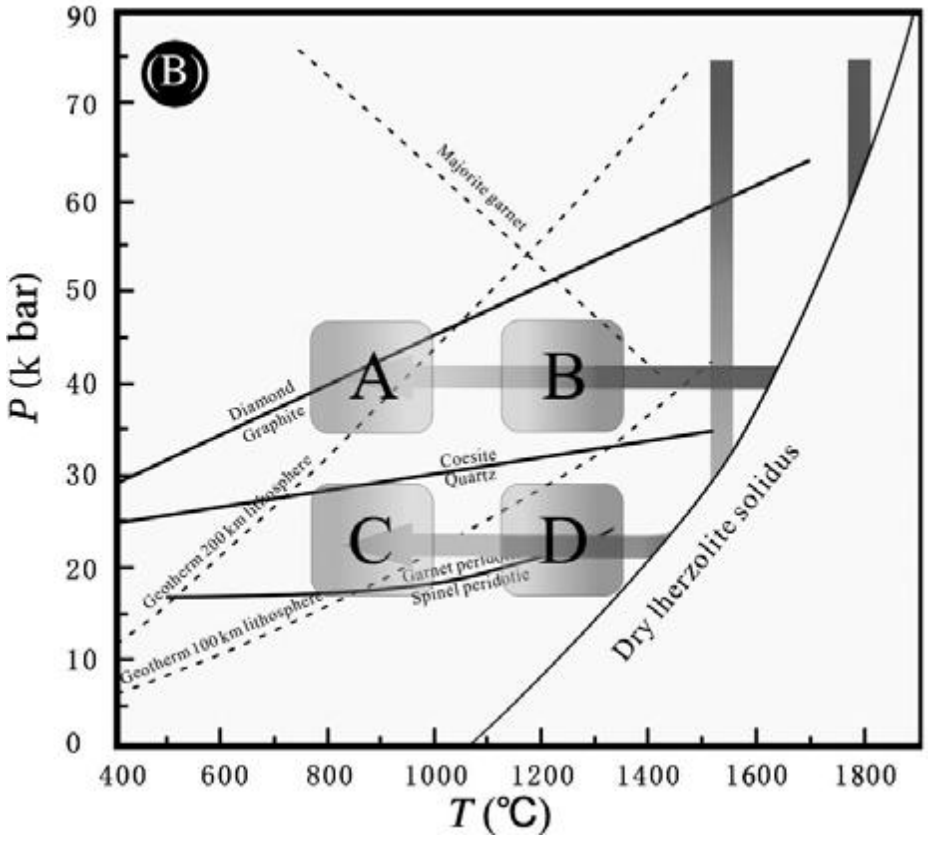

Figure 2.6.2; PT conditions operating in mantle wedges A,B,C & D as proposed in figure 2.6.1 ***(After Cong et al., 2011)***

2.7. The transient hot channel

The transient hot channel is a concept first proposed by *Hsu, (1971).* The concept was a first approach to the explanation of HP terranes in Phanerozoic orogens. The transient hot channel is a low viscosity ductile channel above a subduction zone. The low viscosity of the channel is genereated by dehydration of the subducting slab (and/or dehydration during prograde metamorphism). The transient hot channel has recently been modeled by *Gerya et al. (2007) (Figure 2.7.1)*. Dehydration of subducted passive margin sediments and heating create UHP rocks. These are effectively squeezed out of the lower crust during collision *(Gerya et al., 2007)*. This model does not require slab break-off after collision in order to exhume the UHP rocks. The Seve Nappe Complex is an HP terrane in the Scandinavian Caledonides and the effective mechanism of bringing this HP terrane to the surface is not clear yet. Three different models have so far been proposed, dunk tectonics *(Brueckner & van Roermund, 2004)*, and extensional collapse *(Roberts, 2003).* The transient hot channel is the approach used by many geophysicists in general for UHP terranes in Phanerozoic orogens. As seen in figure 2.7.1, not much of the geometry of a standard fold and thrust belt remains.

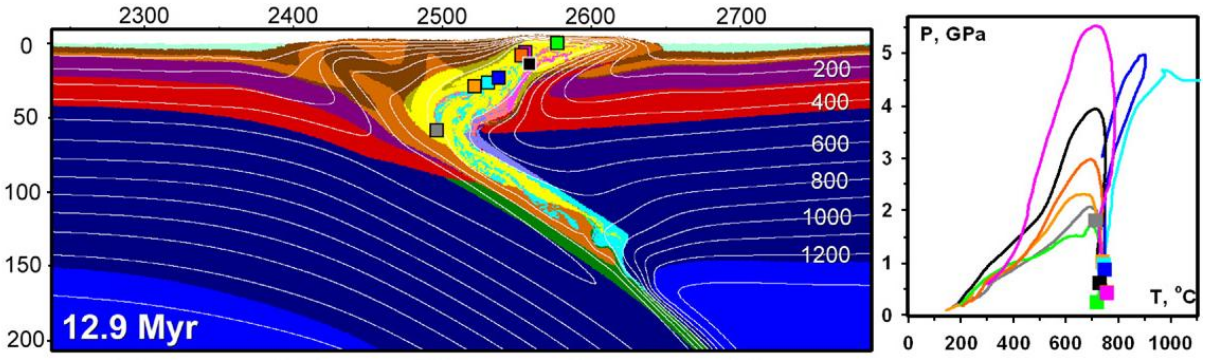

Figure 2.7.1; Modeling of the Transient hot channel. To the right are PT plots of rocks in the hot channel. The Light blue path could be equivalent of exhumed SCLM *(After Gerya, 2007)*

2.8. Magmatism in the Scandinavian Caledonides

The Friningen peridotite lens is cut through by a basic dike which is interpreted not to be found in the enclosing gneisses. This basic dike ought to be correlated with other dikes in the allochtons and/or autochton of the Scandinavian Caledonides. It is important to realize that such a magmatic event postulated for dikes in the Friningen garnet peridotite body are strongly dependent on the type of provenance of the SNC. If the SNC is considered to be an external terrane i.e. foreign to Baltica, the dike in the peridotite will not correspond to any dikes that predate crystalline basement rocks of Baltica itself.

The Sarek nappe forms part of the Seve-Kalak terrane and consists of arkoses and basaltic dikes *(Andreasson et al., 1992)*. These dikes are originally interpreted to belong to the rifting event culminating in the opening of the Iapetus ocean *(Andreasson et al., 1998)*. Dating this dike swarm (608 ± 1 Ma) confirmed this theory (*Svenningsen, 2001)*.

Figure 2.8.1A shows the bulk rock REE data used in the study of *Andreasson et al., (1992)* and normalized to the chondrite values of *Sun & McDonough (1989)*. These data shows a relatively enriched REE profile, with increased enrichment in the HREE.

Bulk rock REE data presented by *Solyom et al., (1992)* also shows this type of pattern for the Central Scandinavian Dyke Group (CSDG), the Protogine Zone Dolerite Group (PZDG) and the Blekinge Dalarna Dolerite Group (BDDG) *(Figure 2.8.1B).* These results were also normalized to values of *Sun & McDonough (1989)*.

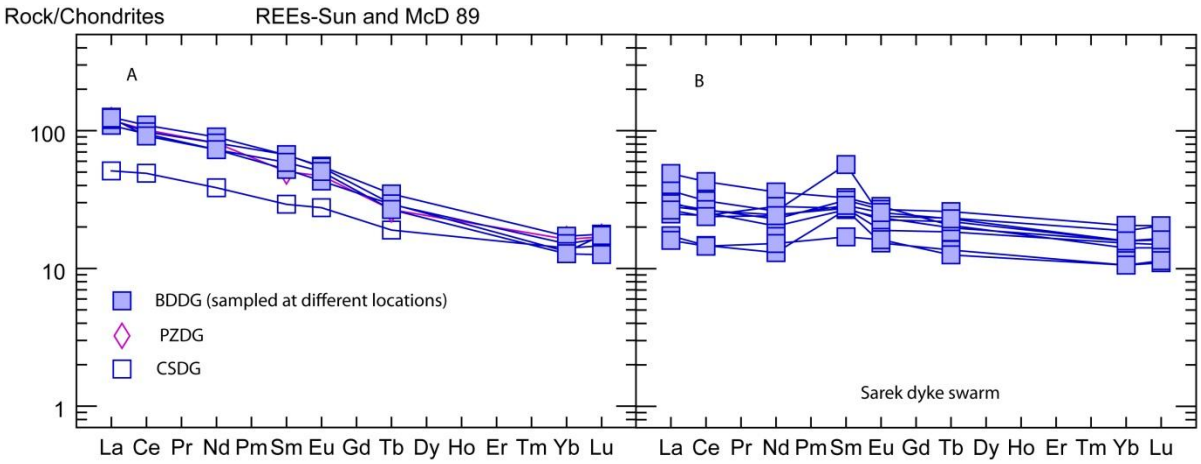

Figure 2.8.1; A) Bulk rock REE data of the BDDG, PZDG and CSDG normalized to chondrites *(Data from Solyom et al., 1992)* B) Bulk rock REE data of the Sarek Dike Swarm , normalized to chondrites *(Data from Andreasson et al., 1992)*

The time of intrusion of the PZDG and CSDG was dated 1180 and 1220 Ma respectively *(Johansson & Johansson, 1990)* and interpreted to reflect an incipient breakup of the Baltoscandian shield. These two dike swarms are very similar to the Sudbury and Abitibi dike swarms occurring in the Superior province of Canada *(Solyom et al., 1992)*. The BDDG has been dated at 930 Ma *(Patchett, 1978; Johansson & Johansson, 1990)*.

2.9. Eclogites and garnet pyroxenites

Controversy exists about the possible genesis of eclogites and garnet pyroxenite dikes occurring in orogenic garnet peridotite bodies. Garnet pyroxenite is interpreted as (U)HP melts which are in equilibrium with its host peridotite *(Gonzaga et al., 2010)*. Note the difference with UHP cumulate melt, an interpretation favored for spinel pyroxenites *(Liu et al., 2005)*. The currently most favored interpretation of eclogites is that they represent recycled oceanic material *(Barth et al., 2001; Jacob 2004)*. This line of reasoning has been questioned in recent work by *Griffin & O'Reilly, 2007* who concur the interpretation that eclogites are exclusively metamorphosed basalts. They are not in favor of ubiquitously interpreting eclogites as subduction related oceanic crust/basalt and present results from a statistical analysis of xenolith suites and point out that eclogites are concentrated in the lithosphere-asthenosphere boundary (South African craton). However a recent revision of xenolith data from multiple locations within cratons has shown that eclogites do host oxygen isotope compositions and REE patterns that point to crustal origins of their protoliths. The heterogeneous oxygen isotopes are not concurrent with isotopic compositions of peridotitic mantle. This is indirect evidence that indeed the eclogites represent recycled oceanic crust. This does not give any information on whether subduction was coeval with entrainment of these eclogites in the mantle and the residence time of subducted material. The bulk rock REE plots of *Gonzaga et al., (2010)* are shown in figure 2.9.1. The $\delta^{18}O$ composition are shown in figure 2.9.2, these are the best discriminating factor for eclogites and garnet pyroxenites according to *Gonzaga et al., (2010)*.

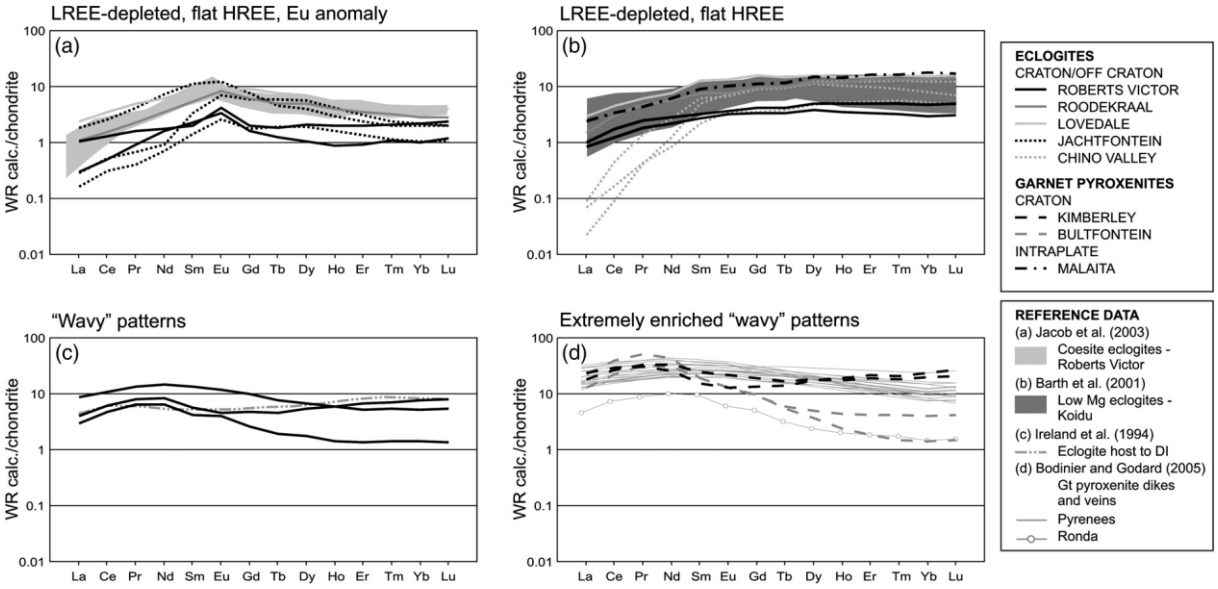

Figure 2.9.1; Bulk rock REE data recalculated from garnet and pyroxene REE data from *Gonzaga et al., (2010)*.

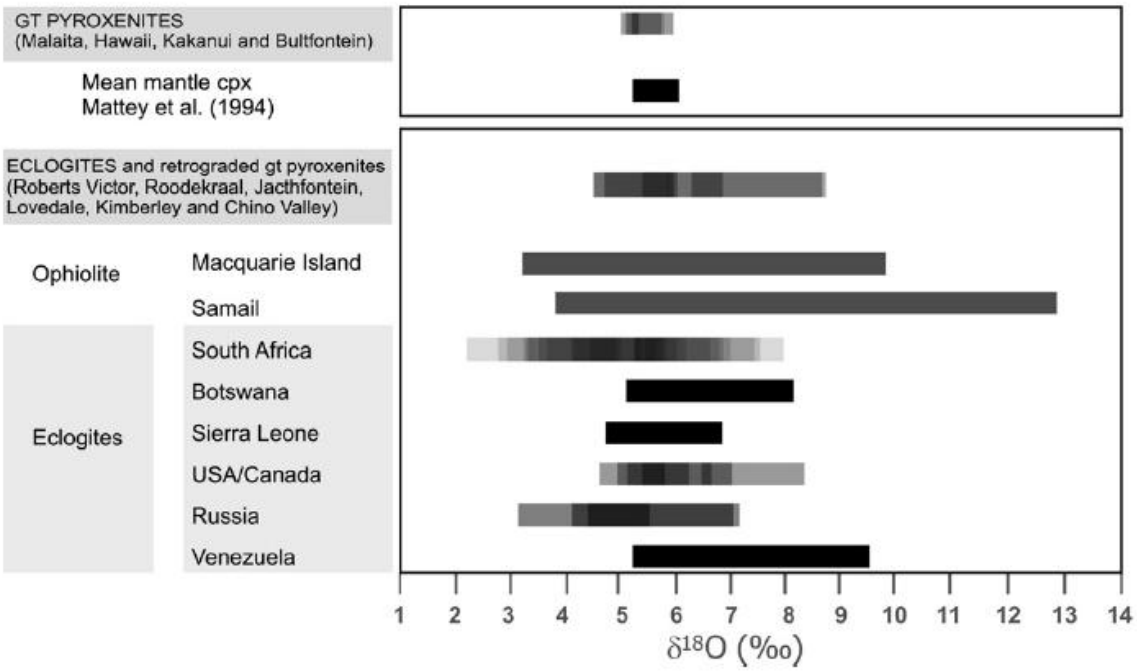

Figure 2.9.2; $\delta^{18}O$ compositions of cratonic garnet pyroxenites and eclogites. Note the spread in eclogites compared with that in garnet pyroxenites *(after Gonzaga et al., 2010)*

3. Methods

X-Ray Fluorescence

Samples for XRF analyses were crushed with a hammer mortar and pestle until no grains exceeded 5 mm. In between each sample the equipment used for crushing were cleaned with demi water, dried, cleaned with ethanol and then dried with compressed air. After this procedure, samples were crushed in a crusher to a uniform grain size of 73 micrometer. 10 Gram of each sample was taken to press into a tablet and 3 gram was taken to melt into a pearl. The samples were measured on a sequential ARL 9400 WD-XRF. For further discussion and details of this technique the reader is referred to Jenkins (1988).

Inductively Coupled Plasma Optical Emission Spectrometry (ICP-OES) and Mass-Spectrometry (ICP-MS)

ICP-OES is an analytical technique using inductively coupled plasma to excite the subject material and obtain specific optical emission spectra. Optical spectrometry is applied to convert the emission spectra to usable data. ICP-MS uses mass spectrometers and samples totally dissolved in HF acid *(Montaser, 1998).*

Extraction of Accessory minerals

In the search for zircons, accessory minerals were extracted from approximately 8 kg of mafic dike samples, the separation has taken place entirely in the mineral separation lab of the VU, Amsterdam, the Netherlands. These samples were crushed and sieved untill a fraction of 125 – 250 µm and a fraction of 30 – 125 µm remained. These were separated on the basis of magnetic susceptibility and density (heavy liquid separation with di-iodium methane). After the separation, accessory phases with different magnetic susceptibility and grain size were placed on a polished section in order to analyze them with the EMP.

Optical microscopy

Thin sections of each hand sample were made for investigations using optical and electron optical techniques. Of the peridotite, samples were cut were microstructures in the handsamples showed the least retrogression. Two thin sections of each dike hand sample (7 in total) were cut parallel and orthogonal to the main elongation and or foliation visible in the hand samples.

Electron microprobe analysis

Electron Microprobe (EMP) analyses were done using a JEOL JXA-1800 at Utrecht University. Mineral chemical analyses are obtained from an interaction volume of a cubic micrometer. EMP analyses were done using Electronic Dispersal Spectometry (EDS) for the quick identification of minerals and Wavelength Disperal Spectometry (WDS) for high resolution mineral chemical analyses. Samples were carbon coated prior to EMP analyses in order to induce conductivity for sound analyses. The obtained data have been corrected for backscatter and retardation effects, absorption effects and secondary fluorescence effects using the ZAF routine correction procedure.

Geothermobarometry

Estimates for PT conditions were obtained using EMP mineral analyses as input for the PTEXL program written by *Brey & Kohler (2008).* This program is iterative and relies on an educated 'guess' for input. Iteration is done three times with the calculated values in order to reach a good estimate for PT conditions based on a number of different thermometers.

Theriak Domino

Theriak Domino or the TD suite is a selection of programs that thermodynamically calculates phase diagrams. The software uses Gibbs Free Energy minimization *(De Capitani & Petrakakis, 1987)* to calculate phase diagrams under the assumption of chemical equilibrium throughout a certain bulk rock volume. The program uses the thermodynamic database of *Berman et al. (1985).*

Field sampling

During field work, 7 large mafic dike, 4 peridotite, and 3 thin (cm-scale) pyroxenite dike samples were gathered. Samples were labeled GP1-GP4 (GP for Garnet perditotite), D1-D7 (D for Dike) and MD1-MD3, (the smaller dikes). The locations of samples that were gathered directly from the outcrop are depicted in figure 4.1.8. Other samples were gathered from the talus directly below the outcrop. In order to be certain that pyroxenite samples originated from the peridotite these have been only sampled from peridotite boulders that still contained the pyroxenites.

From D1-D7 and GP1-GP4 thin sections were made. 2 Thin sections of each of the samples D1-D7 and GP1-GP4 were created and of MD1-MD3 one thin section each. These have all been created for the optical microscopy analyses. The best of these thin sections were used subsequently for EMP analyses.

Samples D1-D7 have been used for XRF, ICP-OES and ICP-MS bulk rock compositions. Sample GP3 has been subjected only to XRF analyses. Sample D5 and GP3 were used for Theriak Domino thermodynamic calculations.

An attempt has been made to gather zircons from these samples. This has been done using two complete (10*10*10) samples, D3 and D4 and smaller amounts (5*5*5 cm) of each other sample D1,D2 and D5-D7. Of sample D3 and D4 approximately a small piece remains of approximately 1*4*4 cm.

4 Results

4.1 Field observations

4.1.1 *Location*

The Friningen garnet peridotite is located in Northern Jämtland, approximately 30 km from the Swedish-Norwegian border (GPS: 64°44´430´´N, 014°33´444´´E). The location of the peridotite is shown in figure 4.1.1. The peridotite outcrop lies structurally in the HP Ertsekey lens of the Central belt of the Seve Nappe Complex *(Van Roermund, 1985; 1989).*

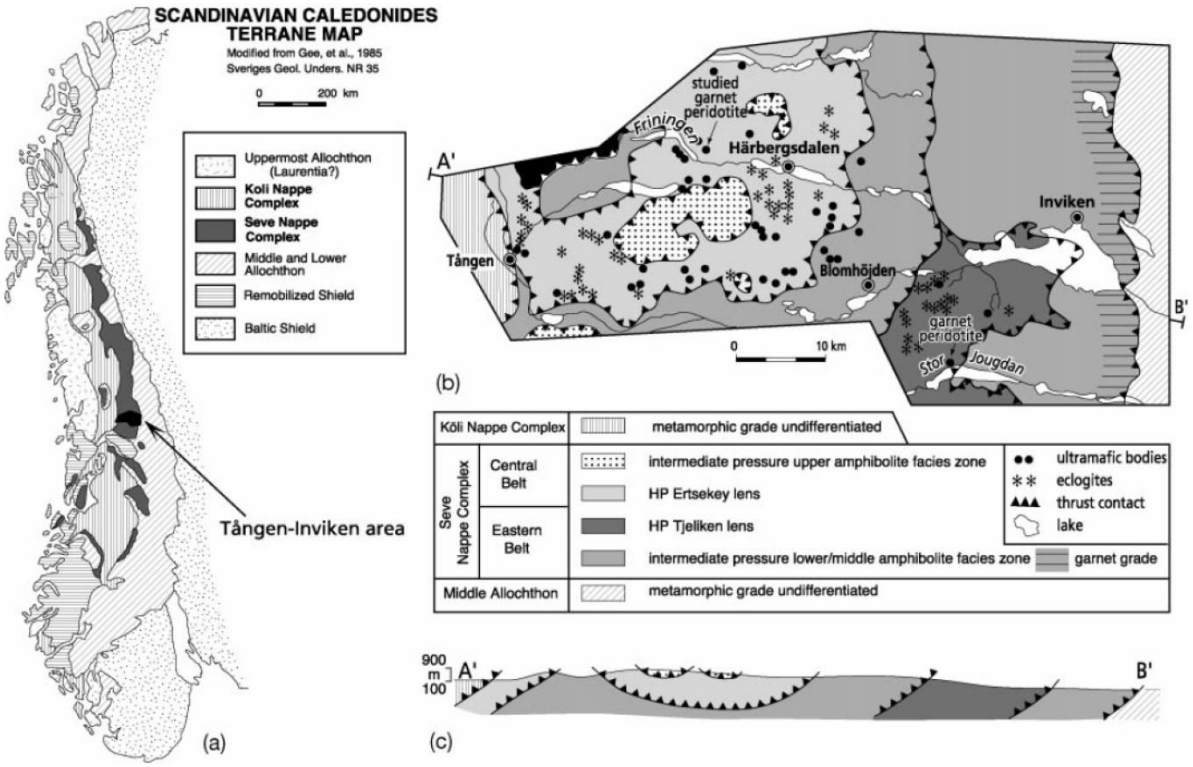

Figure 4.1.1; Location of the garnet peridotite body. A) Overview of the Scandinavian Caledonides. B) overview of the fieldwork area with ultramafic bodies and eclogites represented as dots and stars, respectively. C) structure of the area in an E-W profile. ***(After van Roermund, 1985; Brueckner et al., 2004)***

The peridotite can be reached from Härbergsdalen in the east (accessible by car) along a walking trail of approximately 10 km. The outcrop is located a 45 minute walk from the Sielkentjakkstugan, a wooden cabin which can be used for overnight stay. Figure 4.1.2 shows a panorama of the outcrop. The country rocks of the peridotite lens are heavily deformed HP gneisses (not visible on figure 4.1.2).

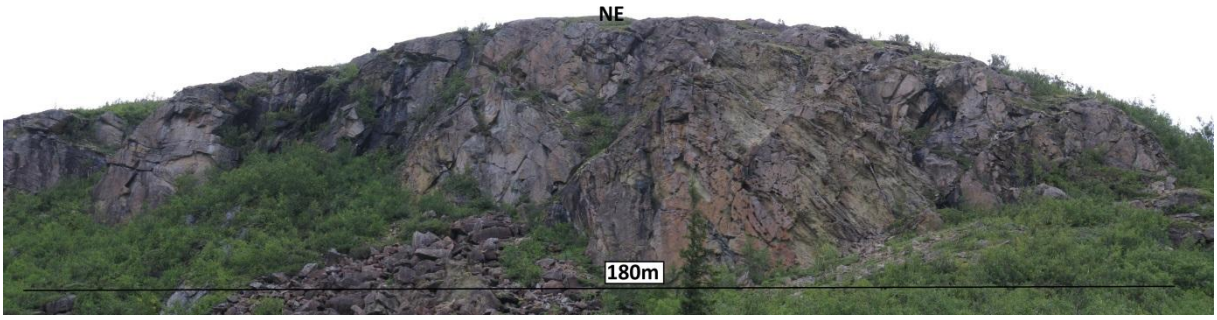

Figure 4.1.2; Panorama of the Friningen garnet peridotite lens.

4.1.2 *Lithologies*

The Friningen garnet peridotite lens consists of banded dunite – lherzolite and is approximately 180 m wide and 30 m high. A garnet pyroxenite dike (garnet + diopside), without plagioclase or olivine, runs through the outcrop from the upper NW to the lower SE *(Figure 4.1.3a)*.

The peridotite grain sizes range from locally granular to very fine grained. In some places the peridotite contains garnet of up to 2 cm; in some places spinel *(Figure 4.1.3b)*. Garnets occasionaly host inclusions of spinel and clinopyroxene. The variation in grain size cannot be correlated to the rock-forming minerals. Garnets and spinels are usually larger than clino- and orthopyroxene and olivine, although the latter can reach dimensions of 2.5 cm.

The garnet pyroxenite dike consist of diopside and garnet, garnet is megacrystic, clinopyroxene has a finer grain size *(Figure 4.1.3c)* Garnets are often very elongated *(Figure 4.2.7)*, no elongation is seen in the clinopyroxenes. The garnet-diopside ration is 2/3 to 3/2.

Thin garnet pyroxenite dikes crossscut the outcrop, which have an overall much smaller grain size than the main dike but similar mineralogy.

Figure 4.1.3; a) Garnet pyroxenite dike (upper left to lower right) in the Friningen garnet peridotite lens. B) Coarse spinels, pyroxenes and olivine. Possible subhedral hexagonal pseudomorphs after garnet. C) megacrystic garnets (reddish) in finer graind clinopyroxene matrix (green)

4.1.3 *Structures*

Compositional banding (S_0)

In previous work, *Brueckner et al., (2004)* report compositional banding in the peridotite. In this study, compositional differences of the peridotite were found. These compositional differences are expressed in the peridotite as different percentages of the rock forming minerals in different parts of the outcrop. Unfortunately no constraint on the orientation of the compositional banding was found with the exception of one part of the outcrop in the SE *(figure 4.1.5c)* where the compositional banding is at an angle of approximately 30° to the main foliation.

Main foliation (S_x)

The main foliation in the garnet peridotite lens is visible throughout the outcrop and the intersection lineation with outcrop plane 164/90 (strike dip) dips approximately 35° in the SW part of the peridotite. This gradually changes to the NE of the peridotite, where the lineation becomes approximately horizontal *(see also figure 4.1.5a+b)*.

Foliation (S_{x+1})

A second foliation is present as a disjunctive anastamosing foliation and makes an angle of approximately 60° with the main foliation. This foliation is very weakly developed *(see also figure 4.1.5a+b)*.

Late shear zones with the same orientation as the second foliation (S_{x+1}) were found in the SE half of the peridotite lens *(see also figure 4.1.5c)*. These are straight and have a displacement of up to 50 cm. The late shear zones will be called S_{x+2}.

For the orientation of the different structures in the peridotite see figure 4.1.4.

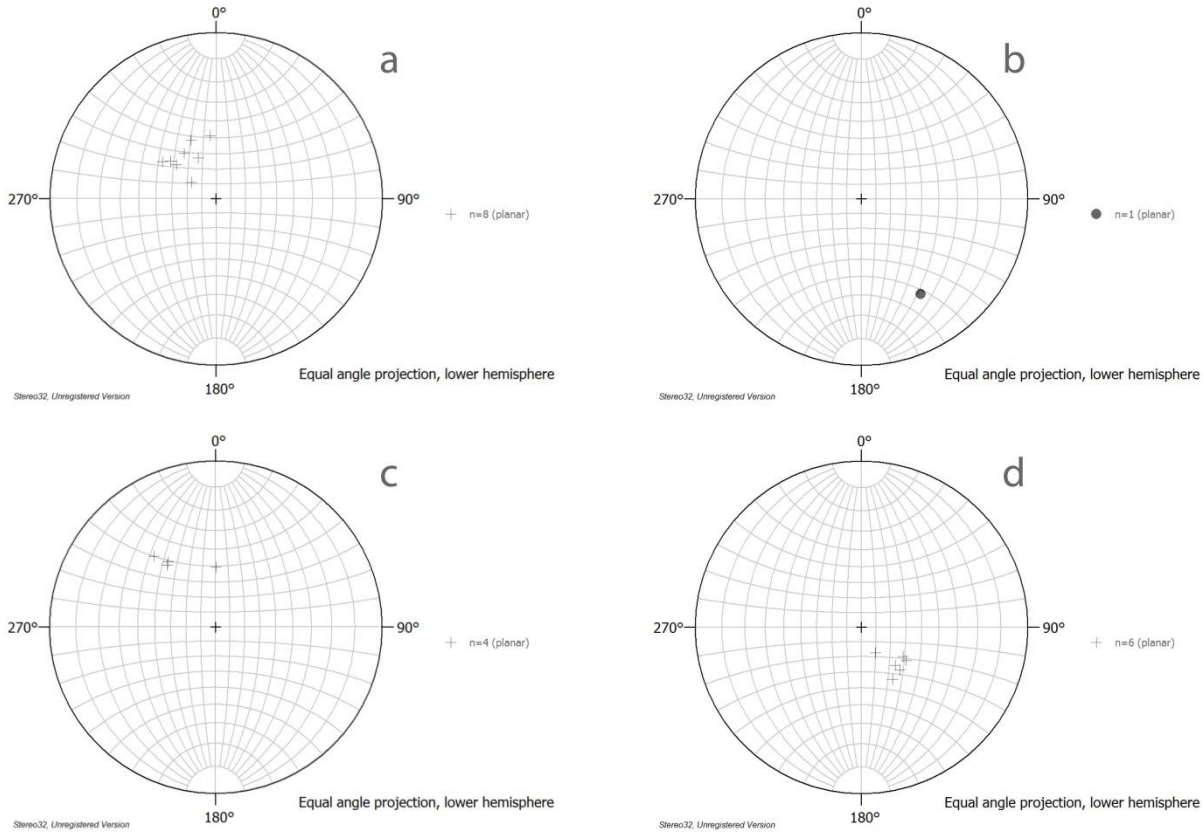

Figure 4.1.4; Stereoplots, all planar features are plotted as poles in equal angle projections. A) Poles of main foliation S_x. B) Poles of shear zones S_{x+2}. C) Poles of dike orientation. D) poles of late fractures in the dike

Figure 4.1.5; a) main foliation S_x (cyan) and second foliation S_{X+1} (green) in very fine grained dunite. The second foliation is defined by amphibole minerals. b) main foliation S_x (cyan) and second foliation (S_{x+1}) in the peridotite. Note the cleavage refraction at the transition between dike and peridotite, indicating a rheology difference. c) S_3, late shear semi-brittle shear zone (red) with an approximate displacement of 0.5 m. The blue line shows a thin (5 cm) pyroxenite vein being offset by the shear zone. In cyan is again the main foliation, which is at an angle to the compositional banding

Overprinting relations

S_x is a folded foliation (On a larger scale than visible in figure 4.1.4a); it dips 35° in the SE part of the peridotite body and is horizontal in the NW part. The axial plane foliation of this fold is defined by the S_{x+1} foliation which must be due to a later tectonic event. The late shear zones (S_{x+2}) are straight and parallel to S_{x+1}. It is most probable that the shear zones have formed using planes of weaknesses defined by S_{x+1}. The main foliation S_x will be termed S_1 and the axial plane foliation of the open folds in S_1 will be termed S_2. The late shear zones in the peridotite have the same orientation as S_2 but as these have likely formed on former planes of weakness these will be termed S_3.

No overprinting relations or relative ages have been found regarding the compositional differences in the peridotite outcrop. This presents a problem as the relative age cannot be determined. The compositional banding is assumed to be S_0 for this outcrop, although no evidence was found that supports this assumption. This automatically implies that the compositional banding has been deformed by S_1, S_2 and S_3.

Main dike structures

Isoclinal folds are found in the garnet pyroxenite dikes. The folds have half wavelengths of approximately 0.5 m and are clearly visible in parts of the outcrop. The axial plane of the folds are subparallel to the S_x foliation, the plane of symmetry is parallel to the S_1 foliation. These folds will be called F_x *(see also figure 4.1.6).*

The garnet pyroxenite dike is also boudinaged, with the length axis of the boudins (sub) parallel to the S_x foliation. Boudins range in length from several meters to 1 m and the thicknesses vary from 50 cm to 20 cm. Boudin traces are connected meaning, the length axis of one boudin is in line with the following boudin. The boudinage of the dikes will be termed D_x.

The envelope of the dike and its isoclinal folds is folded itself, by large open folds with a maximum wavelength of around 100 m. The open folds have interlimb angles of ~135°. These folds will be called F_{x+1} *(see also figure 4.1.6).*

The dike shows cusp and lobe structures which, although not necessarily representing a single deformation event, should be discussed. The cusp and lobe structures are best visible in the isoclinal folds.

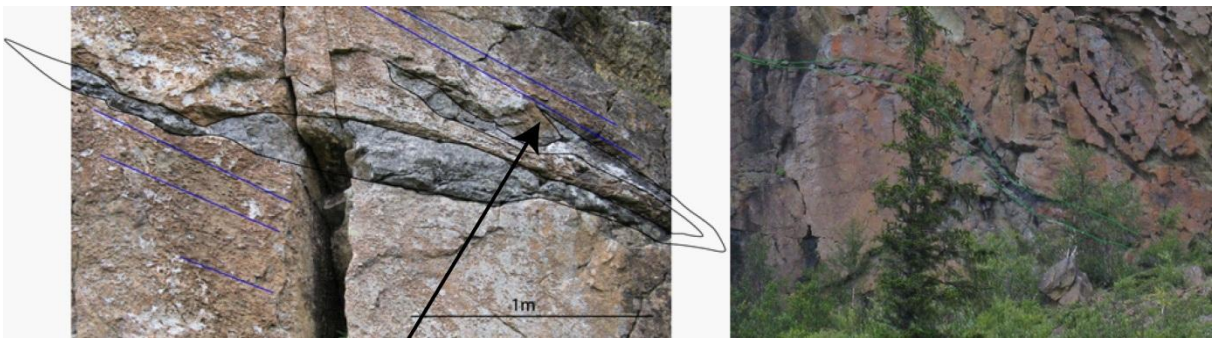

Figure 4.1.6; left) Isoclinal fold and cusp and lobe structures in the dike. Cusp and lobe structure is indicated with an arrow. Right) open fold in the dike envelope, envelope in green. The tree in the lower right of the photograph is approximately 3m high

Overprinting relations

As the isoclinal folds of the dike are themselves folded, they must represent an earlier tectonic event than the open folding. On the basis of this relative timing, the isoclinal folding will be termed F_1 and the open folding F_2. The boudin traces are connected which implies that they are syn- or later than the F_1 folding. The bouding traces are also (sub)parallel to the main foliation. Boudinage is either due to progressive deformation coeval with the isoclinal folding or due to another tectonic event. If this is another tectonic event the stretching must have been perfectly orthogonal to the former compression which created the isoclinal folds. There are no extensional crenulation cleavages or foliation boudinages in the outcrop. Therefore, boudinage as an expression of continued progressive deformation is the most likely.

The cusp and lobe structures in the garnet pyroxenite indicate that the garnet pyroxenite acted as a low viscosity layer in peridotite during deformation. This corroborates a study by *Barnhoorn et al. (2010)* who has shown garnet rich layers can act as low viscosity layers in the mantle over a range of PT conditions. The cusp and lobe structures are mainly seen in the

isoclinal folds. It might therefore be possible that only during the deformation which formed F_1 folds the garnet pyroxenite was substantially weaker than the peridotite.

4.1.4 *Discussion*

No macroscopically observable deformation occurred in the peridotite prior to the intrusion of the garnet pyroxenite dike. Optical microscope analyses however indicate a strong crystallographic preferred orientation (CPO) of early olivine grains. Therefore on the basis of field evidence it can be said that the garnet pyroxenite intruded in a tectonite. The garnet pyroxenite might have intruded in a compositionally banded peridotite or in a completely dunitic peridotite. In the latter case the dunite was refertilized after the intrusion of the garnet pyroxenite which formed the compositional banding. If the compositional banding is due to the dike intrusion the compositional banding must be parallel to the dike orientation and to the main foliation. If the compositional banding existed prior to the intrusion of the dike the orientation can have a random angle with respect to the dike. The compositional banding is at an angle of approximately 30° in the SE of the outcrop *(see also figure 4.1.5c).* The compositional banding which of the teconite is therefore interpreted to have existed prior to the intrusion of the garnet pyroxenite dike and comprises S_0.
The garnet pyroxenite was isoclinally folded (F_1 folds) and an axial plane foliation S_1 developed in the peridotite. The S_1 axial plane foliation is (sub) horizontal in the NW of the peridotite and dips approximately 30-35° in the SE of the peridotite body. This is also the main foliation in the peridotite. These are later folded by F_2, which comprises open folds with a wavelength on a larger scale (10 m scale). S_2 defines the plane of symmetry of the F_2 open folds and is a weakly developed axial plane foliation. S_2 is at an angle to S_1 of approximately 60°. The shear zones have formed on former planes of weaknesses defined by S_2 and must therefore represent S_3.

4.1.5 *Conclusion*

The garnet pyroxenite dike intruded in a compositionally layered peridotite body. This body contained a strong CPO of olivine (not determined) and is hence interpreted as a tectonite during which S_0 was formed. The compositional layering is at an angle to the dike. Subsequently, isoclinal F_1 folds and the S_1 foliation developed in the dike and the peridotite. These were later deformed when F_2 folds formed, with an axial plane foliation S_2 at an angle to S_1. Some planes of S_2 were reactivated during a third deformation phase as semi-brittle S_3 shear zones formed. The structural history of the peridotite lens and intruded dike is shown in figure 4.1.7. A panorama of the peridotite lens including the dike and foliations, (stitched from 3 individual photographs) can be seen in figure 4.1.8.

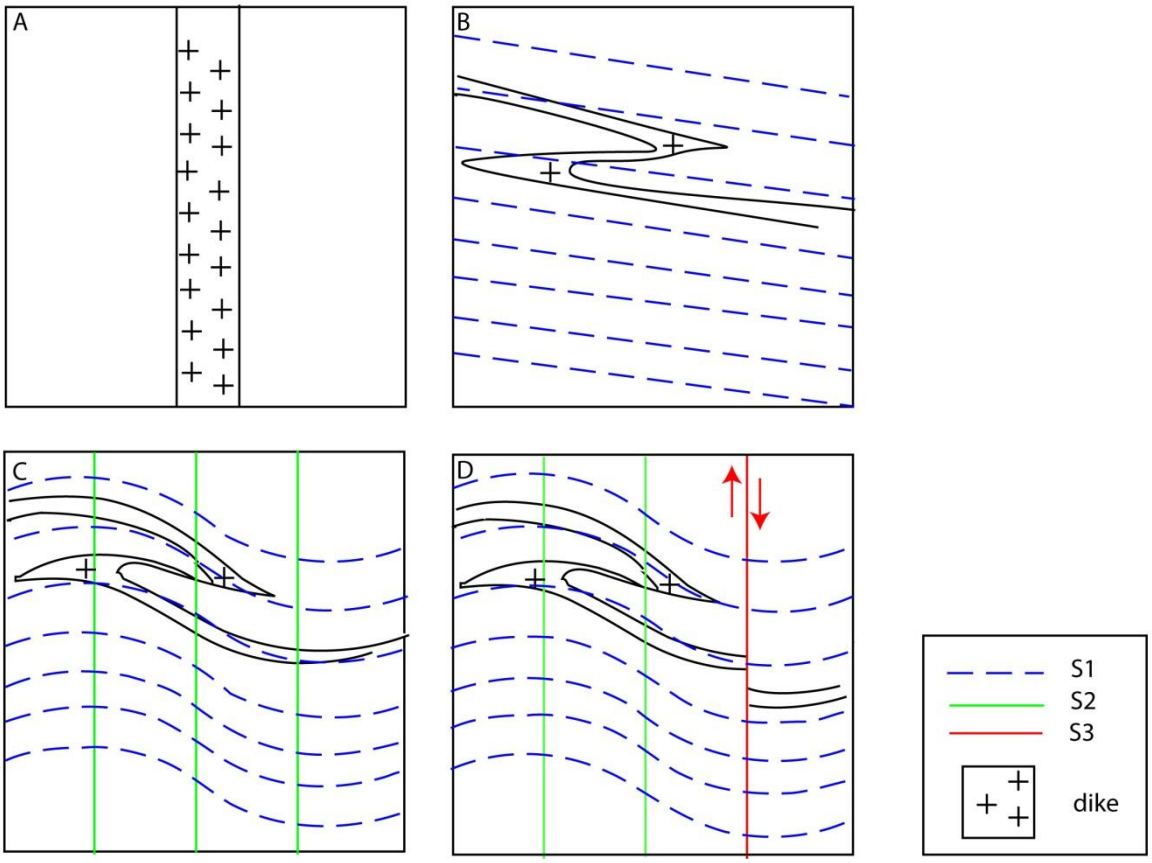

Figure 4.1.7; Overview of the structural history of the peridotite lens and the intruded dike. The compositional banding is omitted from this reconstruction. A) The intrusion of the dike in a compositionally layered solid peridotite tectonite. The relation between the dike and S_0 is unknown; B) F_1 isoclinal folding (which also boudinaged the dike) and the formation of the S_1 foliation C) F_2 open folding of the isoclinal folds and the S_1 foliation. The S_2 foliation comprises the axial plane foliation of F_2 folds. D) Occasional S_3 dextral semi-brittle shearing along S_2 foliation.

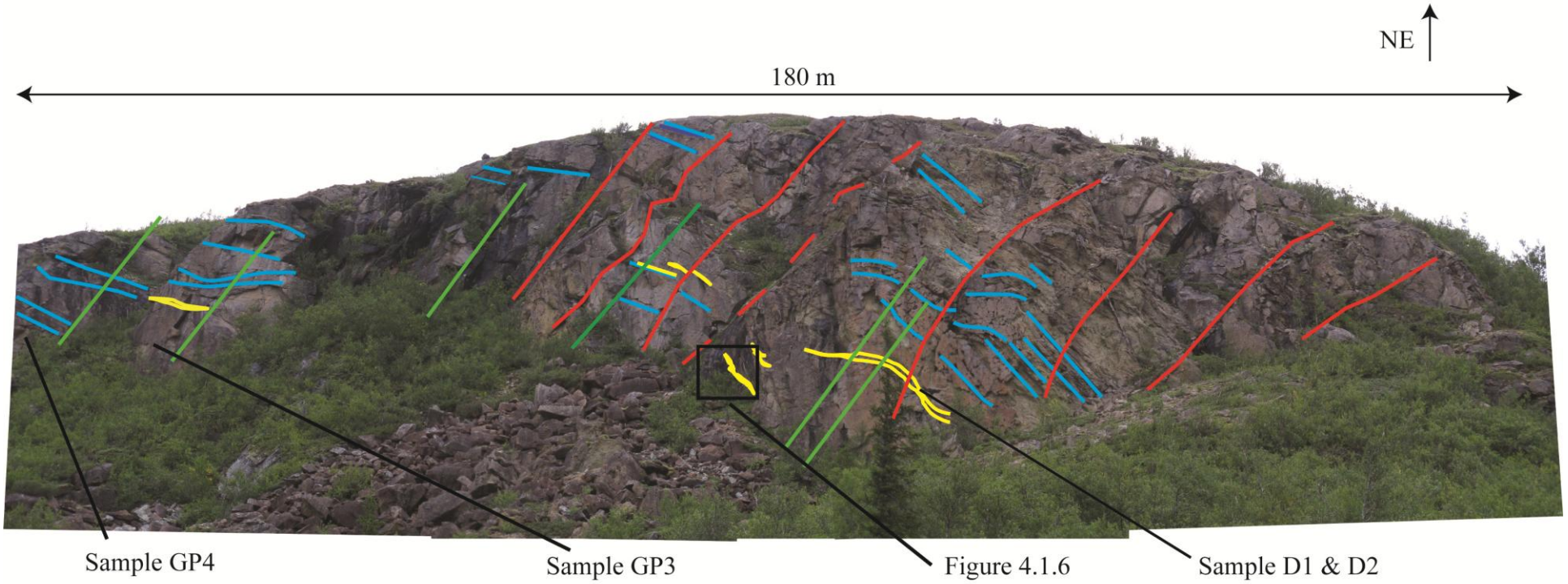

Figure 4.1.8; Overview of the Friningen garnet peridotite
The panorama shows a first foliation, S1 in cyan, which is folded by a later tectonic event, F2. F1 is inferred to have progressively deformed the dike and created the dike boudins (in yellow). The green solid line indicates S2 and is the second foliation which can be observed in the outcrop. The red lines indicate late semiductile shear zones (S3) which transect the peridotite lens, parallel to S2.

4.2 Microstructures

The mineral assemblages of both peridotite and pyroxenite will be given in a relative chronological order for increased readability. After the description of the stable assemblages of the peridotite the chronological order of these assemblages will be discussed. Subsequently this will be done for the garnet pyoxenite. The discussion contains a comparison between the garnet pyroxenite and the garnet peridotite and the probable coeval mineral assemblages of these lithologies.
Fractures will be termed similarly to the mesoscale foliations in the peridotite body *(Section 4.1 'field observations')*. This does not necessarily imply coeval formation of these foliations and fractures. The final discussion of this section will contain a comparison between the deformation features seen on the meso- and microscale *(Section 4.1 and 4.2)*.

Used abbreviations

Grt	garnet
Spl	spinel
Opx	orthopyroxene
Cpx	clinopyroxene
Di	diopside
Omp	omphacite
Ol	olivine
Amp	amphibole
Chl	chlorite
Plag	plagioclase
Srp	serpentine

4.2.1 *Garnet peridotite microstructures*

Assemblage	M_{1A}	M_{1B}	M_2	M_3	M_4	M_5
Grt	x		x			
Spl	Hi-Cr	x	x	x		
Opx	x	x	x	x	x	
Cpx	x	x	x	x		
Ol	x	x	x	x	x	
Amp		x			x	
Srp						x
Chl						x

Table 4.2.1; Petrogenetic grid of garnet peridotite

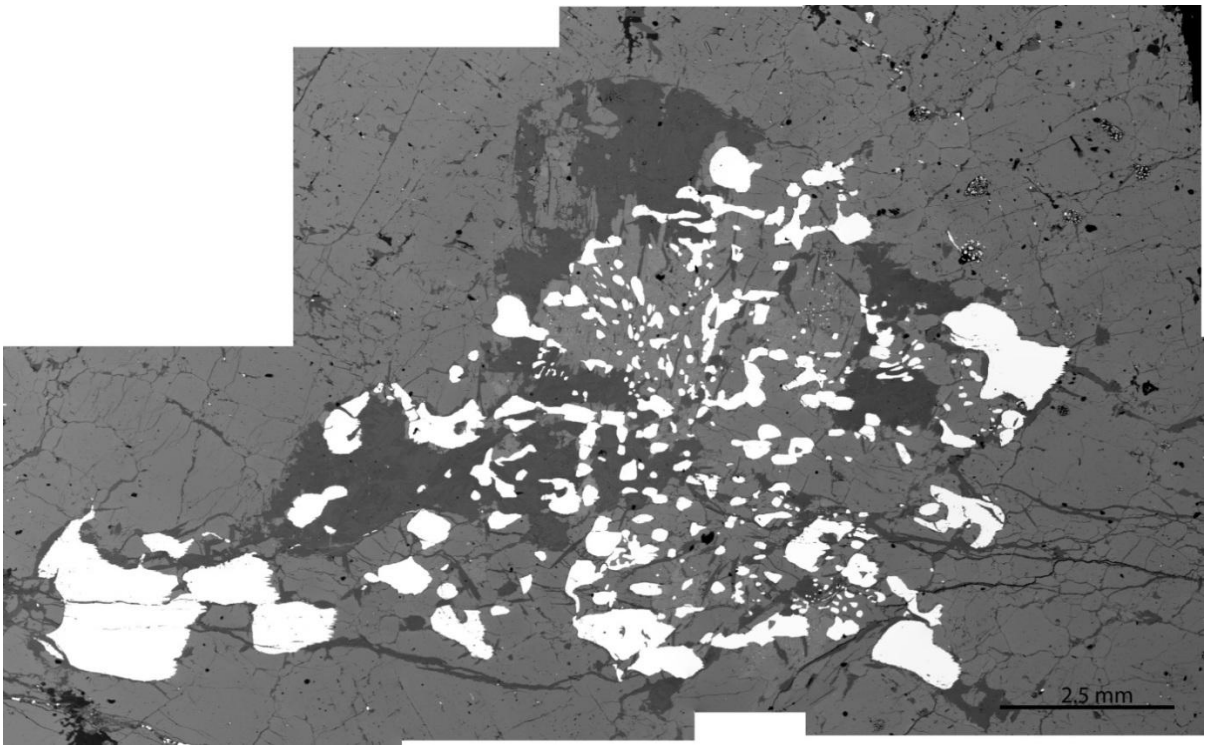

Figure 4.2.1; BSE micrograph illustrating polymineralic cloth after M_{1A} garnet: Large globular spinels (white), light grey is olivine, dark grey is light orthopyroxene and amphiboles. Note spinel grain size decreases from rim to core (thin section gp11).

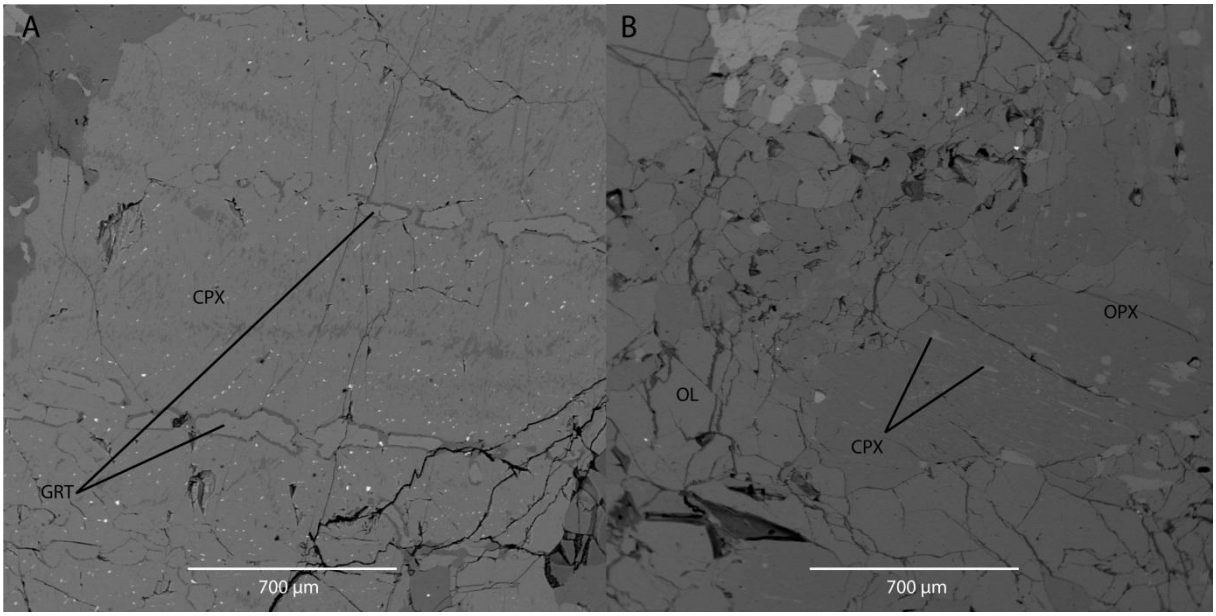

Figure 4.2.2; BSE micrograph of A) Exsolution of garnet in M_{1A} clinopyroxene (sample GP4), B) exsolution of clinopyroxene in orthopyroxene (sample GP4)

M_{1A} assemblage

The M_{1A} assemblage comprises garnet, orthopyroxene, clinopyroxene, olivine and spinel. The M_{1A} crystals can be recognized by deformation and size. All of the M_{1A} minerals are heavily deformed, with S_x fractures. M_{1A} olivines and orthopyroxenes show undulatory extinction. M_{1A} garnets are megacrystic and larger than the other M_{1A} crystals with sizes of up to 1.5 cm.

M_{1A} olivines and pyroxenes usually have grain sizes up to 0.5 cm, although in thin section GP1-1 and GP1-2, olivines reach 1 cm in size. Although not measured the olivines optically show a strong CPO indicating a tectonic origin.
The M_{1A} olivine crystals show undulatory extinction kinking and fractures oriented in at least three different directions. These fractures will be called S_x fractures. The angle defined by undulatory extinction (folding) of the olivine crystal lattice can roughly be measured with the rotation stage of the optical microscope and reaches a maximum angle of 40°. S_x fractures in the olivine crystals are straight. Euhedral, undeformed olivines formed by dynamic recrystallization of approximately 100 µm occur along grain boundaries of M_{1A} olivines. Trains of fluid inclusions transect many of the M_{1A} olivines.
Globular spinel + pyroxenes symplectites occur together with the protolith olivines, with a maximum size of < 1 cm *(Figure 4.2.1)* . These globular symplectites have a grain size which increases from core to rim *(Figure 4.2.1)*. Between the spinel globules fibrolitic pyroxene and amphibole occurs. EMP chemical analysis of globular spinel grains gives a chromium content of ~45% *(Table 4.4.2)*.
The S_x fractures in M_{1A} garnets are up to 30 µm broad and contain lower grade minerals (spl + opx + cpx + amp). The S_x fractures terminate at the garnet grain boundary. Some fractures do crosscut the adjacent minerals (all mineral assemblages), and do not host lower grade minerals. These will be called S_{x+1} fractures. Some of the garnet hosts inclusions of clino- and orthopyroxene. The interface between adjacent garnets comprises lower grade minerals and/or symplectites. The fractures present in M_{1A} garnets do not crosscut the pyroxene inclusions. A reaction rim borders the garnet rim and the envelope of this reaction rim is interpreted to represent the former M_{1A} garnet grain boundary. The enveloping surface is roughly hexagonal and thus M_{1A} garnets were euhdral crystals. Garnet megacrysts of thin section GP4 show the exsolution of rutile needles.
M_{1A} clinopyroxenes are up to 0.5 cm large and show exsolution of garnet along principal mineral planes *(Figure 4.2.2a)*. Often M_{1A} clinopyroxenes host kink bands which might make up 40% of the mineral volume.
M_{1A} orthopyroxenes and olivines show undulatory extinction *(Figure 4.2.3c)* and are up to 0.5 cm large. M_{1A} orthopyroxenes occasionally show exsolution of clinopyroxene *(Figure 4.2.2b)*.

M_{1B} assemblage
The M_{1B} stable mineral assemblage consists of spinel, ortho- and clinopyroxene and olivine. In dunitic thin section GP11 *(Figure 4.2.1)* amphibole occurs in the M_{1B} assemblage. Pyroxenes and olivine of the M_{1A} assemblage are stable during spinel growth. M_{1B} spinels occur along the edges of the M_{1A} garnet megacrysts as anhedral crystals *(Figure 4.2.4d)*. EMP BSE images indicate the chromium content of the spinel grains decreases from core to rim *(Figure 4.2.3)*. The grain size of the spinel crystals decreases from the outer envelope of the M_{1A} crystal to the core of (former) M_{1A} garnets. Thin section Md1 is taken near the garnet pyroxenite dike and shows a strain gradient in M_{1B} crystals. The strain increases near the dike. The M_x matrix is undeformed.

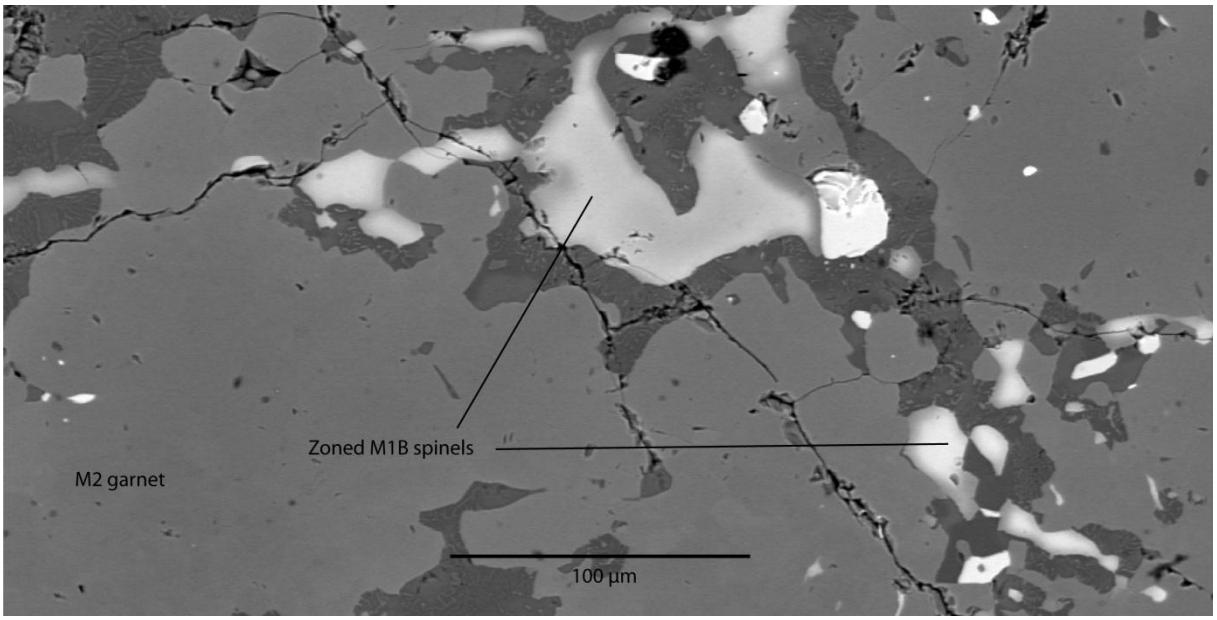

Figure 4.2.3, Zoned M_2 spinels embedded in M_2 garnets. The BSE coefficient (a measure of density of the minerals) decreases from core to rim. This zoning is due to the growth of the M_3 kelyphite in between M_2 garnets and spinels

M_2 assemblage

M_2 garnets are present as anhedral overgrowths in the reaction rim of M_{1A} garnets. These garnets incorporate many tiny spinel and/or rutile inclusions. EMP analysis shows M_2 garnet contains less chromium than M_{1A} garnets *(Table 4.3.1)*.

The M_{1A} crystals float in a matrix of M_2 olivine, clinopyroxene and orthopyroxene *(Figure 4.2.3b)* defined by a very consistent grain size (200 – 250 µm) and a conspicuous microstructure consisting of strain free crystals with triple point junctions of 120° and straight grain boundaries. This is called the foam matrix. M_2 clinopyroxene is often present near M_{1A} clinopyroxenes, therefore this matrix is interpreted as recrystallized M_{1A} crystals. Some trains of fluid inclusions transect the M_2 matrix.

M_3 assemblage

The M_3 assemblage is defined by spinel, clino- and orthopyroxene present in fine-grained spinel symplectites along grain boundaries of M_2 garnets *(Figure 4.2.3)* in equilibrium with olivine in the matrix *(Table 4.2.1)*. The grain size of these symplectites is on the order of micrometers. These can be seen as a brown crystal mush in xpl and using the microprobe. These can be distinguished from M_{1B} spinels by their orientation with respect to the M_2 and M_{1A} garnets. The M_3 symplectites are connected to the M_2 garnets while M_{1B} symplectites are connected to M_{1A} garnets.

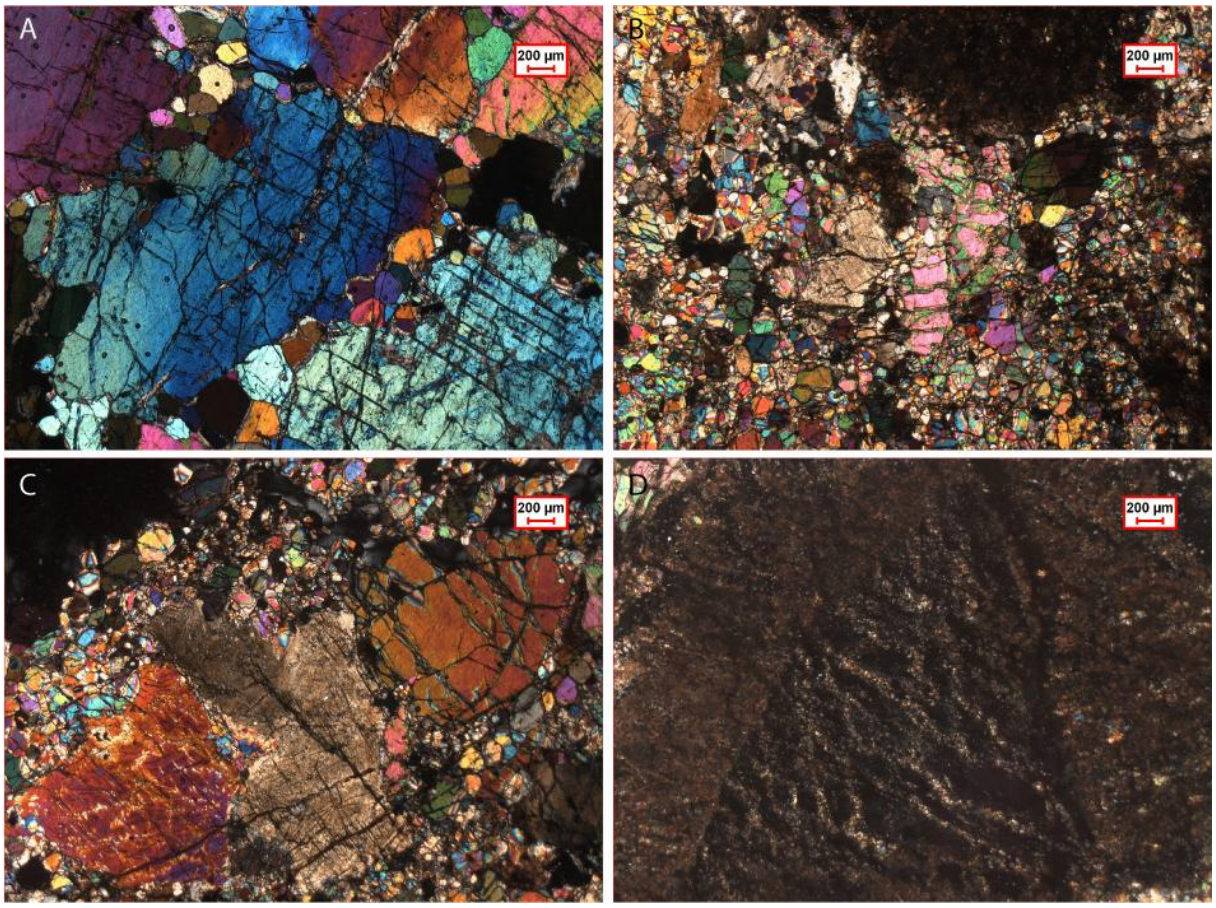

Figure 4.2.4 Optical micrographs of A) Very large olivines (M_{1A}) with recrystallized foam olivines (M_2) at the grain boundaries. B) Large symplectite after M_{1A} garnet in top of figure, megacryst of olivine and orthopyroxene in the middle, floating in a fine grained foam matrix. C) Megacrysts of olivine, clinopyroxene and orthopyroxene in a foam matrix, upper left shows edge of thin section. D) Garnet M_{1A} megacryst, showing at least 2 directions of fractures and a large symplectite surrounding it. Note that M_2 garnet overgrows the M_{1B} spinel and pyroxene symplectites. All pictures were taken with crossed nichols.

M_4 assemblage

The M_4 assemblage consists of amphibole, olivine, and orthopyroxene *(Table 4.2.1)*. Amphibole overgrows spinel (M_{1A} and M_3), garnet (M_1 and M_2), and pyroxene of the reaction rims around M_{1A} garnet and in M_{1A} garnet fractures. Amphibole reaches a maximum size of approximately 30 µm.

M_5 assemblage

The M_5 assemblage is characterized by stable chlorite and/or serpentine, which is present near S_{x+1} fractures crosscutting entire thin sections. The grain size is on the order of µm's making individual grains impossible to see using the optical microscope. Weak pleochrosim and green colour in PPL characterize the bulk of these retrogressed parts of thin sections as chlorite.

Chronology of mineral assemblages in peridotite

Garnets of the M_{1A} assemblage are overgrown by the M_{1B} mineral assemblage *(Figure 4.2.1)*. M_{1B} spinel grain sizes decrease from the edge of the reaction rim around M_{1A} garnets to the core of the garnet (or the inner part of the reaction rim). The larger M_{1B} spinels in the edge of the reaction rims are zoned, with chromium contents decreasing from core to rim. The

replacement microstructure implies a pressure decrease after the transition from M_1 garnet-olivine to M_{1B} mineral assemblages. The S_x fractures crosscut the M_{1A} assemblage but terminate at the M_{1B} reaction rim. Although they might represent different events, these fractures will collectively be termed S_1 fractures.

The M_2 garnets overgrow the kelyphite reaction rim around the M_{1A} garnets and do not contain S_x fractures. M_2 garnets host numerous inclusions of rutile and spinel, in contrast to M_{1A} garnets. This indicates that during the crystallization of M_2 garnets, less titanium and chromium could be incorporated in the growing crystal structure. This implies a difference in mineral chemistry as confirmed by EMP chemical analysis (Table 4.4.1) and evidence for a distinct period (M_2) of garnet growth in the peridotite. The M_2 foam assemblage contains clino-, orthopyroxene, olivine ± garnet ± spinel. It is an annealed microstructure, based on the straight grain boundaries and triple point junctions of the foam texture. The occurrence of olivine-garnet (M_2) ± spinel in the foam matrix implies it has formed during renewed residence of the peridotite in the garnet stability field after being in the spinel stability field (M_{1B}). The second period of garnet growth is likely to have been paired to a large tectonic event called F_1 which induced recrystallization of the garnet peridotite.

With the exception of grain size the M_3 assemblage is similar to the M_{1C} assemblage as this is also defined by the symplectite (spinel + pyroxenes) assemblages around garnet. The M_3 symplectite however, grows around M_2 garnets and is finer grained than the M_{1B} symplectites. The M_4 assemblage overgrows all spinel + pyroxenes symplectites and contains amphibole. This overgrowth relationship constrains the relative timing. The M_5 assemblage consists mainly of chlorite and other retrograde minerals. Chlorite and/or serpentine occurs as a very fine grained crystal mush and overgrows all former minerals. Chlorite and/or serpentine is concentrated near S_{x+1} fractures which crosscut entire thin sections and all mineral assemblages. It is likely that this occurred along S_2 fractures which served as fluid pathways assisting retrograde reactions. S_2 fractures are therefore placed between the M_4 and M_5 assemblage.

4.2.2 *Garnet pyroxenite microstructures*

Deformation	**S_1**		**S_2**	
Assemblage	**M_1**	**M_2**	**M_3**	**M_4**
Microstructures	Megacrysts	matrix		
Grt	x	x	x	
Cpx	x	x	x	
Opx	x	x		
Plag/spl			x	
retrograde				x

Table 4.2.2; petrogenetic grid of garnet pyroxenite

M_1 assemblage

The M_1 assemblage consists of heavily deformed and somehow recrystallized garnet megacrysts and pyroxenes *(Figure 4.2.5-7)*. Most of the pyroxenes are clinopyroxene but some orthopyroxene is also present. M_1 megacrysts show fractures in multiple directions and float in a M_2 matrix. The fractures terminate at the M_1 grain boundaries, with the exception of

large late fractures crosscutting all mineral assemblages. The M_1 garnet megacrysts reach grain sizes up to 1 cm. M_1 pyroxenes are not larger than 0.5 cm.
Sample D7 is a small sample of approximately 10 cm in size, taken from the interface between garnet pyroxenite and country rock peridotite. Thin sections were made from the edge of the garnet pyroxenite and the host peridotite *(Figure 4.2.7)*. With the naked eye a green mineral in handsamples (grey in xpl) can be seen along the transition. Some relict M_1 megacrysts are present close to this boundary and float in a M_2 matrix *(Figure 4.2.7)*.The green mineral in the transition zone has not been characterized but is possibly an amphibole formed by metasomatism between dunite and garnet pyroxenite.

M_2 assemblage
The M_2 assemblage has a similar mineralogy as the M_1 assemblage but a much smaller grain size. In addition, the M_2 assemblage defines a foam texture and is not transected by all fractures present in the thin section, only by late fractures transecting all mineral assemblages. Garnets and pyroxenes of the M_2 assemblage are both approximately 100-200 µm in size. M_2 garnets occur in clusters after former recrystallized M_1 garnets. This garnet domain boundary is often elongated, this elongation is interpreted to be due to F_1. In triple junctions of M_2 clinopyroxene small garnets (< 50 µm) occur which are part of the M_2 assemblage. Inside some of the aggregates of former M_1 garnets bands of M_2 clinopyroxenes occur. Often these are adjacent to deformation tails of M_2 garnets *(Figure 4.2.6C)*. The clinopyroxene bands are not interpreted as inclusions but form part of the M_2 assemblage and interpreted as an F_1 deformation effect.

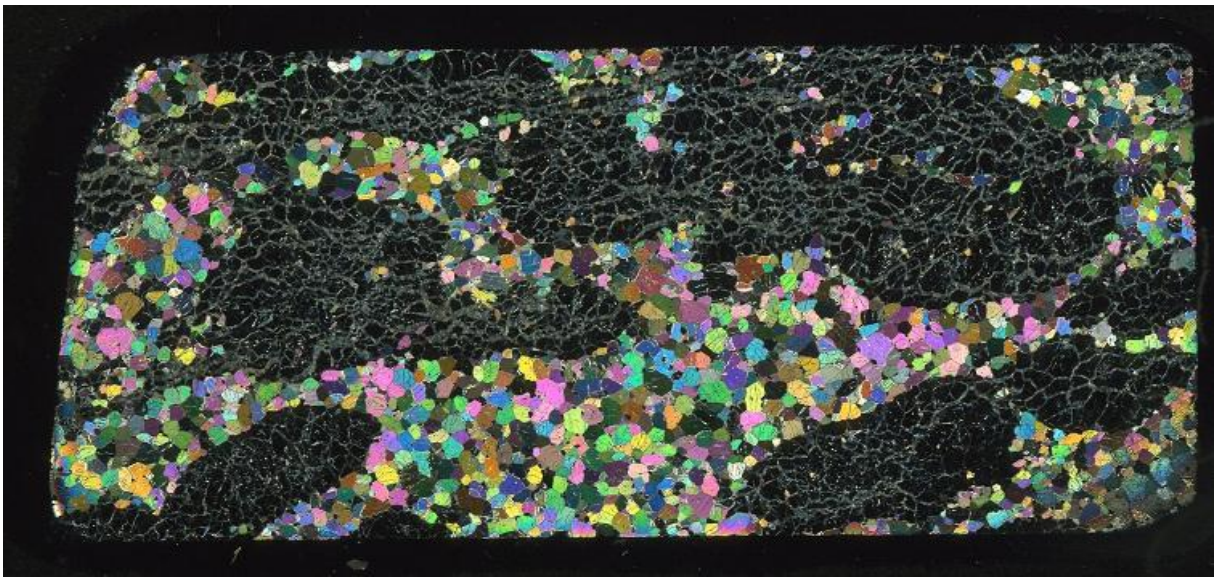

Figure 4.2.5; Cross polarized scan of thin section D51, aggregates of M_1 garnet and clinopyroxene are fully recrystallized to M_2. Consequently the recrystallized garnet domains float in a foam texture of M_2 diopside

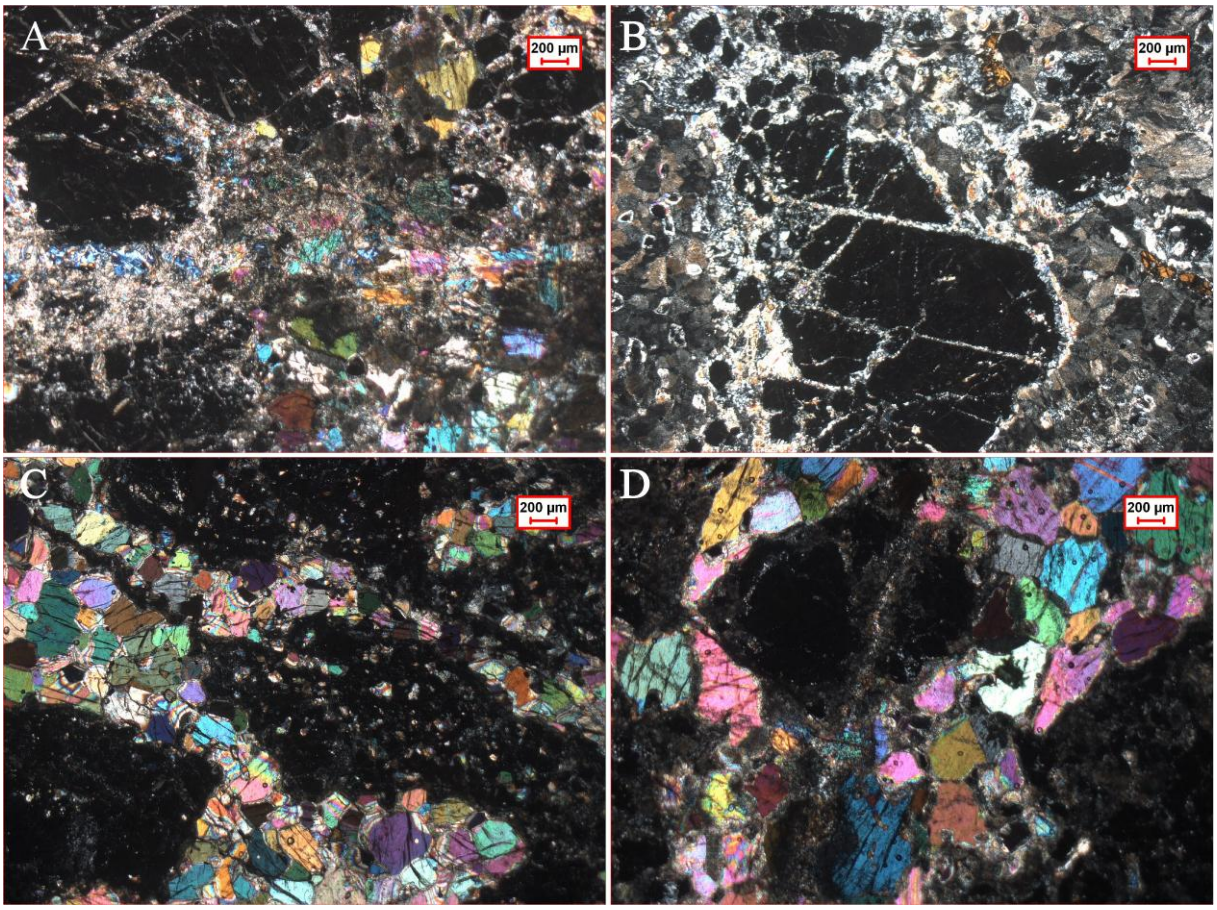

Figure 4.2.6; Optical micrographs. A) typical microstructures of sample D1 showing retrogressed clinopyroxene and fractured garnet megacrysts. The reaction rims around garnet show clear plagioclase rims due to decompression. B) Typical microstructures of sample D2, showing fractured megacrysts with clear plagioclase rims retrogressed clinopyroxene fully replaced by symplectites. To the right of the garnet crystal a large rutile crystal is visible. C) M_2 garnet tails along recrystallized M_2 garnet aggregates D) Late fracture through garnet megacryst and diopside in sample D3. Garnet is more retrogressed than diopside (note also the relict garnet megacryst in the lower right which is nearly completely retrogressed.

M_3 assemblage

The M_3 assemblage is visible as intergrowths of plagioclase + pyroxenes and/or spinel + pyroxenes around garnet crystals. These kelyphites occur around M_1 as well as M_2 garnet crystals. Plagioclase + pyroxene symplectites form on the grain boundary between Na-bearing pyroxenes and garnets, implying the pyroxenes are (partly) omphacitic in composition *(Figure 4.2.6A+B)*. Sample D2 shows S_x fractures but no elongated garnet domain boundaries were observed.

The microstructural difference between various thin sections of garnet pyroxenite dike samples is large. Key differences are the M_3 assemblage described above and retrogression of garnet and clinopyroxene. In two out of seven samples (D1+D2) clinopyroxene is nearly 100% retrogressed. The M_2 clinopyroxene crystallographic orientation is retained in these relict clinopyroxenes present in the symplectites. In three out of seven samples (D6-D7) clinopyroxene is not retrogressed at all. The latter all being garnet + diopside garnet pyroxenites without an eclogitic component.

In sample D3+D4 garnet is more prone to alteration to M_3 and M_4 assemblages than the clinopyroxene. This is most likely due to variations in mineral chemistry from sample to sample and to variability in fluid availability beween samples. Pyroxenes in this sample are only retrogressed near late fractures and although they do contain > 1% Na *(Table 4.3.1)*. Other evidence from bulk rock chemistries *(Section 4.3)* show these are garnet pyroxenites.

M_4 assemblage

Near fractures which transect all former mineral assemblages retrogression occurs. Along these fractures retrogression occur and grains are retrogressed to a very fine grained crystal mush. Retrogression likely occurred near fractures which served as fluid pathways. These fractures are termed S_2.

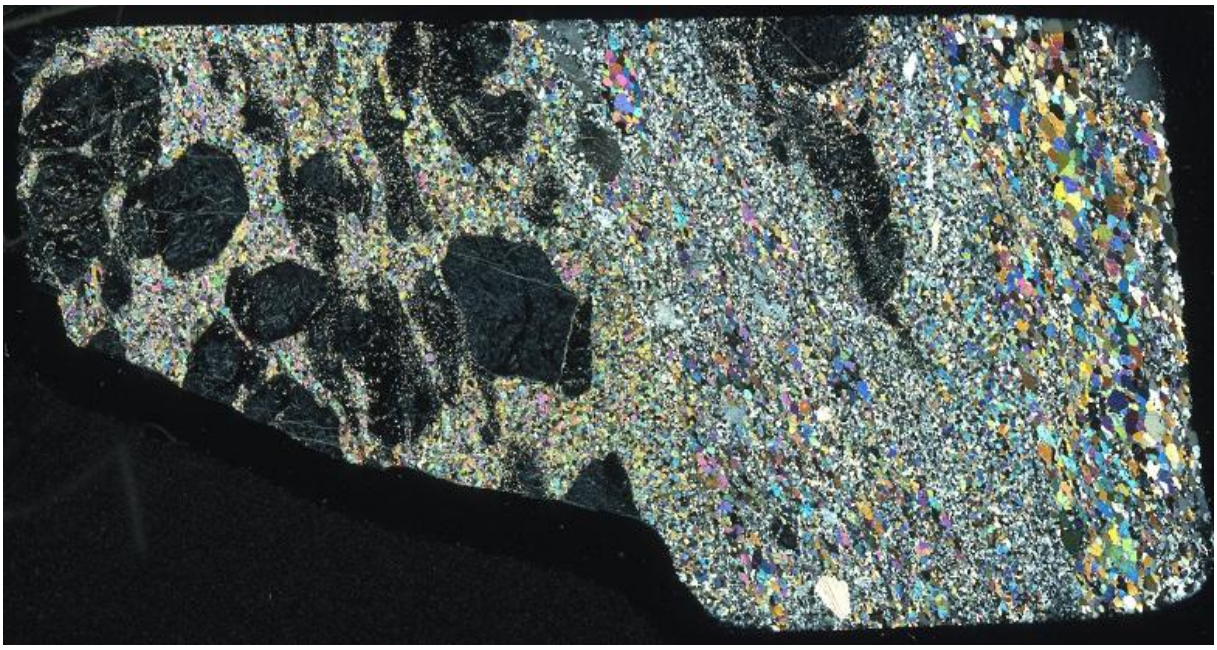

Figure 4.2.7; Thin section D7-1, a recrystallized garnet pyroxenite on the left, a band of grey minerals in the transition zone and dunite to the right where grainsize increases again (crossed nichols). Note at the left the inhomogeneously deformed garnet pyroxenite; undeformed M_1 garnets are adjacent to recrystallized and elongated M_2 garnets.

Differences between dike samples

In garnet pyroxenite samples D1 and D2 retrogression of clinopyroxene is nearly 100%. A change in the orientation of M_3 symplectite (after M_2 pyroxene) lamellas is interpreted to mark former grain boundaries of M_2 pyroxene. M_1 garnets are only partly retrogressed and not recrystallized into M_2 crystals. Plagioclase + pyroxene kelyphites are present around garnets.
In sample D3 and D4 the retrogression of garnet into M_3 sypmlectite is up to 70%. In contrast to the two samples described above, clinopyroxene is now only partly replaced by pyroxene-plagioclase symplectites (up to 10%). The volume % of garnet comprises 60% in these samples; other samples do not contain more than 40-50% garnet.
In samples D5-D7, no retrogression to M_4 assemblages occurs at all. The M_3 assemblage is weakly developed and only present in fractures between M_2 garnets (sample D5). The M_3 assemblage around garnet in this sample consists of spinel + pyroxene kelyphite.
These differences in the microstrures are most evident after the M_2 assemblage and an explanation should be sought in the mineral chemistry and/or presence of fluids.

Differences between garnet pyroxenite samples D1, D2 and D3-D7

Sample D1 and D2 do not record garnet megacrysts recrystallized to smaller M_2 foam textures. In addition, the garnets in these samples are not elongated, in contrast to those of sample D3-D7. Sample D1 and D2 record M_1 garnets and clinopyroxene is either fully retrogressed or present as small crystals, reminiscent of the M_2 foam texture in sample D3-D7. The polygonal foam texture and triple point junctions are not very well developed

however. In addition to that, the grain sizes of clinopyroxene are not very consistent. The M_3 assemblage consists of plagioclase + pyroxene reaction rims around garnet and retrogressed clinopyroxene. In addition biotite clusters after phengite are present and occasional kyanite occurs as inclusions in garnet. Rutile is also present in the thin sections. The former clearly illustrates a difference in bulk rock composition of the dike samples.
In thin section D5-D7 garnets do record M_2 assemblages and M_3 compositions are present as spinel + pyroxene symplectites around garnet. The M_1 garnet grain boundary of M_2 aggregates are often elongated as opposed to those of garnets of sample D1-D4.

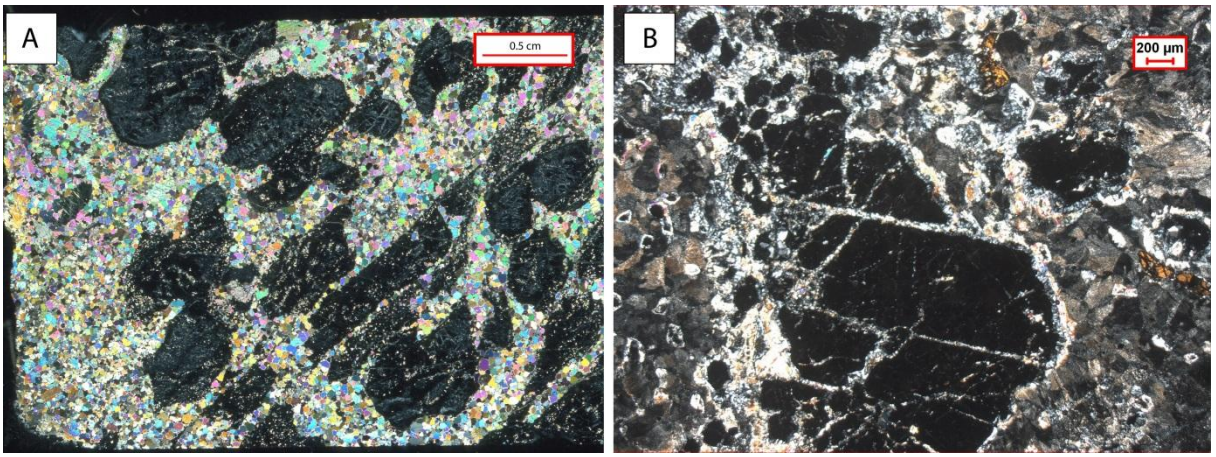

Figure 4.2.8; A) elongated garnets in sample D6, thin section D6-2 and B) fractured M_1 crystals which are not recrystallized to M_2 assemblages in sample D2, thin section D2-1

At the moment no conclusion can be drawn for these contrasting microstructures. The implied difference in bulk rock compositions and the absence of the M_2 foam texture in sample D_1 and D_2 clearly indicates two generations of dikes are present in the country rock peridotite.

Chronology of mineral assemblages in garnet pyroxenite
The M_1 assemblage of the garnet pyroxenite samples predates the M_2 assemblage since recrystallized domains of M_2 garnets and M_2 clinopyroxene outline the sizes of former larger M_1 crystals. In addition to this, M_1 minerals contain S_x fractures which do not transect M_2 crystals. The M_3 assemblage is retrograde after garnet and pyroxene. Lamellar symplectites of plagioclase/spinel + pyroxenes and symplectites after pyroxene (in sample D1-D4) show that this mineral paragenesis was stable after the M_2 mineral assemblage. The M_4 assemblage occurs near S_2 fractures which transect all prior mineral assemblages.

4.2.3 *Discussion*

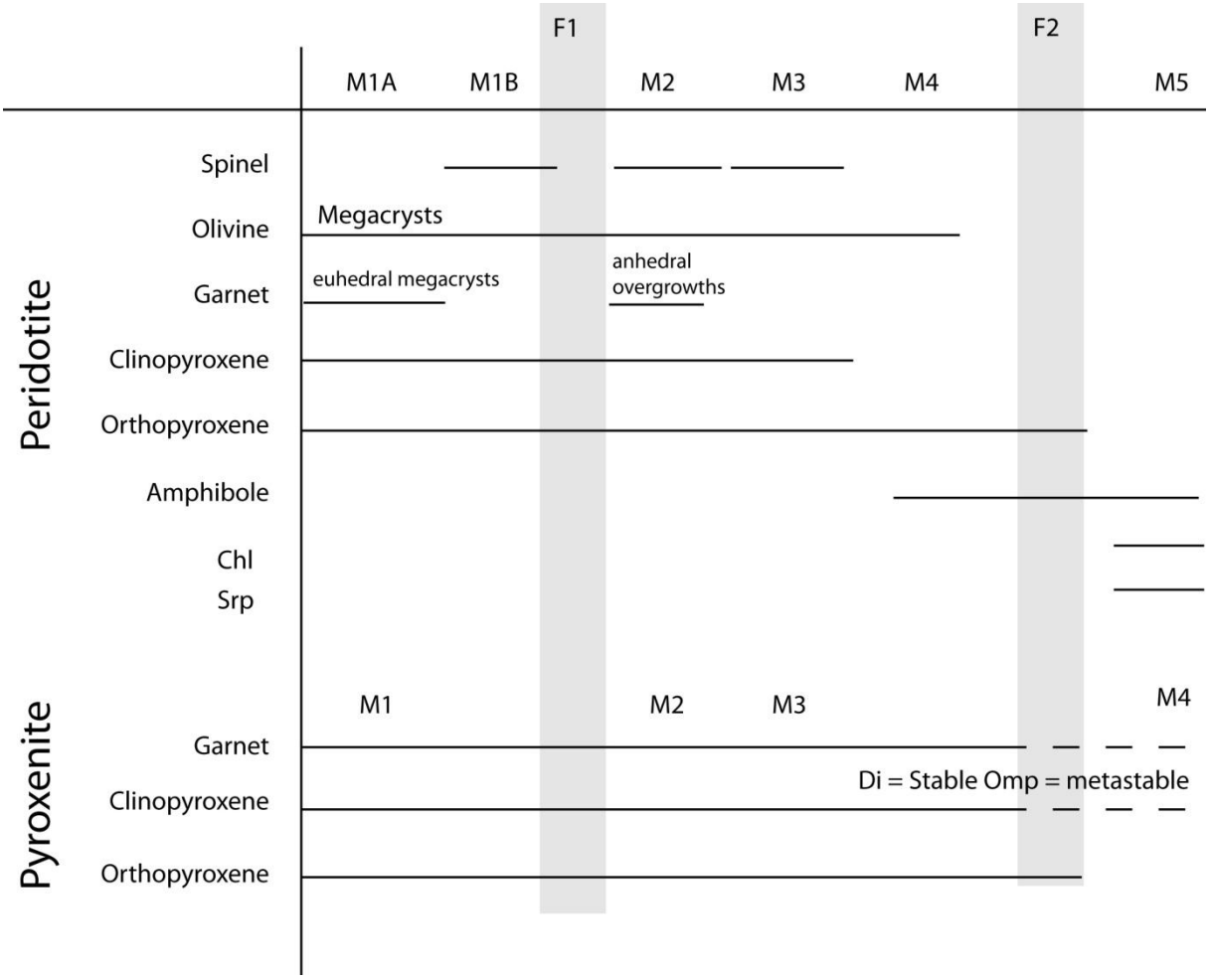

Figure 4.2.9; Petrogenetic grid of peridotite and garnet pyroxenite.

In the peridotite, the M_{1A} assemblage contains megacrystic garnet which indicates that the peridotite resided under (U)HP conditions in the mantle. The $M_{1A} \pm M_{1B}$ assemblage of peridotite is correlated to the M_1 assemblage of the garnet pyroxenite which is the first stable assemblage after the crystallization of the dike. The S_1 fractures present in M_{1A} and M_1 minerals as well as the comparable grain sizes of relict megacrysts indicate a coeval stable mineral paragenesis. This conclusion is supported by thermobarometric results *(Section 4.5)*. S_1 fractures in peridotite do not transect M_{1B} reaction rims which might be due to reworking of the M_{1B} reaction rims, the overprinting by the M_2 assemblage or by the relative timing of the fractures. The S_1 fractures do not transect the M_2 annealed microstructure. These must therefore be pre-M_2. It cannot however not be ruled out that they are syn- or pre-M_{1B} so the time constraint of S_1 is $M_{1A} < S_1$ M_{1B}. In the petrogenetic grid *(Figure 4.2.9)* they are placed as post-M_{1B}.

The transition from the garnet stability field to the spinel stability field of peridotite is due to decompression. The decrease in size of M_{1B} spinel in reaction rims from outer to inner rim is interpreted to be due to a coeval temperature decrease. M_1 garnet and pyroxene in the garnet pyroxenite remained stable during this decompression period. This indicates limited decompression depth in the olivine-spinel field.

Stretching of M_1 and M_{1B} minerals in thin section M1d (peridotite) is interpreted to be coeval with elongation of M_1 garnets in garnet pyroxenite. This places the F_1/S_1 deformation phase

either syn- or post M_{1B}. On the basis of the M_1 domain boundaries into M_2 aggregates (in pyroxenite) the stable mineral assemblage (in the pyroxenite) was formed by the M_2 – assemblage during F_1 deformation. The time constraint on F_1 is $M_{1B} \leq F_1 < M_3$. However, the M_2 assemblage is most likely coeval in pyroxenite and peridotite on the basis of M_2 grain sizes of the foam texture. This is an annealed microstructure formed by strain free grains with straight grain boundaries. The M_2 assemblage must therefore have formed after F_1. The F_1 deformation phase is present in the pyroxenite (seen in both garnet and pyroxene) and peridotite (mainly seen in recrystallized strain free olivine grains).
The M_2 assemblage that formed in the peridotite is evidence of renewed deformation in the garnet stability field of peridotite. The foam texture is interpreted to correlate to the M_2 assemblage and this is present in both peridotite and pyroxenite.
During the M_3 phase in peridotite garnet remained stable in pyroxenite. During decompression and cooling of the peridotite lens the M_4 (peridotite) and M_3 (pyroxenite) assemblages grew. These are correlated as they are both evidence of decompression and cooling under crustal conditions. However, the exact PT conditions of both these mineral assemblages might be different.
The S_2 fractures are late fractures which are present in both peridotite and pyroxenite. Retrogression to very low grade assemblages is evident in both lithologies near S_2 fractures. Therefore S_2 fractures and the M_5 (peridotite) and the M_4 (pyroxenite) assemblages are interpreted to be coeval.

Very recently UHP PT conditions have been determined in some of the mafic dikes corresponding to sample D_1 and D_2. Kyanite, phengite, sapphirine and coesite were found in addition to garnet and clinopyroxene *(Majka & Jának, 2011)*. These minerals now also been found in thin sections D1 and D2 but are retrogressed.

4.3 Bulk rock geochemical analyses of garnet pyroxenite samples

4.3.1 *Bulk rock Major elements (XRF)*

Major element analyses on garnet pyroxenite samples obtained by XRF are given below in table 4.3.1. The XRF is calibrated for certain major element distributions. Samples similar to the samples used for the calibration of the XRF can in this manner be reliably measured. Both the magnesium and iron contents of the samples subject to analysis are a few percent above the calibration line of the XRF. Hence XRF results on the dike samples have been checked by subsequent ICP-OES analyses *(Appendices)* and were reproduced. The peridotite sample has not been checked and since this is magnesium rich the error on the magnesium content of the peridotite might be substantial. Note that all iron measured was taken as FeO in this table. The elemental iron content ranges from 4.27% to 6.39%. No effort was taken to recalculate the FeO and Fe_2O_3 contents of the garnet pyroxenite samples.

	weight percentages (% wt.)										
Sample #	**SiO_2**	**Al_2O_3**	**TiO_2**	**FeO**	**MnO**	**CaO**	**MgO**	**Na_2O**	**K_2O**	**P_2O_5**	**Sum**
d1	45.48	16.18	0.17	9.11	0.16	14.53	13.34	1.29	0.01	0.06	100.32
d2	47.28	17.08	0.18	8.30	0.14	13.77	11.70	1.69	0.05	0.05	100.23
d2x	48.45	17.05	0.21	8.44	0.14	13.44	11.74	1.73	0.08	0.06	101.34
d3	46.40	15.66	0.08	8.59	0.19	11.15	16.90	1.24	0.02	0.06	100.30
d4	45.69	17.63	0.09	9.14	0.23	8.99	18.09	1.07	0.04	0.04	101.01
d5	48.60	10.60	0.21	5.55	0.17	16.54	19.60	0.26	0.02	0.05	101.60
d5x	47.47	12.02	0.23	6.11	0.18	15.10	19.22	0.31	0.03	0.06	100.74
d6	46.25	15.85	0.23	8.49	0.20	10.87	18.28	0.79	0.02	0.05	101.04
d6x	46.29	15.80	0.24	8.65	0.20	11.18	17.98	0.84	0.02	0.05	101.24
d7	46.31	15.98	0.22	8.29	0.20	10.77	18.38	0.81	0.04	0.05	101.05
GP3	44.85	2.85	0.11	8.29	0.0	2.77	40.04	0.13	0.0	0.0	100.0

Table 4.3.1; Representative XRF bulk rock measurements on garnet pyroxenite dike samples. During the preparation of the samples doubles were taken. These have been analyzed and are denoted with an 'x' behind the sample number

The P and K content in the garnet pyroxenite samples are extremely low. Mn is homogeneously distributed but also very low, as is Ti. The Na content ranges from 0.26 to 1.73 %. In an alkali-silica diagram the bulk rock composition is basaltic *(Figure 4.3.1).* According to the discrimination diagram of *Pearce et al. (1977)* this basaltic composition overlaps with that of oceanic arcs.

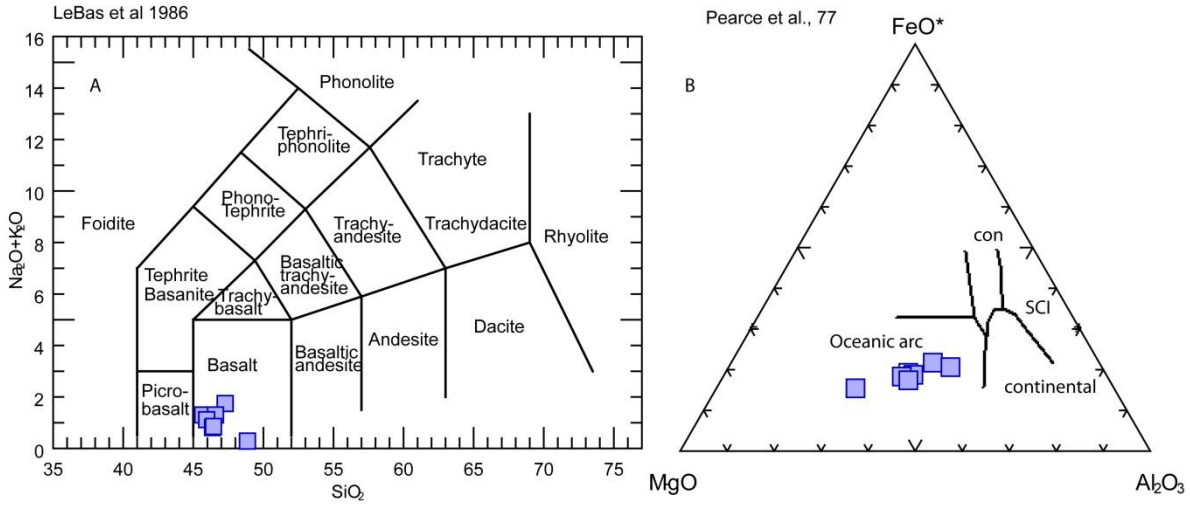

Figure 4.3.1; Discrimination diagram A) for igneous rocks *(Lebas et al., 1986)*. All garnet pyroxenite samples plot in the basalt field and B) For basalts *(Pearce et al., 77)* all garnet pyroxenite samples plot in the 'oceanic arc' field

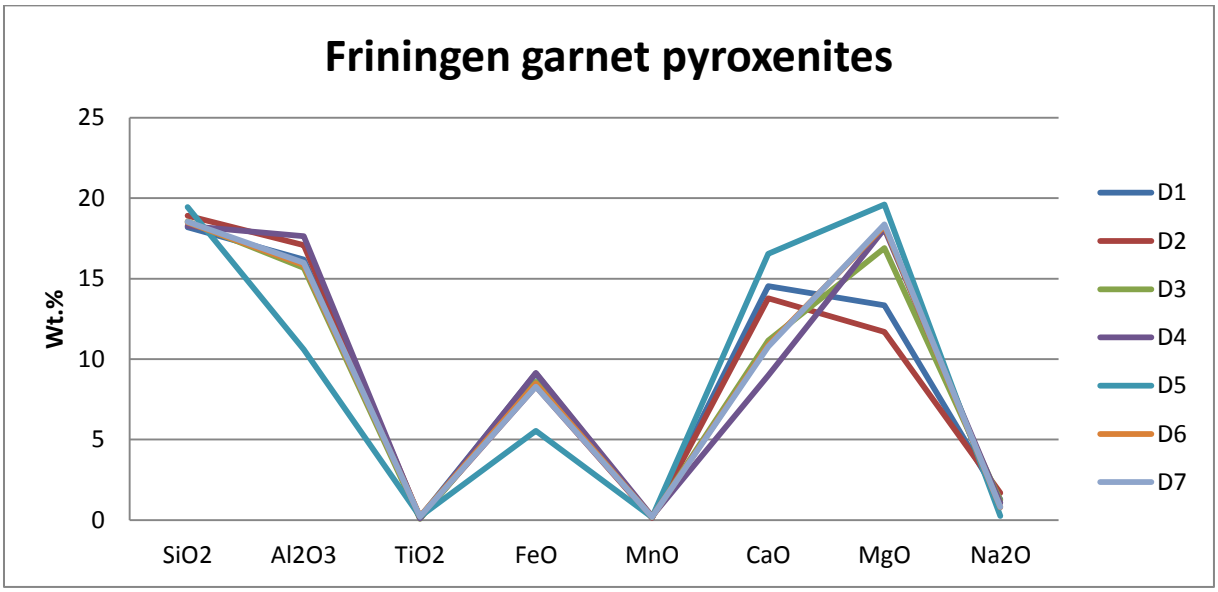

Figure 4.3.2; Variation of major element oxides of garnet pyroxenites. Note differences in CaO, MgO and FeO. Sample D1 and D2 deviate from the other samples in their MgO and CaO content. D5 has a very low FeO content, but higher CaO and MgO than other samples.

Al_2O_3 *CaO										
	D1	D2	D2x	D3	D4	D5	D5x	D6	D6x	D7
Wt % CaO	14,53	13,77	13,44	11,15	8,99	16,54	15,1	10,87	11,18	10,77
Wt % Al_2O_3	16,18	17,08	17,05	15,66	17,63	10,6	12,02	15,85	15,8	15,98
Al_2O_3 *CaO (*10^{-2})	2,35	2,35	2,29	1,75	1,59	1,75	1,82	1,72	1,77	1,72

Table 4.3.2; Al_2O_3*CaO values. Most likely, sample D1 and D2 require an alternative origin than other garnet pyroxenite samples.

Figure 4.3.2 and 4.4.3 show that there are essentialy three different sets or suites of samples. D5 Is the sample which most evidently differs from the other samples in the Fe, Ca, Mg and Al content. This sample also has the lowest sodium content (Na = 0.26 % wt.). There are 2 samples, D1 and D2, which show relatively high CaO and low MgO contents. The rest of the element oxides these samples are comparable with the other samples except for Na. These samples have a Na content > 1% wt. The samples D3,D4 and D6,D7 shows high MgO and low CaO contents. These samples can be plotted in a ternary diagram on the basis of the CaO, MgO and FeO contents. The latter is illustrated in figure 4.3.3.

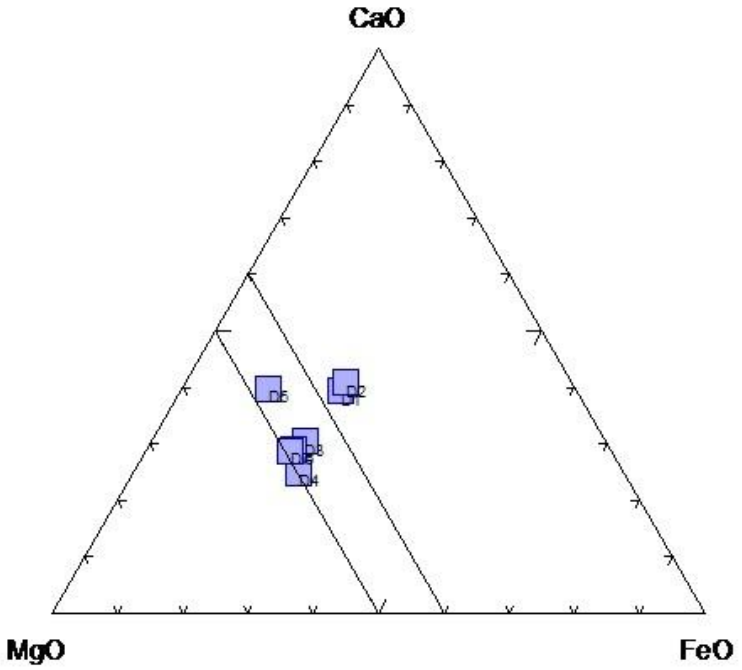

Figure 4.3.3; Ternary diagram with CaO, MgO and FeO (total Fe). Note the difference in MgO Wt% of D1 and D2 with respect to other samples

In order to check whether different magmatic pulses were the source of the differences in chemistry, 8 elements are plotted versus the MgO content (*Figure 4.3.4)*. The scale of the graphs varies, so possible trends should be treated with care as this might be an effect of the y-axis scale. MgO is plotted versus the Al_2O_3*CaO content in figure 4.3.5 and shows two clear groups, D1 and D2 and D3-D7.

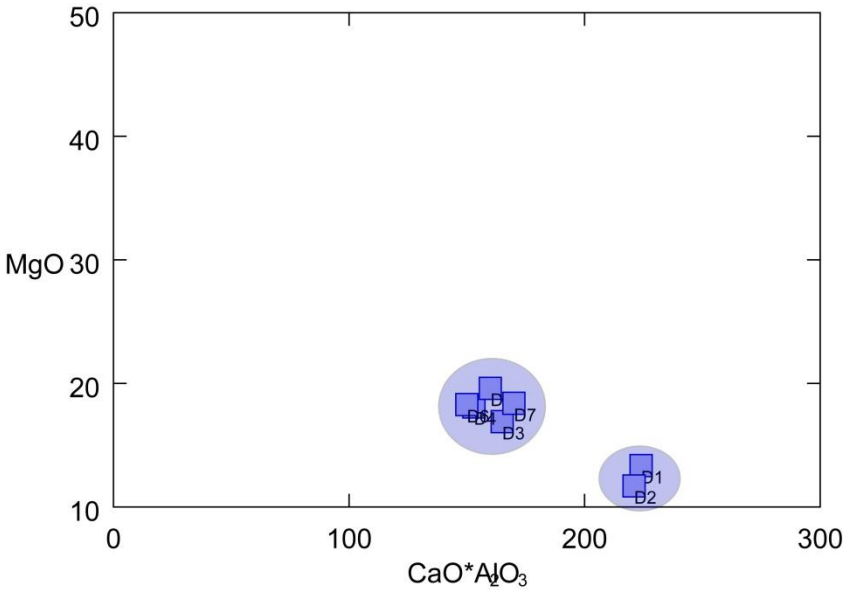

Figure 4.3.5; MgO versus Al_2O_3 contents of dike samples D1-D7. Note that D1 and D2 clearly differ from the other samples.

4.3.2 Bulk rock major elements results

The bulk rock major elements show that sample D1 and D2 differ from the other samples with respect to their magnesium contents, Al_2O_3*CaO values and the magmatic trends depicted in figure 4.4.4. The magmatic trends that become visible when D1 and D2 are not taken into account show that the bulk rock composition of sample D3 –D7 are consistent with those produced by basaltic melt derivation from peridotite. The Na_2O contents indicate a partly eclogitic composition, although sample D3 and D4 are similar in their Na_2O content to sample D1 and D2, containing 1 - 1.2 % of Na_2O. The Al_2O_3*CaO values very clearly plot in two groups, indicating that D1 and D2 should be separated from the other samples.

Considering that sample D3-D7 are produced by basaltic melt extraction from peridotite, the Na_2O contents of sample D3 and D4 requires an explanation. This Na_2O content must have been introduced later and indicates metasomatism of the garnet pyroxenite samples or influence from a crustal component. The possibility that sample D3 and D4 represent an entire other group of samples is rejected as they plot on the magmatic trends visible in figure 4.4.4 and have similar CaO*Al_2O_3 values *(Table 4.3.2)*. Figure 4.3.5 very clearly shows that samples D1 and D2 differ from sample D3-D7. This might indicate an alternative origin and/or age of sample D1 and D2. The possible origins of the dikes will be discussed in section 5.

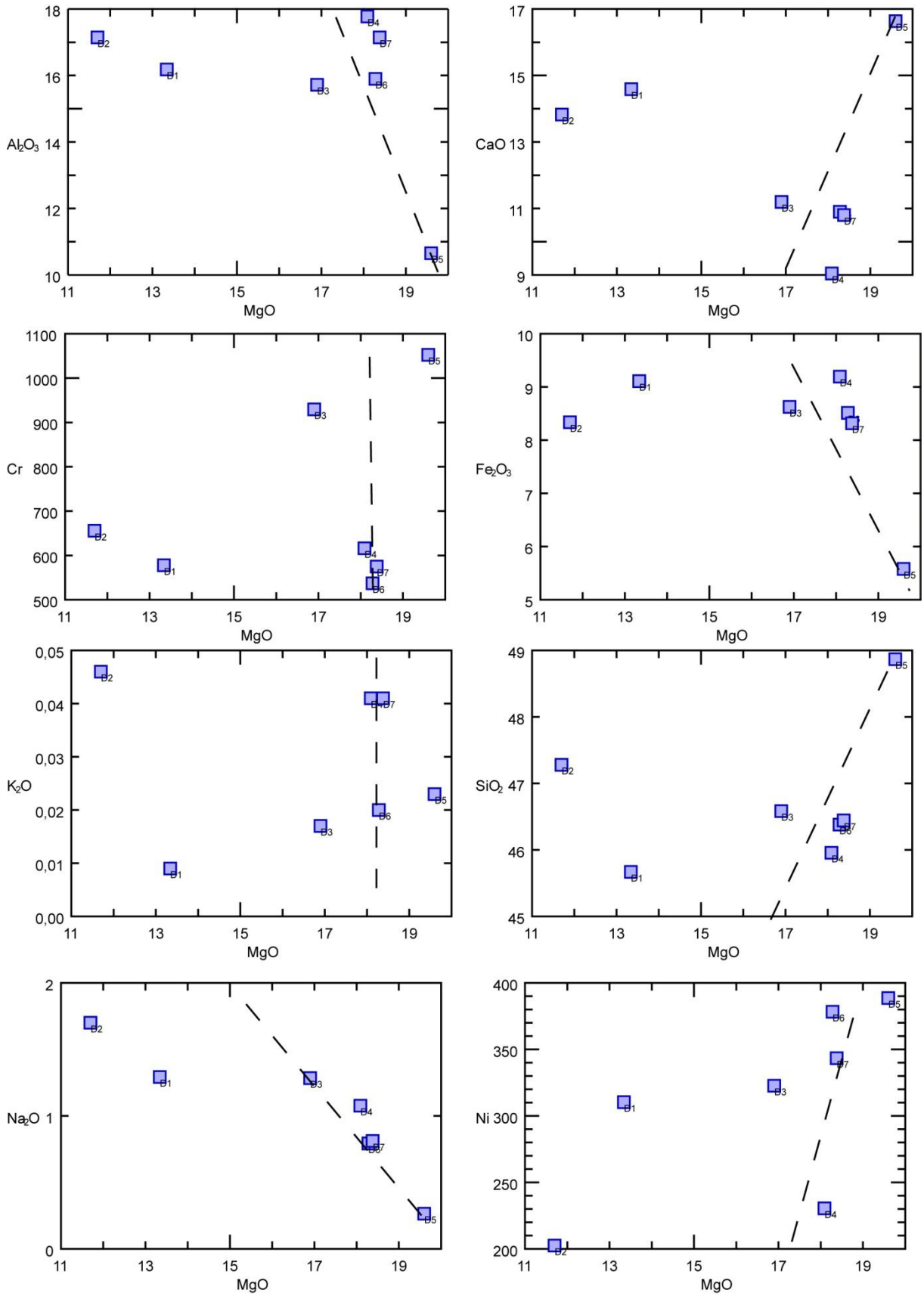

Figure 4.3.4; Major and trace elements oxides of garnet pyroxenites plotted against their MgO content versus different bulk rock elements and trace elements. Note that the scale is chosen as a best fit and therefore varies.

4.3.3 Extended bulk rock Rare Earth Element analysis

Bulk rock garnet pyroxenite extended REE data obtained by ICP-MS and all normalized to primitive mantle values after Sun & Mcdonough *(1989)* can be seen in figure 4.4.6A & B. Sample D3 and D4 are plotted separately as their extended REE composition is slightly different *(Figure 4.3.6B)*. The latter extended REE composition is depleted relative to the other elements except for HREE *(compare figure 4.3.6A+B)*.

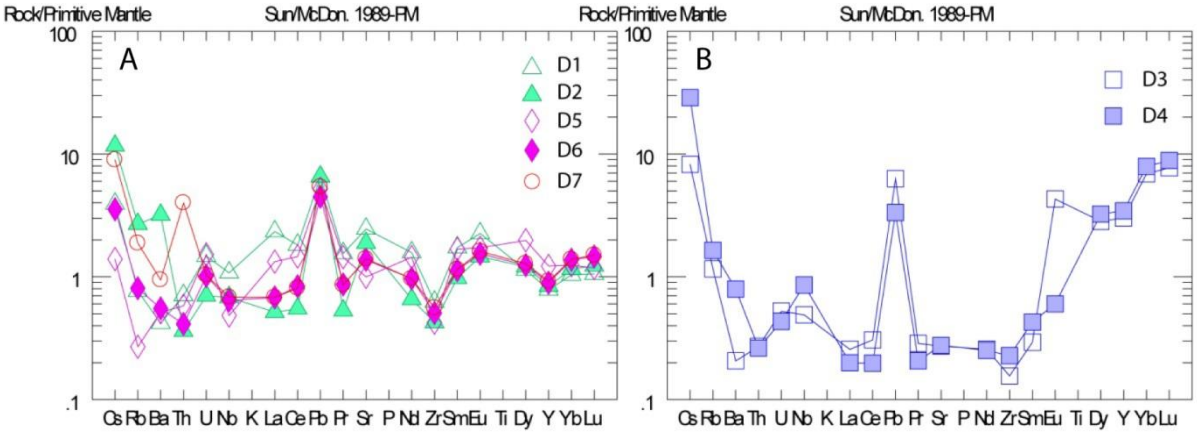

Figure 4.3.6; Bulk rock extended REE diagram (values normalized to Chondrites after *Sun & McDonough, 1989)*. A) sample D1,D2 and D5-7. B) Sample D3 and D4

The ICPMS extended REE results show different patterns between samples *(Figure 4.3.6)*. All samples except D3 and D4 show relatively flat enriched profiles *(Figure 4.3.6A)*. There is a slight EU anomaly in all but sample D5. The LREE pattern differs mutually in enrichment from slightly enriched to enriched, in contrast the HREE pattern is very consistent . Sample D3 and D4 *(Figure 4.3.6B)* are very distinct and show a normal to slightly depleted *(Figure 4.3.5A)* LREE pattern and extremely enriched HREE patterns. In addition to this, a very large EU anomaly is observed in sample D3 while no EU anomaly is visible in sample D4.
Based on the extended trace element patterns, there are a number of important characteristics between figure A & B. Most of the samples (D1,D2,D6 & D7 in Figure 4.4.6A) show flat enriched patterns. While the LREE enrichment differs but the level of HREE enrichment is approximately equal. There is a small but still visible Eu anomaly in all of these samples, which is positive. Sample D3 *(Figure 4.3.6B)* shows normal chondritic values for the LREE, a very large positive Eu anomaly and a large enrichment in HREE. This differs from sampe D4 in the Eu anomaly and the fact that D4 is slightly more depleted in LREE. Sample D3 shows a wavy enriched pattern without any Eu anomaly. The degree of HREE enrichment declines towards the lighter elements but is depleted with respect to the other patterns. In order to check the validity of the Eu anomaly, Eu* was calculated according to the following formula: $Eu^* = Eu_{PM} / [Sm_{PM}*Gd_{PM}]^{1/2}$.

	D1	D2	D3	D4	D5	D6	D7
Eu*	1.40	1.39	8.43	0.87	0.97	1.30	1.36

Table 4.3.3; Quantification of the Eu* anomaly in the different garnet pyroxenite samples, according to the methods of *Niu and Ohara (2009)*.

In this formula, the PM subscript denotes that the original values are normalized to primitive mantle values (The values used here are: Gd = 0,2055; Sm = 0,153; Eu = 0.058; after *Sun & McDonough (1989)*). An Eu* < 1 corresponds to a negative Eu anomaly and an Eu* > 1 corresponds to a positive anomaly. These values reflect the difference between the samples, D1,D2,D6 & D7 have comparable positive values, D3 has a very high positive anomaly, D4 a slightly negative anomaly (Eu* < 1) and D5 does not show any Eu anomaly at all. See also table 4.3.3

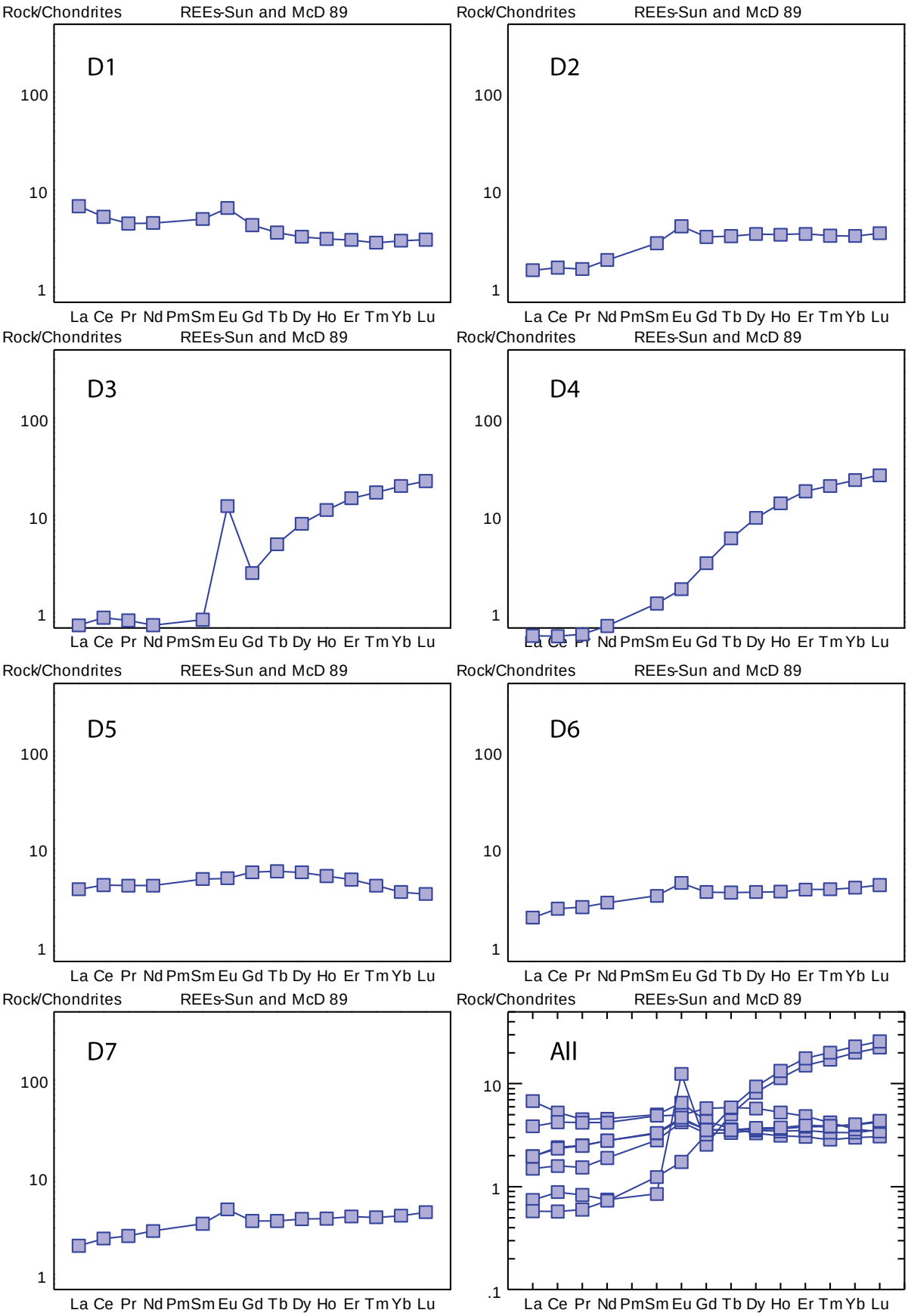

Figure 4.3.7; Bulk rock REE patterns of all analyzed dike samples plotted in individual compositional diagrams D1-7; In the lower right all REE patterns of analyzed dikes are plotted together (Note the erratic EU anomaly and the difference in relative LREE enrichment and HREE enrichment.

4.3.4 Discussion

It is necessary to discriminate between the primary and secondary characteristics of the bulk rock compositions of the dike samples. The bulk rock composition shows major differences in Ca, Mg and Al amounts of ~5 %. This cannot be related to the melting of the material as there is no clear evidence for fractional melting (but this may be due to inappropriate sample compositions) *(Figure 4.3.3)* and there are no clear groups of samples to be discerned.
The rare earth element analyses show a number of interesting features which should be explained, such as:

1) A positive Europium anomaly that differs in magnitude from sample to sample *(Table 4.4.3)*
2) Different degrees of LREE enrichment *(Figure 4.3.7)*
3) Large HREE enrichment of sample D3 & D4 *(Figure 4.3.6B)*

There are a number of different processes which can govern the Europium anomaly in rocks. The lower crust is generally enriched in Europium and crustal fluid contamination of samples can give rise to a positive Europium anomaly. Subduction processes involving fluids can elevate earlier Europium concentrations. Europium also replaces Ca^{2+} in plagioclase hence plagioclase bearing rocks can have positive Europium anomalies provided there was Europium present during crystallization. The latter process occurs during crystallization, the former two processes can occur after crystallization. Sample D3 and D4 *(Figure 4.3.6B)* have very similar trace element patterns with the exception of the Europium anomaly. Assuming that the two samples have inherited the general REE pattern (HREE enriched, normal to slightly depleted LREE, Figure 4.3.6B) during crystallization, automatically implies the Europium anomaly was imposed later in the history. Another possibility is that Europium was eratically distributed throughout the garnet pyroxenite melt during crystallization. Other REE are equally distributed between sample D3 and D4. Hence, the former interpretation is favored.
The various degrees of LREE depletion might be due to different minerals incorporating LREE elements. Here garnet is a dominant storage for HREE, while clinopyroxene incorporates the LREE. In sample D3 and D4 the HREE enrichment is as large as the LREE depletion. Dike sample D3 and D4 consist mostly of garnet, hence there are no or relatively few minerals available to store LREE.
The other samples, D1, D2 and D5-D7 have REE patterns with different amounts of LREE enrichment. Sample D5 lacks the Europium anomaly the other samples share and this again implies a Europium anomaly which was superposed on the general REE pattern. A Europium rich subduction-related fluid is inferred to have altered the samples late in the history. The latter is inferred to be responsible for the Eu anomalies present and the different degrees of LREE enrichment. On the nature and source of this fluid more will be said in the final discussion.
Bulk rock REE plots clearly do not correspond with either the REE data of *Solyom (1992)* or *Andreasson (1992),* the latter are illustrated in section 2.8.1. This makes the correlation with either of these dike swarms problematic. The Eu anomaly is very dependent on oxygen fugacity and fluids so this discrepancy can be easily explained. However, the LREE depletion

in the samples presented and those formerly described is very different. The relative amounts of garnet and pyroxene in sample D3 and D4 are different with respect to the other samples. Hence, sample D3 and D4 are interpreted not to be representative of their bulk rock compositions.

Garnet pyroxenite and eclogite

Nickel and Chromium content and Mg#								Medaris discrimination
Sample	**D1**	**D2**	**D3**	**D4**	**D5**	**D6**	**D7**	**Eclogite**
Na_2O (%)	1.29	1.69	1.73	1.24	0.26	0.79	0.81	> 0.75 %
Ni (ppm)	310	202	322	230	388	378	343	< 400
Cr (ppm)	577	655	929	616	1052	537	574	< 1500
Mg#	59.4	58.5	66.3	66.4	77.9	68.3	68.9	> 80

Table 4.3.4; The three values which Medaris uses to distinguish between eclogite and garnet pyroxenite

Bulk rock basaltic compositions of these samples suggest a basaltic precursor of all samples. The sodium content is of large importance in this respect as sodium > 1% content cannot directly be related to melting of mantle material. This divides the samples analyzed in two groups, D1-D4 and D5-D7.

Figure 4.3.4 does not show evidence of fractional melting. Different samples do not show similar grades of depletion/enrichment with increasing magnesium content. Also when different groups of samples are checked for fractional crystallization such as D1,D2 and D5-7 the degree of depletion/enrichment is erratic.

Table 4.3.4 shows the nickel, chromium and Mg#, which are used by *Medaris et al., (1995)* to distinguish between garnet pyroxenites and eclogites in the Gföhl nappe in the Bohemian massif. Eclogites are considered to have Mg# < 80%, Na > 0.75 %wt, Cr < 1500 ppm and Ni <400 ppm.

According to *Medaris et al., (2006)* classification schemes all of these samples would plot in the eclogite field (with the exception of the Na_2O content of sample D5 *(Table 4.3.4)*). This raises questions to the actual mechanisms involved in the formation of the garnet pyroxenites. The recycling of oceanic material is consistent with the sodium content but according to this study, the sodium can be introduced later in tholeiitic meta-basalts. Eclogites of the Central Belt are usually more sodium rich, > 4 % versus a maximum of 1.5 % for samples of this study *(van Roermund, 1985)*, so on this basis garnet pyroxenites can still be distinguished from eclogites. The classification scheme used by Medaris is thus not applicable to the Friningen peridotite dike samples as a sodium content of < 4% makes it unlikely that these dike samples are eclogitic.

The variable sodium contents and Eu anomalies of the Friningen dike samples make it unlikely that these are primary. Dike sample D5 has no Eu anomaly at all and a very low sodium content (< 0.3 %) which makes it likely that this sample is the least altered by secondary effects. Possible secondary influences that have given rise to the erratic sodium contents and Eu anomalies will be discussed in the final discussion.

The bulk rock REE patterns are not consistent with the bulk rock major elements, as sample D1 and D2 cannot be distinguished from other samples. The reason for this might be that diffusion after the intrusion of the dike has homogenized the distribution of the REE. This is

dependent on the minerals that host them as can be seen in sample D3 and D4 which consist mostly of garnet. Of the handsamples, a small piece (up to 4 cm) was taken in order to determine bulk rock REE and bulk rock major elements. These were the same pieces of sample.

4.4 Mineral chemistries

In this section mineral chemistries obtained with the electron microprobe. Garnet, clinopyroxene, olivine and orthopyroxene minerals have been subjected to EMP chemical analyses. EMP linescans, i.e. a number of analyzed points over one or multiple minerals have been used to check for homogeneity of the crystals of primarily the M_{1A} assemblage.

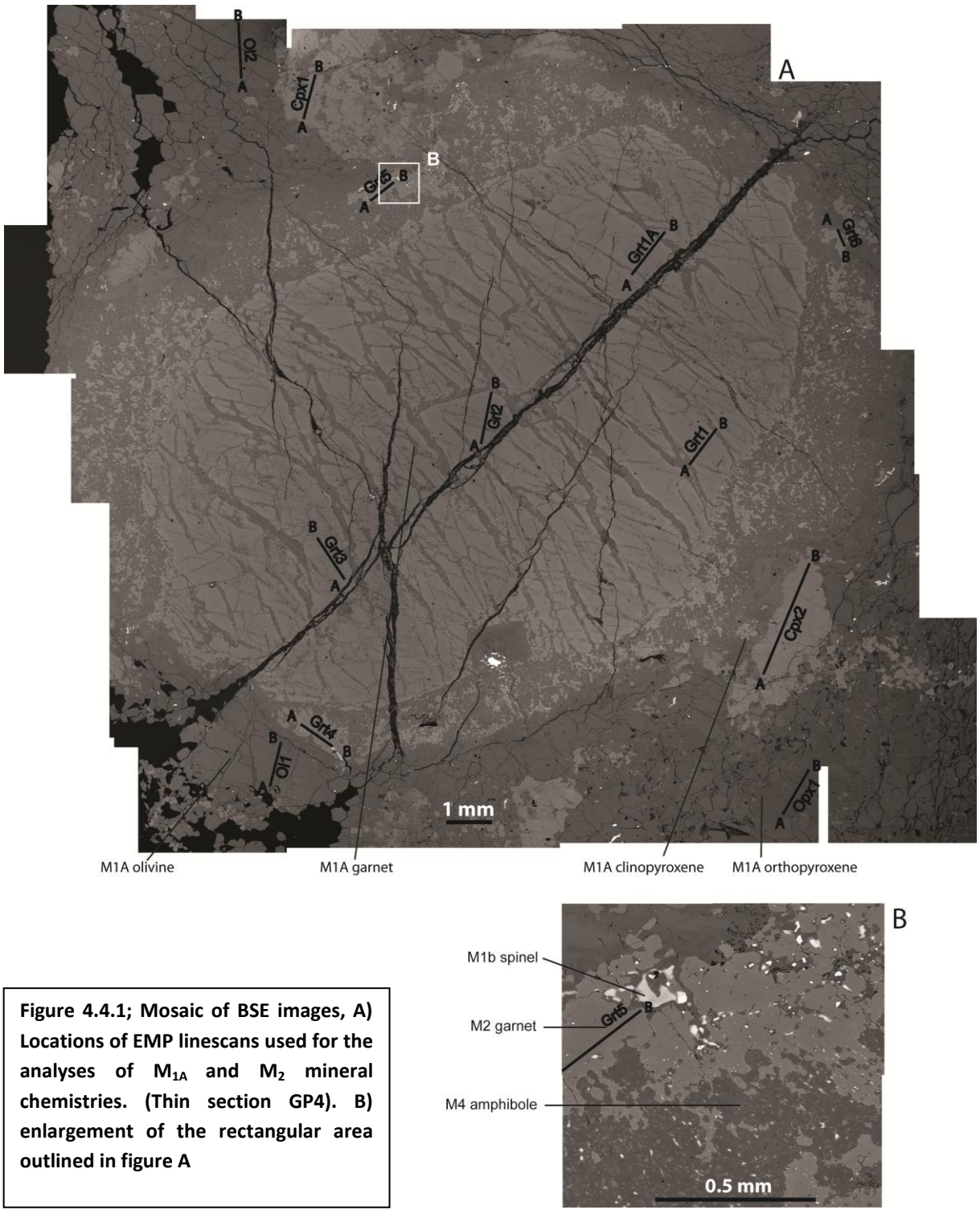

Figure 4.4.1; Mosaic of BSE images, A) Locations of EMP linescans used for the analyses of M_{1A} and M_2 mineral chemistries. (Thin section GP4). B) enlargement of the rectangular area outlined in figure A

Figure 4.4.1 shows the location of the linescans which have been used in order to determine the mineral chemistry of the M_{1A} assemblage. Linescans were checked for homogeneity, joined and averaged in order to reach the best approximation of the stable M_{1A} compositions. EMP results of linescans over M_{1A} minerals are shown in figure 4.4.2 and clearly illustrate that M_1 minerals are homogeneous.

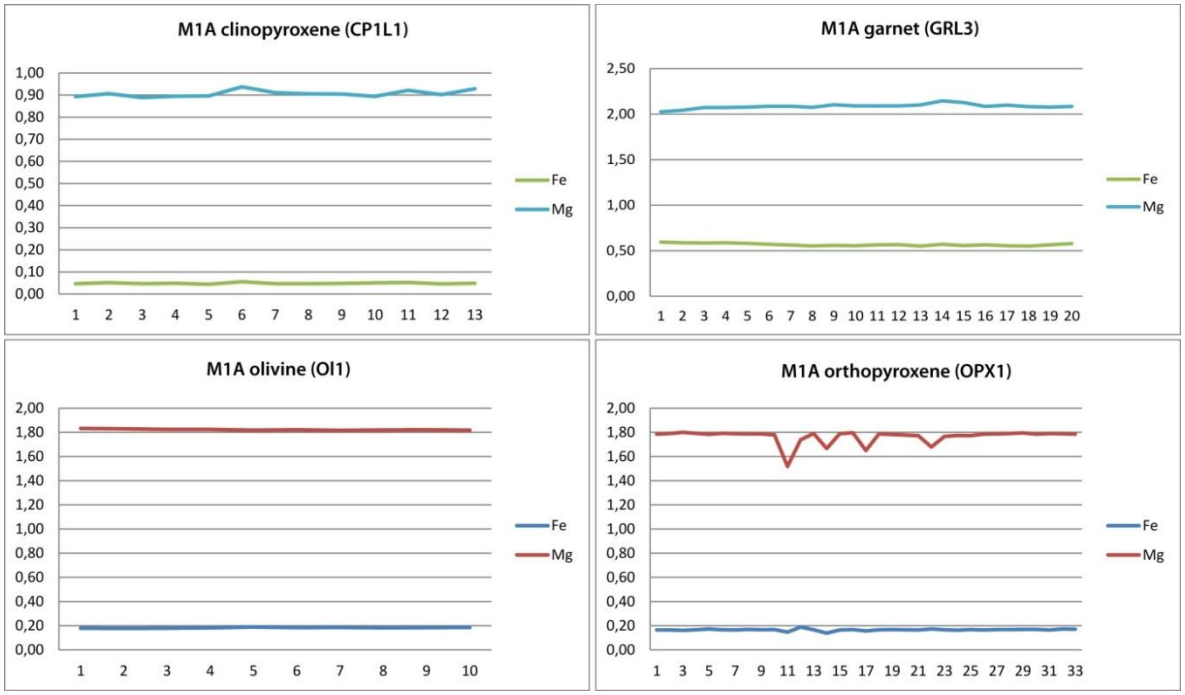

Figure 4.4.2; Uniform Fe-Mg levels expressed in cations per formula unit in M_{1A} minerals. For the location of the linescans see figure 4.4.1. As the exchange reaction between Fe and Mg is the basis of many thermo- and barometers only these are plotted.

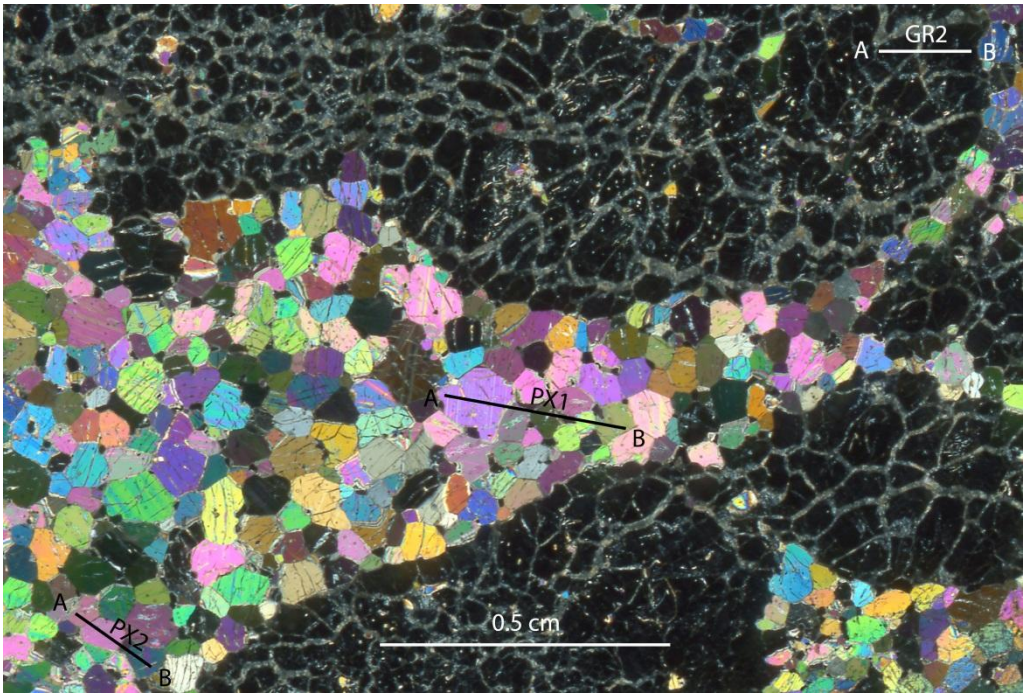

Figure 4.4.3; Optical light microscopy photograph (crossed nichols) of garnet pyroxenite sample D5-1 with the locations of linescans used for the M_2 composition

Representative EMP mineral analyses are illustrated in tables 4.4.1-5. The letters GP in the sample code stand for garnet peridotite, the letter D stands for dike and denote garnet pyroxenite samples.

Garnets									
Sample	**GP4***	**GP4**	**GP4***	**GP3**	**D41**	**D11**	**D41**	**D31**	**D52***
Mode	**M_{1A}**	**M_{1A} cpx_{ex}**	**M_2**	**M_2**	**M_1**	**M_1**	**M_2**	**M_2**	**M_2**
SiO_2	41,85	42,32	41,28	41,79	42,25	41,15	41,98	41,16	41,97
Al_2O_3	22,15	22,56	22,74	22,96	23,26	22,77	23,19	22,94	23,17
FeO	9,39	9,17	12,41	11,30	11,64	12,01	12,49	15,28	9,93
MnO	0,41	0,57	0,75	0,30	0,35	0,28	0,36	0,45	0,35
MgO	19,60	19,09	17,06	18,05	17,55	14,38	16,97	15,47	18,53
CaO	4,81	4,69	5,06	4,64	4,95	8,93	5,54	4,46	6,10
Na_2O	0,01	0,02	0,01	0,02	0,01	0,00	0,01	0,02	0,01
TiO_2	0,13	0,04	0,09	0,03	0,00	0,02	0,02	0,01	0,03
Cr_2O_3	1,88	1,12	0,60	0,15	0,19	0,17	0,09	0,10	0,31
sum	99,97	99,58	100,00	99,24	100,19	99,71	100,64	99,88	100,35

Table 4.4.1; EMP Garnet compositions in peridotite. M_{1A} cpx_{ex} is the mineral code for garnet exsolved from M_{1A} clinoproxene. A star (*) behind the sample code indicates this mineral chemistry has been obtained by averaging homogeneous linescan measurements

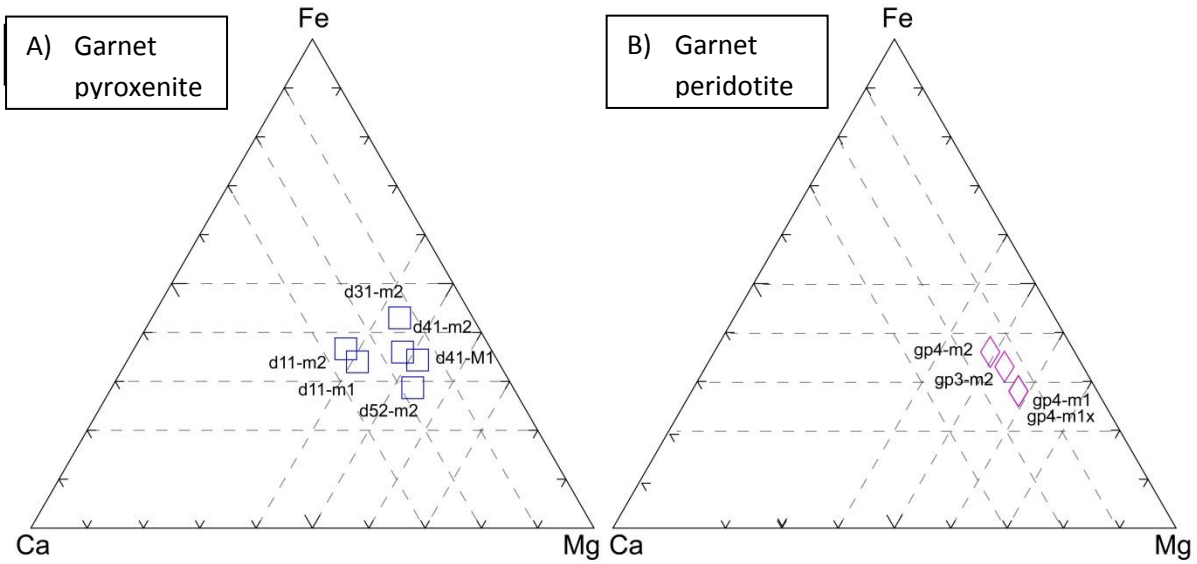

Figure 4.4.4; Garnet mineral chemistries expressed in end-member plots of A) garnet pyroxenite dike samples and B) garnet peridotite samples. Mg, Ca and Fe stand for the cation # in the mineral calculated as cation # / (Mg+Ca+Fe) and corresponds to almandine (Fe), grossular (Ca) and pyrope (Mg). These names are not used in the graphs to avoid confusion

The M_1 and M_2 garnet chemistries of garnet pyroxenite samples do not differ significantly in their grossular content *(Figure 4.4.4)*. However, the M_2 garnets have a higher almandine and lower pyrope content than the M_1 garnets. The difference is approximately 5 %. The difference in end-member composition between different samples is an expression of the variable bulk rock chemical compositions. A similar trend is observed in peridotite samples, with a difference of 5-10 %. The chromium content of garnets in peridotite is between 1 – 2 % in the M_1 assemblage and up to 0.60 for the M_2 garnets. There is no chromium (maximum of

0.19 %) in garnets of the garnet pyroxenite dike. This is an effect of the compatibility of chromium, which is not incorporated in melts during fractional melting.

Spinel compositions									
Assemblage	Thin section	Al_2O_3	FeO	MnO	MgO	TiO_2	Cr_2O_3	Sum	Cr*
M_{1B} spinel	GP11	22,59	20,52	0,77	10,13	0,14	44,50	98,71	66 %
M_{1B} spinel	GP3	27,86	20,14	0,63	11,34	0,10	38,77	99,08	58 %

Table 4.4.2; M_{1B} spinel chemistries. M_2 spinels could not be reliably measured

Spinel compositions vary from chromium contents of ~45 % to chromium contents of ~39 % in garnet lherzolite sample GP3 and spinel dunite sample GP11 respectively *(Table 4.4.2)*. The FeO and MgO contents are similar. The aluminum content varies as much as the chromium content as chromium replaces aluminum in the crystal lattice.

Clinopyroxene chemistries								
mode	**M_{1A}**	**M_{1A} recalculated**	**M_2**	**M_1**	**M_2**	**M_2**	**M_1**	**M_2**
sample	**GP4***	**GP4**	**GP4***	**D31**	**D41**	**D31**	**D1**	**D5***
SiO_2	53,53	52,97	50,48	54,86	55,39	55,67	53,99	54,89
Al_2O_3	2,71	3,7	1,42	5,27	4,78	5,06	6,08	1,21
FeO	1,57	1,95	3,47	1,76	1,61	1,69	1,82	1,46
MnO	0,06	0,08	0,06	0,06	0,03	0,02	0	0,02
MgO	16,41	16,54	25,22	14,02	14,43	14,37	13,22	17,56
CaO	22,13	21,25	17,47	20,00	20,65	19,95	20,49	24,13
Na_2O	1,21	1,15	0,61	0	2,62	2,81	2,62	0,38
TiO_2	0,67	0,64	0,12	2,86	0,12	0,09	0,16	0,1
Cr_2O_3	1,13	1,13	0,53	0,12	0,13	0,16	0,08	0,08
NiO	0,00	0	0	0,16	0,10	0,10	0	0
sum	99,42	99,42	99,39	99,09	99,90	99,95	98,49	99,83

Table 4.4.3; Clinopyroxene chemistries. As above, a star (*) indicates an average chemistry obtained with multiple linescans.

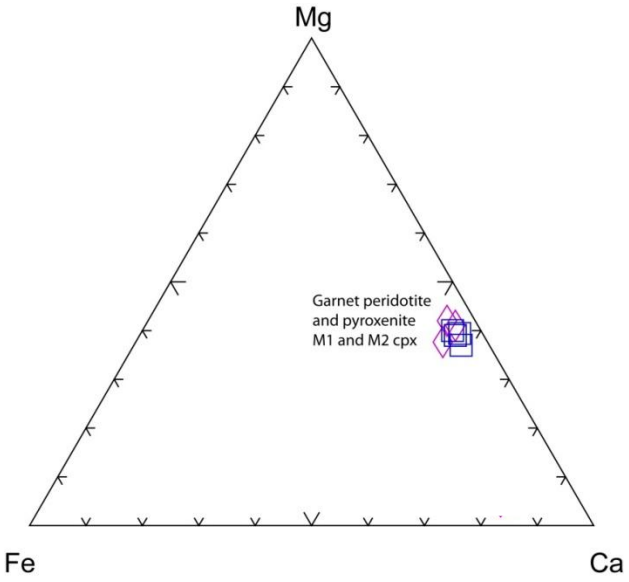

Figure 4.4.5; Clinopyroxene Ca#, Mg# and Fe# end member diagram. Note the similarity between the different samples (also when dike and garnet samples are compared)

M_1 and M_2 clinopyroxene chemistries of garnet pyroxenite and garnet peridotite have very similar end member compositions *(Table 4.4.3; Figure 4.4.5)* except for chromium content. A low amount of Fe is present in clinopyroxenes which averages 5 %. The Ca content is ~45 % and unlike the grossular content in garnet this does not reflect bulk rock compositions. In peridotite samples, the Mg# is 89 % for M_1 clinopyroxene in pyroxenite to 88 % for M_2 clinopyroxene. In garnet pyroxenite dike sample D3 the Mg# of M_1 clinopyroxene is 89%, similar to that of M_2 (89%).

Olivine chemistries							
assemblage	**sample**	**SiO_2**	**FeO**	**MnO**	**MgO**	**sum**	**Mg#**
M_{1A}	GP4*	40,85	8,95	0,08	49,99	99,90	84,82%
M_2	GP4*	40,88	9,18	0,1	49,85	100,03	84,45%
M_{1A}	GP11	41,27	6,75	0,08	51,51	99,99	88,4

Table 4.4.4; Olivine chemistries of garnet lherzolite sample GP4 and of garnet dunite sample GP11. GP4 M_{1A} and M_2 olivine is similar in chemistry and has a Mg# of approximately 85%. GP11 M_{1A} olivine has a Mg# of 88.4 %

The Mg# of olivine in garnet lherzolite sample GP4 and dunite sample GP11 *(Table 4.4.4)* ranges from 84.5 % - 88.4 %, respectively. This is significantly lower than the previously reported Mg# of 90 % -92 % of *Brueckner et al. (2004)* in dunite . There is no difference in chemistry between the annealed M_2 microstrure and the M_{1A} megacrystic assemblage.

Orthopyroxene chemistries					
assemblage	**M_{1A}**	**M_{1A}, recalculated 5% exsolution**	**M_{1A}. Recalculated 10% exsolution**	**M_2**	**M_1 *(B.e.a., 2004)***
sample	**GP4***	**GP4**	**GP4**	**GP4**	**D**
SiO_2	57,09	56,76	56,43	54,68	55,94
Al_2O_3	1,38	1,38	1,38	4,74	2,46
FeO	5,79	5,67	5,56	6,82	5,56
MnO	0,11	0,11	0,10	0,12	0,08
MgO	34,69	34,22	33,75	32,91	34,33
CaO	0,15	1,02	1,89	0,45	0,14
Na_2O	0,01	0,04	0,07	0,08	0,01
TiO_2	0,06	0,06	0,06	0,23	0,06
Cr_2O_3	0,21	0,22	0,24	0,33	0,21
sum	99,49	99,47	99,45	100,37	98,83

Table 4.4.5; Orthopyroxene mineral chemistries. The recalculated orthopyroxene chemistry combines 5/10% exsolution of clinopyroxene, assumed to be of M_2 composition (see table 4.4.2) and the M_{1A} orthopyroxene chemistry. The M_1 orthopyroxene chemistry of the garnet pyroxenite (D) is from *Brueckner et al. (2004)*.

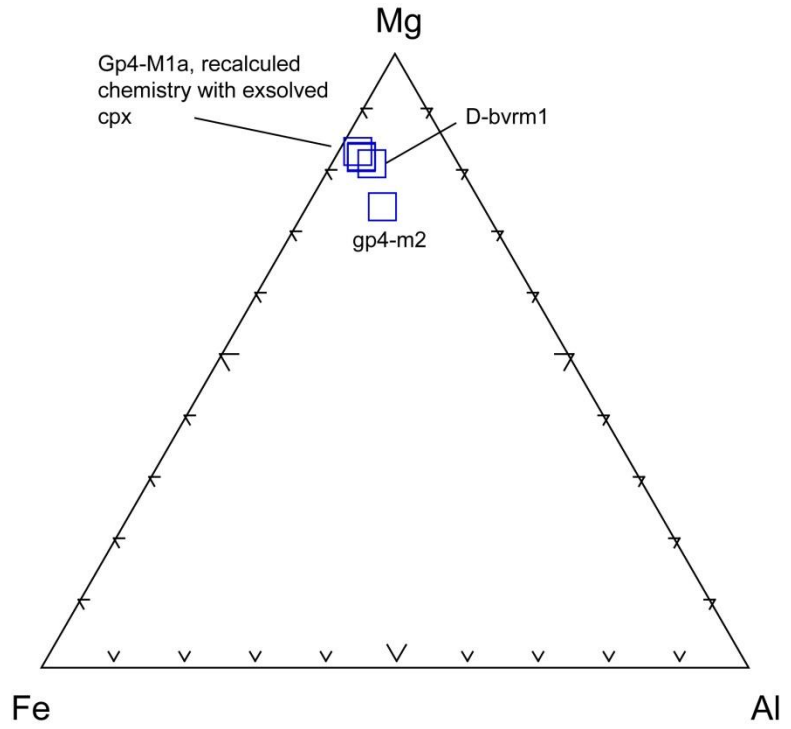

Figure 4.4.6; Orthopyroxene mineral chemistries plotted in end member diagrams. Note that M_1 assemblages are consistent in the dike and peridotite. The M_2 assemblage of the peridotite has a higher Fe/Mg ratio and higher Al content.

Orthopyroxene chemistries *(Table 4.4.5; Figure 4.4.6)* of the M_1 assemblage are similar in composition and record Mg# of ~86 %. The M_2 orthopyroxene is richer in Aluminum and has a Mg# of 83 %. M_{1A} orthopyroxene has been recalculated under the assumption that the exsolved clinopyroxene has a similar composition to M_2 clinopyroxene due to lack of a good analysis of the exsolved clinopyroxene.

M_4 Amphibole compositions										
Sample	**Si**	**Al**	**Fe**	**Mn**	**Mg**	**Ca**	**Na**	**Ti**	**Cr**	**sum**
GP4	42,40	17,16	2,99	0,04	16,97	12,05	2,89	1,06	0,81	96,36
D41	46,93	13,45	4,40	0,05	18,57	10,78	2,49	0,51	0,17	97,69

Table 4.4.6; amphibole compositions of both peridotite and pyroxenite

Amphibole compositions have been determined for the M_4 assemblage in both peridotite and garnet pyroxenite *(Table 4.4.6)*. The difference in both samples is likely due to differences in bulk rock compositions. Note again the chromium content in M_4 amphibole in peridotite, which is approximately 4 times that of the garnet pyroxenite M_4 amphibole.

4.5 Thermobarometry

4.5.1 *Results*

Garnet peridotite results

Using the mineral compositions depicted in tables 4.4.1 and 4.4.3-6 the overall assemblage of the peridotite M_{1A} microstructure gives a temperature of approximately 950 °C for opx-cpx solvus based thermometers *(Brey & Kohler, 1990; Wells, 1977; Bertrand & Mercier, 1985)*, 680-880 °C for Fe/Mg based thermometers *(Krogh, 1988; Krogh & Ravna, 2000; Harley, 1984; Ellis & Green, 1979; Powell, 1985; Brey and Kohler, 1990a & 1990b)* and >2000 °C for thermometers based on reactions with olivine *(Brey & Kohler, 1990; O'neill, 1979)*. All these temperatures are obtained using the iterative approach of PTEXL with a pre-set pressure of 2.5 GPa. Olivine based thermometers are rejected, since at these temperatures the system would be magmatic. A temperature of 840 °C gives the best fit to the different barometers used *(Brey & Kohler, 1990; Brey et al., 2008; Nickel & Green, 1985; MacGregor, 1974; Nimis & Taylor, 2000; Ryan et al., 1996)* and associated pressure is 2.3 ± 0.3 GPa.

The peridotite M_2 assemblage, based on the foam texture of clinopyroxene, olivine, garnet and orthopyroxene give temperatures of 600 ± 40 °C and pressures of approximately 2.3 ± 0.4 GPa. The clinopyroxene and olivine by themselves give a pressure of 2.3 GPa *(Nimis & Taylor, 2000; Kohler & Brey, 1990a)*. Olivine and clinopyroxene and garnet and clinopyroxene thermometers *(Kohler & Brey, 1990b, Krogh and Ravna, 2000)* give temperatures of 600 ± 30 °C. Another set of thermometers and barometers, *(P from Nimis and Taylor, 2000; T from Harley, 1984; Ellis and Green, 1979 and Powell, 1975)*, give pressures of 2.85 Gpa and T = 750 ± 50 °C. The best estimates can be seen in table 4.5.1.

Garnet pyroxenite results

The recrystallized M_2 foam texture of garnet pyroxenite D5 has been used for multiple EMP analyses. The linescans over recrystallized megacrystic garnets and foam clinopyroxene have been used for these analyses *(sample D51, D52, Figure 4.4.3, Table 4.4.1 and 4.4.3)*. Only the barometer of *Nimis & Taylor (2000)* can be used for clinopyroxene and garnet. This gives PT conditions of 1.6 GPa and 690 °C if used with the thermometer of *Ellis & Green (1979)* and *Powell (1985). Nakamura (2009)* noted that the thermometers of *Ellis & Green* and *Powell* both show deviations of 200°C for large grossular contents of garnet. The grossular content of these samples are X_{grs} = 0.15, neglecting the possibility of a large discrepancy due to grossular content.

The Ca, Mg and Fe content in garnets is plotted in figure 4.4.4. Both M_{1A} garnets and M_2 garnets were measured. The overall trend is towards a larger Fe/Mg ratio from M_{1A} to M_2 garnets. The chemistry of garnets is relatively consistent with the bulk rock compositions of the dike samples. The best calculated PT estimate can be seen in table 4.5.1 and is based on the thermometers of *Ellis & Green (1979), Powell, (1985), Nakamura (2009)* and the barometer of *Nimis and Taylor, 2000*.

Peridotite and pyroxenite thermobarometric estimates			
Asssemblage	**T (°C)**	**P (GPa)**	**Lithology**
M_{1A}	840	2.3	Garnet peridotite
M_2	600	2.3	
M_1			Garnet pyroxenite
M_2	690	1.6	

Table 4.5.1, best estimates of M_1 and M_2 pt conditions

4.5.2 Discussion

The M_{1A} assemblage has equilibrated at 840 ± 30 °C and 2.3 ± 0.3 GPa. This is based on one thin section (Figure 4.4.1) in which the M_{1A} assemblage is very well preserved. Olivine based thermometers were rejected as these give temperatures at which the system would be magmatic. The thermodynamic calculations have thus been done with cpx, opx and garnet M_{1A} chemistries.
The M_2 assemblage equilibrated at 2.3 ± 0.4 GPa and 600 ± 40 °C. The pressure resembles the pressure of the M_{1A} assemblage but the temperatures are much lower. This discards the possibility that the pressure is confused with the M_{1A} assemblage pressure. This thermobarometric estimate is based on 2 thermometers and 2 barometers. For a different set of thermometers and one barometer *(Nimis and Taylor (2004); Ellis and Green (1979); Powell, 1985)* , the PT conditions are 2.85 GPa and T = 750 ± 50 °C. The migmatites surrounding the peridotite body have formed at conditions of 700 – 800 °C and 2.0 – 3.0 GPa *(Van Roermund, 1985, 1989)*. The latter thermobarometric estimate is therefore inferred to be representative of the conditions under which the M_2 assemblage formed.
The PT conditions of the recrystallized assemblage in the garnet pyroxenite are 1.6 GPa and 680 ± 80 °C. In Theriak-Domino psuedosection of dry peridotite *(Figure 4.6.1)* this plots just in the stability field of garnet peridotite under dry conditions and in the stability field of garnet pyroxenite. The barometry has to be treated with care however as the empirical relationship has been determined on the basis of Cr exchange between garnet and clinopyroxene in peridotite. In garnet pyroxenites, although the exchange mechanism might be similar, the bulk rock composition can influence the equilibrium of this exchange reaction. As no orthopyroxene in the dikes was analyzed in this study pressures are difficult to estimate. *Brueckner et al.(2004)* have analyzed a megacrystic assemblage of opx,cpx and garnet in pyroxenite which yielded a pressure of 1.45 ± .05 GPa and T = 775 ± 25 °C. The temperatures calculated have a small overlap at 760-770 °C and the pressure is interpreted to be in between 1.45 and 1.6 GPa. These pressures cannot be coeval with the M_2 assemblage of the garnet peridotite as they plot in the spinel stability field. The M_2 assemblage of the pyroxenite dike has formed under similar conditions as the M_2 assemblage in peridotite. Therefore, the pressure and temperature estimate of the dike M_2 assemblage is interpreted to be an effect of re-equilibration and is a PT point along the retrograde path of the peridotite.

4.6 Theriak Domino

4.6.1 results

The bulk rock of one peridotite and one dike sample has been used to make phase diagrams with the PT software Theriak Domino. The bulk rock compositions can be found in table 4.6.1. Figure 4.6.1 & 4.6.2 show the resulting pseudosections of the peridotite and pyroxenite samples *(see also A. Prent, BSc thesis)*.

Sample	SiO_2	Al_2O_3	TiO_2	FeO	CaO	MgO	Na_2O	K_2O	P_2O	sum
D5	48.60	10.60	0.21	5.72	16.5	19.60	0.26	0.02	0.05	101.6
GP4-C	44.85	2.85	0.11	8.29	2.77	40.04	0.13	0.0	0.0	100.0

Table 4.6.1; Table with XRF results (D5 and GP4) and the results of GP4

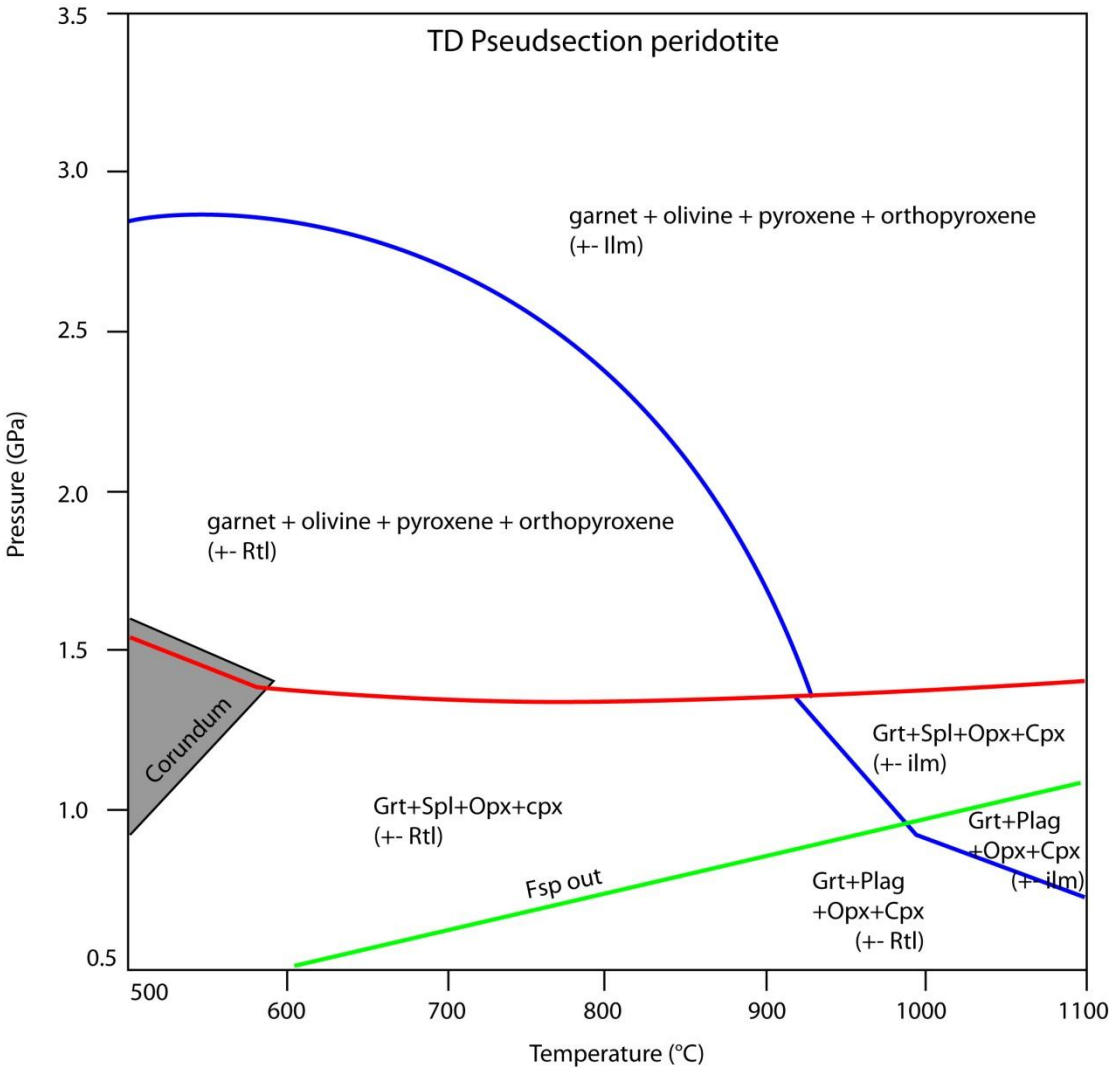

Figure 4.6.1; Pseudosection of peridotite, note that the origin of the diagram, starts at 0.5 GPa and 500 °C.

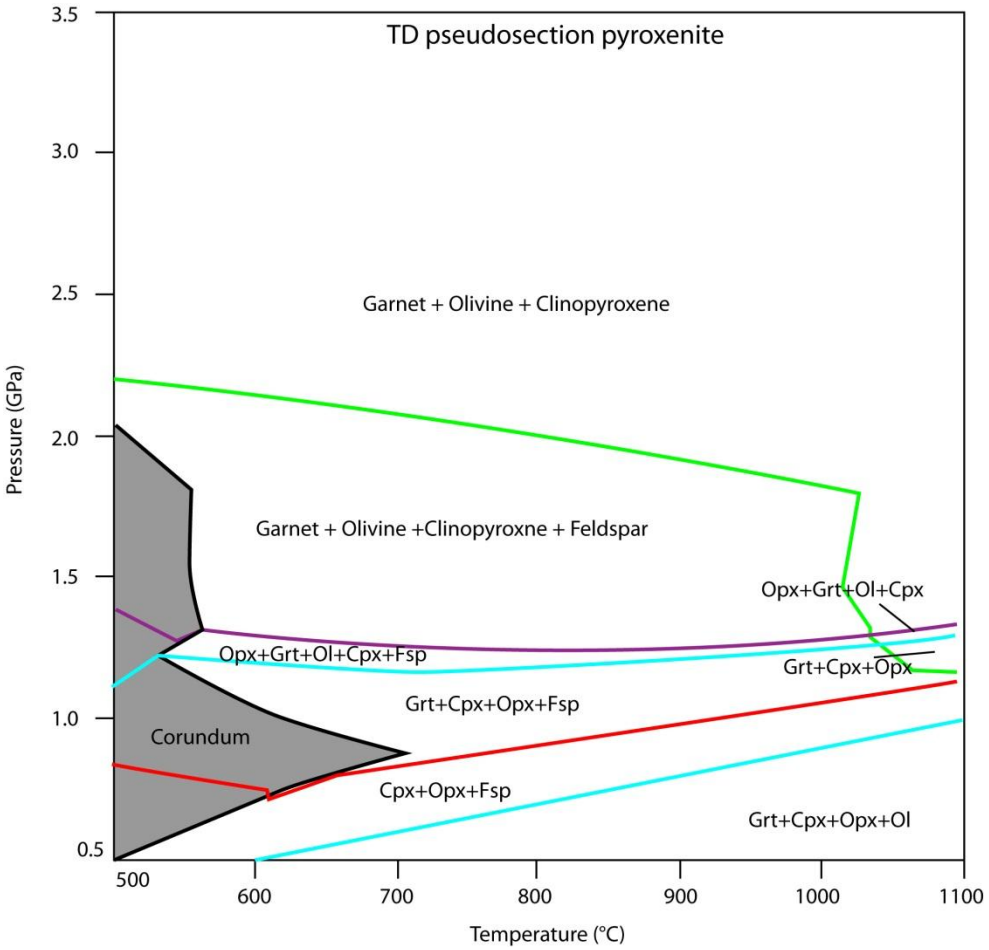

Figure 4.6.2; pseudosection of pyroxenite. As in figure 4.6.1, this pseudosection starts at 5 Kb and 500 °C. Although Fsp is indicated as stable until very high pressures it is not present in quantities of over 1% above approximately 1.0 GPa

As thermobarometric estimates show *(Section 4.5)*, the temperature ranges of interest in the peridotite and pyroxenite samples are 600 – 850 °C. Garnet is stable in pyroxenite above a minimum of 0.65 GPa and 620 °C. Minor amounts of plagioclase are present up to 2.2 GPa but do not comprise more than one percent of the rock volume above 1.0 GPa. Orthopyroxene is stable up to approximately 1.3 GPa and olivine is calculated to be present in almost any PT condition.

The peridotite pseudosection *(Figure 4.6.1)* shows the stability fields of spinel, corundum, garnet, plagioclase (fsp), olivine, clinopyroxene, orthopyroxene, and rutile and ilmenite. Garnet is stable from approximately 1.4 GPa with a weak pressure dependence and plagioclase feldspar is stable up to 0.8 GPa at 850 °C, and has a large positive pressure dependence.

In addition garnet isoploths have been made for dry and wet garnet pyroxenite and garnet peridotite *(see A. Prent, BSc thesis).* Wet bulk rock compositions are compositions in which 5 moles of water have been added. In the garnet isoploths the end-member garnet compositions at different temperatures and pressures are calculated and can thus be compared with garnet compositions give in section 4.4. M_2 garnets of the garnet pyroxenite dike plot at 650 °C and 1.3 GPa under dry conditions *(Figure 4.6.3)*. M_{1A} garnets of the garnet peridotite plot at 650

°C and 1.8 GPa under wet conditions *(Figure 4.6.4)*. Estimated PT conditions calculated using M_1 and M_2 garnet compositions of peridotite and pyroxenite are given in table 4.6.1.

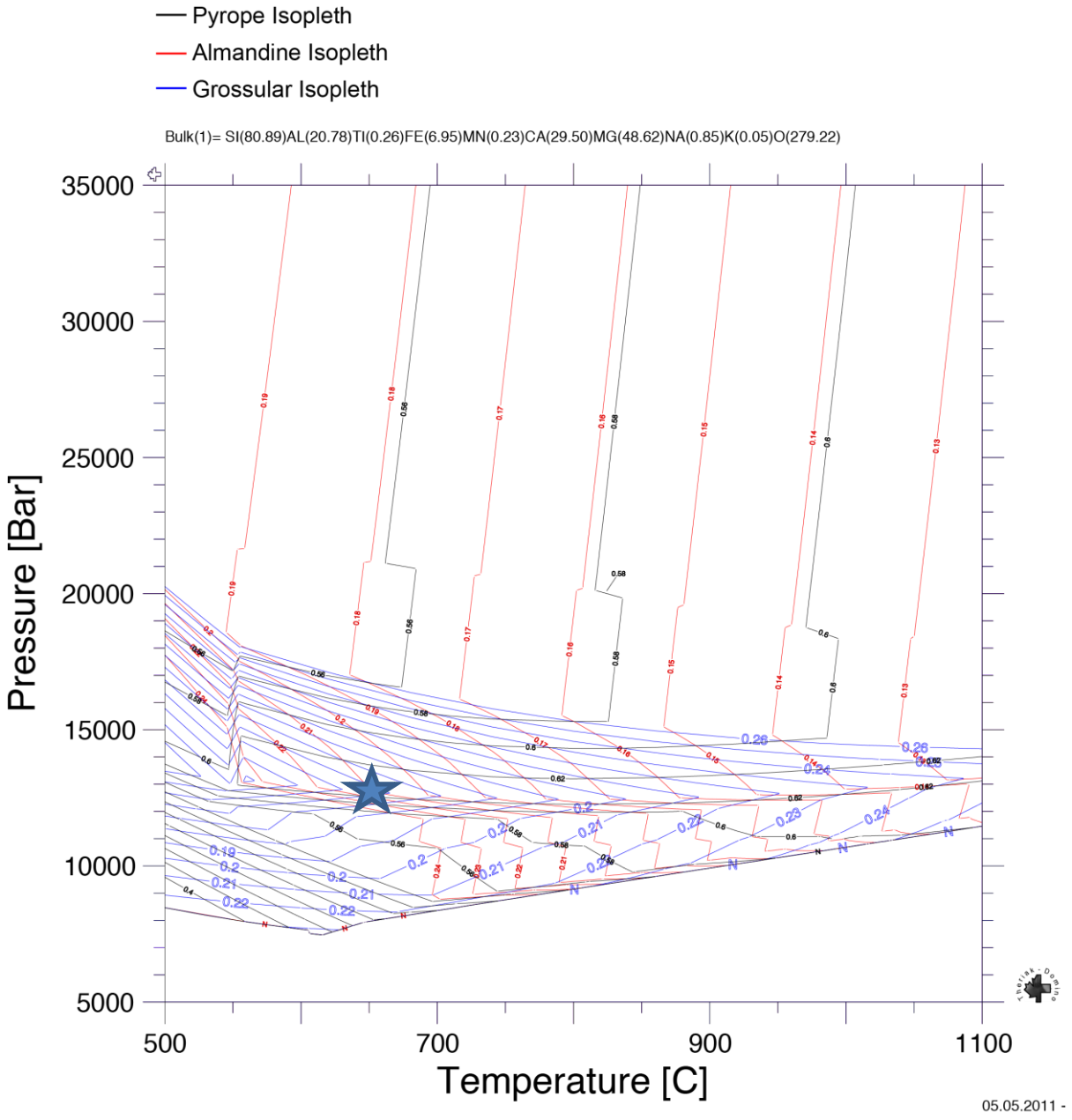

Figure 4.6.3; Isoploth of garnet end-member compositions under dry conditions (no added H_2O in the bulk rock composition). M_{1A} garnet end-members (see section 4.4) plot at 650 °C and 1.3 Gpa depicted with a star. The bulk rock compositiolns used for the thermodynamic calculations are given above the diagram in elements.

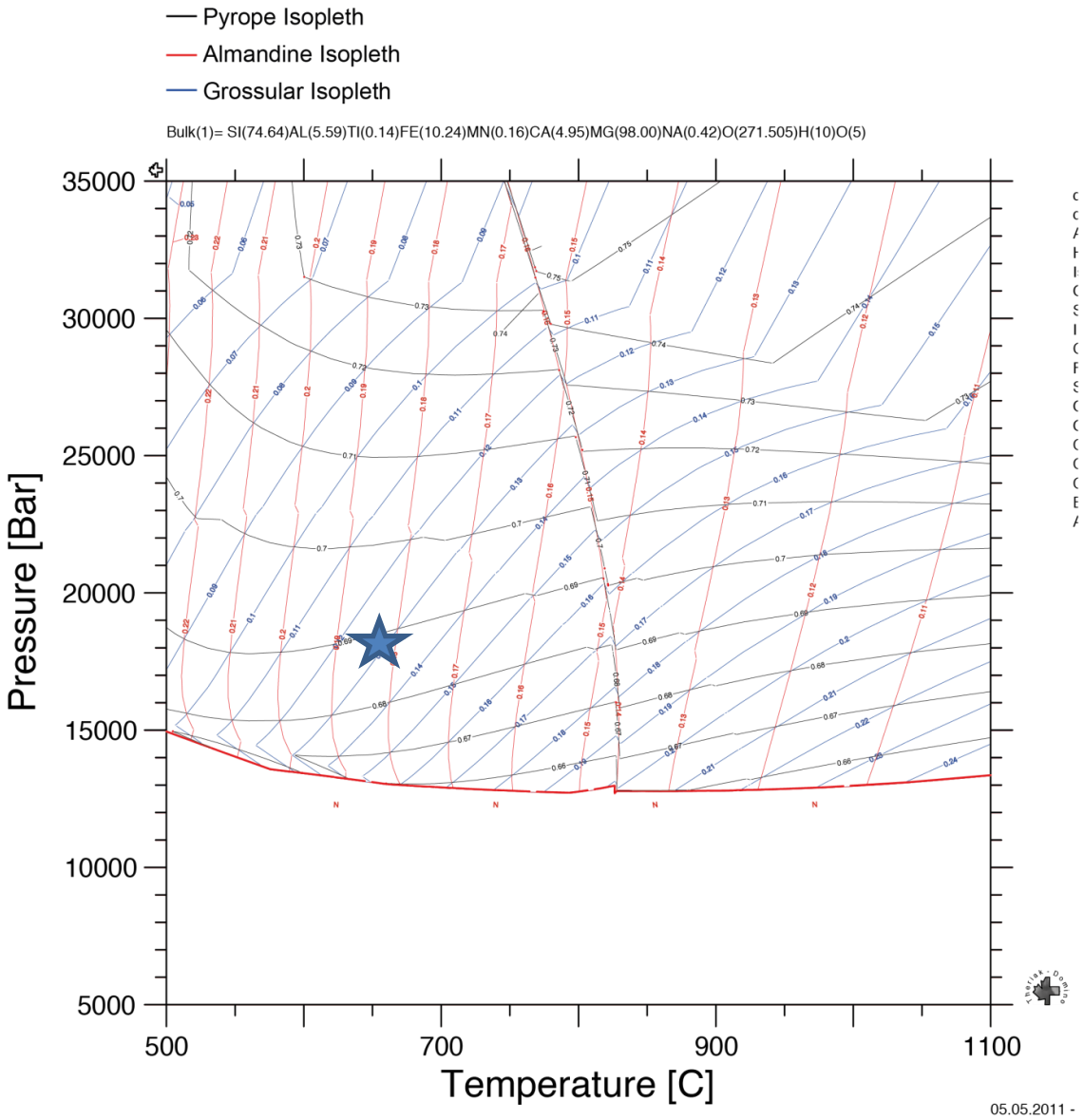

Figure 4.6.4; Isopleth of wet peridotite (5 moles of water added to bulk rock compositions). The M_{1A} end member compositions (see section 4.4) plot at 1.8 GPa and 650 °C. The bulk rock composition used for the calculation is given above the diagram in elements.

PT estimates from Theriak-Domino isoploths				
pyroxenite	M_2	Dry	1.3 GPa	650 °C
Peridotite	M_{1A}	Wet	1.8 GPa	650 °C

Table 4.6.1; TD isopleth fits of M_2 pyroxenite and M_1 peridotite.

The M_2 garnet composition of peridotite does not plot on any intersection of isopleths calculated with Theriak Domino. No M_1 mineral chemistry is available for sample D5 since all are recrystallized to M_2. The M_1 garnet mineral chemistries of other thin sections cannot be uses the pseudosection has been calculated using the bulk rock compositions of sample D5. Comparing the M_1 garnet end member compositions of other samples (with different bulk rock chemistry) cannot be done. Grossular content in the samples *(Figure 4.4.4)* varies according to bulk rock compositions and hence this will lead to a wrong PT estimate.

4.6.2 *Discussion*

As there is no constraint on the error on the peridotite bulk rock compositions these analyses should be treated with care. However, as the peridotite ranges from dunitic to lherzolitic in composition the bulk rock composition will vary substantially in the outcrop itself.
Thermobarometric estimates of M_{1A} and M_2 *(Section 4.4)* are in line with the results of the phase diagrams calculated using Theriak Domino of pyroxenite and peridotite, although the pyroxenite shows some additional features. The pseudosection of pyroxenite shows that olivines should be present in most of the PT space. There is no olivine found in samples of D5 however. At pressures of 1.2 – 3.5 GPa olivine should comprise 10 % of the mineral assemblage. The M_1 boundaries of the annealed foam matrix show that the grain sizes of the M_1 assemblage were up to a cm-scale in size *(Section 2.2)*. This implies that at thin section scale it is possible no olivine is present but it does occur in the hand sample.
In the pseudosection of pyroxenite, between 0.5 – 1.0 GPa *(Figure 4.6.1)* no olivine is present. If no olivine is present in hand-samples the recrystallization to M_2 minerals has occurred under these conditions.
The thermobarometric estimate on the M_2 assemblage of garnet pyroxenite is 1.6 GPa and 680 °C. At these temperatures and pressures, orthopyroxene should not be present and olivine should be present. There is some orthopyroxene in the polygonal foamy matrix but no olivine was found. This implies that the thermobarometric estimate is not correct. Similarly, the thermobarometric estimate of *Brueckner et al.,(2004)* cannot be correct assuming their dike sample has similar bulk rock chemistry. Of course also the phase diagram itself can be at fault, or the interpretation of this phase diagram. This software calculates phase diagrams on the basis of minimizing Gibbs free energy. This leads to the prediction that as soon as a phase has a lower minimum Gibbs energy, reaction will occur and a reaction line is plotted. There is no activation energy implemented in the software. On the other side, an overpressure of 0.5 GPa is considerable for metastable minerals. This is what is approximately needed to create the 1.6 GPa at 680 °C with stable corundum but no olivine. All reactions are also assumed to reach equilibrium by Theriak Domino. There is no evidence to verify this assumption from microstructures.
On the basis of the pseudosections, both the M_1 and M_2 assemblages of the dike are stable below the orthopyroxene out line, assuming low amounts of olivine are present in the garnet pyroxenite hand samples. This is approximately 0.8 - 1.3 GPa and 600-900 °C. Since no olivine is observed, but there is clinopyroxene this pseudosection cannot be used for the observed microstructures in the pyroxenite dike. This also raises questions about the validity of the isoploth garnet end-member diagram. Plots for wet pyroxenite (pyroxenite bulk rock compositions with added H_2O) show amphibole is stable up to > 2.0 GPa high pressures. Amphibole does not occur in the M_1 and M_2 assemblage of pyroxenite, so this pseudosection was rejected.
The decompression needed to get stable spinel after the M_{1A} conditions is at least 0.8 GPa. Converted to depths, this is a minimum of 24 km. This decompression must be a major tectono-metamorphic event. However, again it should be stressed that conclusions based (indirectly) on the XRF analysis of peridotite have to be treated with care.

4.7 Zircon extraction

Of the garnet pyroxenite dike approximately 8 kg of samples were crushed to separate zircons from other minerals. Minerals were separated on the basis of magnetic susceptibility and grain size. After the mineral separation possible zircons were hand-picked and subsequently they have been placed on thin sections and polished. After polishing they were coated with carbon and analyzed with the EMP to determine the accessory phases and minerals that might be used for dating purposes. Minerals that are excellent preservers of crystallization ages such as zircon and baddeleyite are not susceptible to magnetic fields. Therefore, only minerals which were unaffected by the magnetic field have been analyzed with the microprobe. The minerals fall into three categories with respect to grain sizes; 60-90 µm, 90-125 µm, and >125 µm.
The analyses of the accessory phases on the microprobe were done on the basis of their backscatter coefficient. When the brightness in the BSE image is lowered, lighter minerals fade out before heavy minerals. Table 4.5.1 shows the results. Unfortunately no zircon or baddeleyite is present. Much rutile is present but most likely will give recrystallization ages corresponding to Scandian ages. Future studies might also yield Re-Os ages from pentlandite.

30-60 µ	60-90 µ	90-120 µ	>120 µ	Suspect minerals
Corund	Corund	Corund	Corund	SnO/SnO_2
Amphibole	Amphibole	Amphibole	Amphibole	Corund
Rutile	Rutile	Rutlie	Rutile	Rutile
Pentlandite	Pentlandite	Pentlandite	Pentlandite	BrO
				$PbSnO_x$
				Spinel
WCaO	WCaO			Pentlandite

Table 4.7.1; Different minerals found after the extraction of accessory phases. WCaO is a relic from the crusher.

5 Discussion

5.1 Possible PT path

Evidence from microstructures

The M_{1A} assemblage of the peridotite is the first stable assemblage. This assemblage indicates residence in an HP regime. There is no evidence present of prior lower-grade assemblages which implies that the M_1 assemblage is a mantle wedge garnet peridotite mineral assemblage. The M_{1B} spinel symplectites are reminiscent of depressurization and the decreasing grain size from rim to core *(Figure 4.2.1)* indicates coeval deheating.

The M_2 mineral assemblage including garnet-olivine again indicates recompression of the peridotite into the stability field of garnet-olivine. The anhedral and small crystals of the M_2 assemblage overprint M_{1B} corona minerals.

The M_3 to M_5 assemblage are evidence of the retrograde path of the peridotite to the surface where the rocks were collected.

Evidence from thermobarometry and mineral chemistries

Thermobarometry shows the M_{1A} in the peridotite assemblage formed at 840 ± 30 °C and 2.3 GPa. The M_2 assemblage has equilibrated at 600 ± 30 °C and 2.3 ± 0.4 GPa. The M_2 assemblage in the garnet pyroxenite dike formed at 1.6 GPa and 680 ± 40 °C due to the lack of a suitable barometer. This is interpreted as re-equilibration along the retrograde path of the peridotite to the surface.

The magnesium number in olivine (85 – 88 %) implies that no melt extraction event took place prior to the refertilization of the peridotite. However, the outcrop consists partly of dunite e.g. depleted mantle. Further, *Brueckner et al., (2004)* found a magnesium number of 90-92 %. As the peridotite is compositionally layered, the magnesium number will depend on the sample locality. Aditionally, refertilization of the peridotite might lower the magnesium number locally. The occurrence of dunite and the previously reported higher magnesium number show that a melt extraction must have taken place.

Evidence from Theriak Domino

Theriak Domino isoploths on garnet peridotite and pyroxenite yield two possible PT points. M_1 garnet in hydrated peridotite can equilibrate at 1.8 GPa and 650 °C. The M_{1A} assemblage does not contain any amphibole (or other hydrated minerals) however and therefore the calculations might be incorrect. M_2 garnet in pyroxenite can equilibrate in dry conditions at 1.3 GPa and 650 °C. The pyroxenite pseudosection is rejected since there is no olivine and feldspar present in the pyroxenite. There is orthopyroxene present in thin sections of garnet pyroxenite which also does not fit with the predictions of the pseudosections. The transition from M_{1A} to the M_2 assemblage must have involved a decompressional event of at least 0.5 GPa on the basis of pseudosections. Theriak Domino does not take into account the chromium content in garnet and this might also be part of the misfit between Theriak Domino results and the thermobarometric calculation.

Isoploths of garnet cannot give a reliable composition of M_2 garnets. It is very likely that the M_2 garnets did not reach equilibrium during the recompressional M_2 event.

PT path

The M_{1A} assemblage in itself is not full evidence for a mantle wedge garnet peridotite. The dating of M_{1A} clinopyroxenes by *Brueckner et al., (2004)* has shown this a Proterozoic assemblage. They were not able to date garnets implying that it is still possible that the garnets grew later. There is however, not any evidence for a lower pressure assemblage prior to the M_{1A} assemblage. In summary, the lack of pre – M_{1A} lower pressure protolith assemblages and the Proterozoic ages of the M_{1A} assemblage are evidence that this peridotite lens resided in the mantle from Proterozoic until early Caledonian times.

The M_{1A} mineral compositions are interpreted to give reliable results and will be plotted at 840 ± 30 °C and 2.3 GPa. The M_{1B} assemblage is taken as 0.5 GPa lower than the M_1 assemblage which is a maximum pressure estimate based on Theriak Domino pseudosections.

The M_{1B} assemblage must have formed at pressures in the spinel-olivine stability field of peridotite and in the garnet-pyroxene stability field of garnet pyroxenite. This gives a pressure constraint of $1.0 < P < 1.4$ GPa at temperatures in the range of 600 – 800 °C. These temperatures are assumed to be correct due to the temperatures at which the earlier and later M_{1A} and M_2, respectively, assemblages have formed. The relative timing of these assemblages implies that there was a period that the peridotite resided in an HP regime in SCLM, an undefined period of time in the spinel-olivine stability field and was subsequently recompressed in the garnet-olivine stability field.

The M_2 garnets have not equilibrated in the peridotite and therefore thermobarometry on these samples will be rejected. The values calculated by *Brueckner et al. (2004)* for M_2 crystals are T = 700 – 800 °C and P = 2.0 – 3.0 GPa. These are concordant with the host gneiss peak PT conditions and are interpreted to represent the M_2 PT conditions. The M_2 assemblage of the garnet pyroxenite equilibrated at T = 650 – 680 °C and P = 1.3 – 1.6 GPa (data combined from thermobarometry and Theriak Domino) which represents cooling temperatures and pressures. Age dating by *Brueckner et al., (2004)* and *Gademan et al., (2011)* have demonstrated that the M_2 assemblage formed during an Early Caledonian metamorphic event.

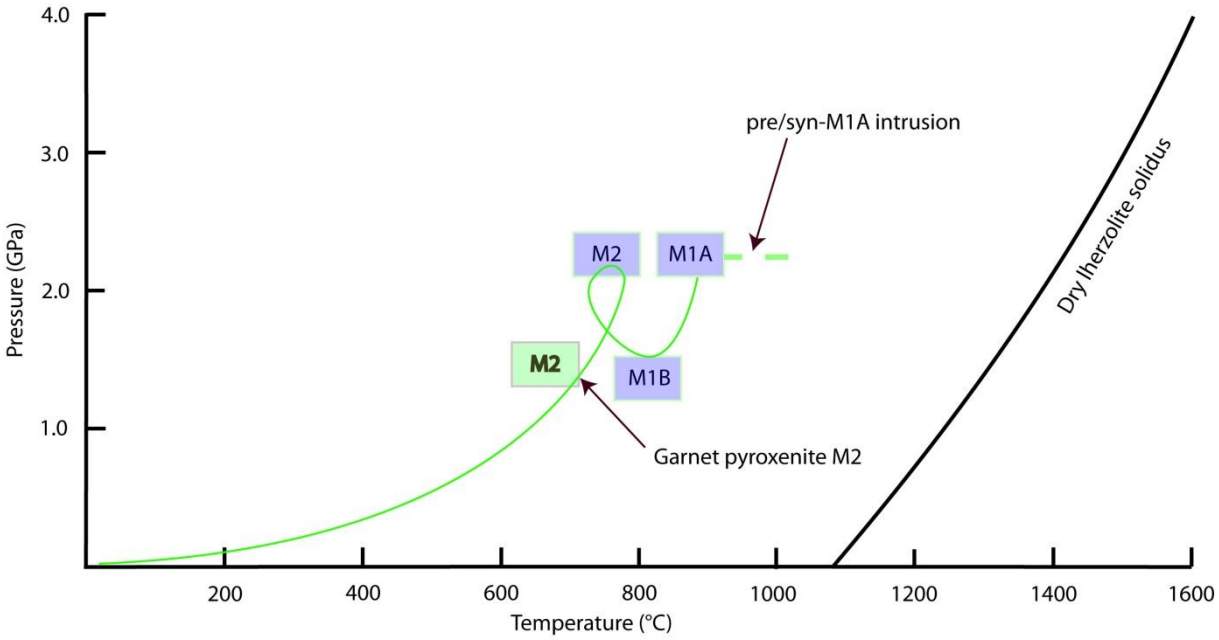

Figure 5.1.2; Composite PT path using evidence from microstructrures, pseudosections and thermobarometry

5.2 Metasomatism

Evidence from bulk rock major elements

The garnet pyroxenite bulk rock compositions show erratic sodium compositions. These are interpreted as secondary features due to the variation between samples. In addition to that, Na is not present in these quantities in lithospheric mantle. Eclogites in the Seve Nappe Complex contain up to 5% sodium which make them impossible to correlate to the Friningen garnet pyroxenite dike. This makes it likely that the sodium was introduced by sodium-bearing fluids. A possible source for this fluid can be subduction related and due to slab dehydration.

Evidence from bulk rock rare earth elements

An erratic europium anomaly is found in the garnet pyroxenite samples. This europium anomly is absent in sample D5 which is also the sample with the lowest amount of sodium. A positive europium anomaly might be a lower crustal signature due to crustal erosion during subduction. Another possibility is that the europium was introduced later while the peridotite lens resided in the crust. It can also be interpreted to be related to the same process that governed the elevated sodium concentrations in the garnet pyroxenite. The latter is the favored interpretation.

The enrichment in LREE inocorporated in the pyroxenite sample is likely the effect of a fluid carrying LREE that percolated the peridotite.

The europium anomaly, the sodium concentrations, and the LREE enrichment are all interpreted to be due to the same LREE and sodium carrying fluid, likely a subduction fluid.

Evidence from Mineral chemistries

Weak evidence for the influx of sodium in the garnet pyroxenite sample comes from EMP analyses on M_1 and M_2 clinopyroxene. In contrast to M_2 compositions, M_1 compositions do not contain sodium. This evidence has to be treated with care as only one M_1 grain was analyzed. The M_2 sodium content also depends on bulk rock compositions.

The evidence for metasomatism presented above implies the peridotite lens resided in a mantle wedge for a substantial time. During this time, the garnet pyroxenite (and the peridotite) was metasomatised by subduction related fluids. This happened with different degrees of metasomatism which might be linked to possible fluid pathways in the peridotite.

5.3 Mantle wedge characteristics

The first stable assemblage of the peridotite is the M_{1A} assemblage. The PT conditions of this assemblage (840 °C and 2.3 GPa) give information on the type of mantle wedge present during collision. The PT conditions can be used to determine the type of mantle wedge that operated during continental collision. Using the classification scheme of section 2.6 *(Zhang et al., 2011)* a type C mantle wedge can be determined. This means that during the collisional event the overhanging mantle wedge was cold (hence, old) and thin. This in turn implies a static mantle wedge overlain by a continental sliver during the collision responsible for M_2 metamorphism.

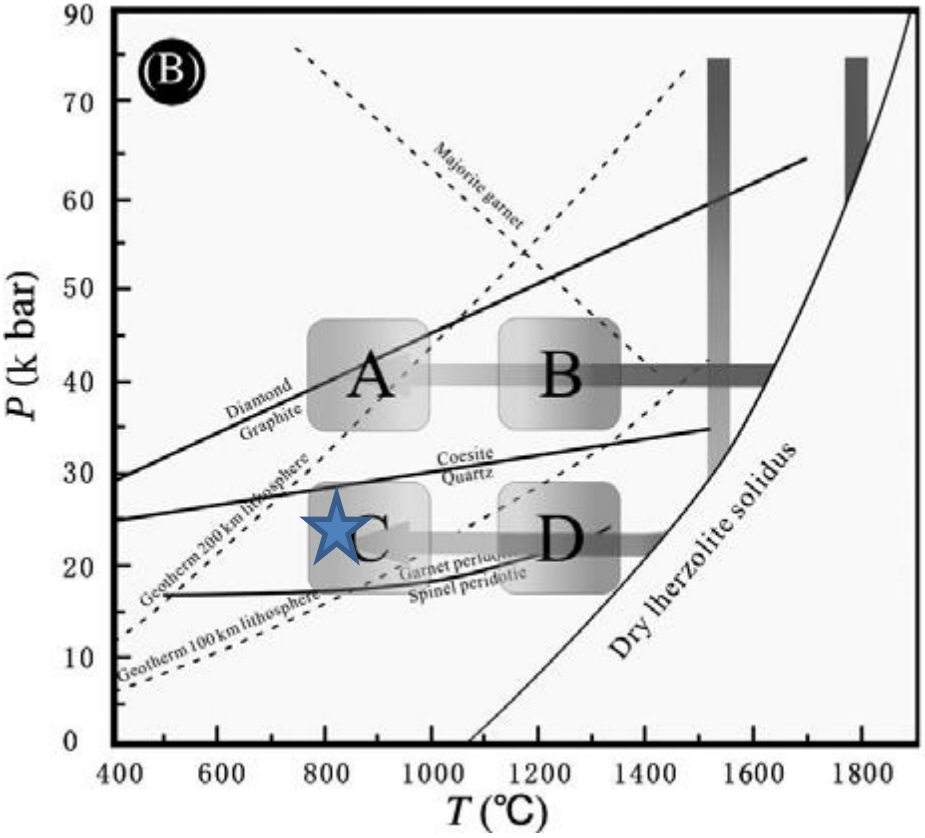

5.4 A geodynamic model

A geodynamic model derived from the observations and mineral chemical data presented in the previous sections is illustrated in figure 5.4.1. This conceptual model is not yet visualized in the context of the Scandinavian Caledonides but illustrates the major steps. The first tectono-metamorphic event (M_{1A}) is interpreted as the making of the SCLM. The detail of this process of how the SCLM is made is not clear and beyond the scope of this thesis.
After the creation of the SCLM a period of refertilization occured. The M_{1A} assemblage was stable when the garnet pyroxenite dike intruded. The age dating done by *Brueckner et al., (2004)* showed that this occurred in the Proterozoic and possibly Archean. Dike sample D5 is correlated to this refertilization on the basis of its lack of sodium and high Mg#. Post-M_{1A} cooling is inferred to be after the fertilization, as different mineral pairs (grt, cpx, opx) all give similar temperatures for M_1. The interpretation that M_1 temperatures are temperatures of mineral closure to diffusion is therefore discarded. The melts are inferred to have intruded the peridotite at $\geq$ 840 °C. Still, the M_{1A} assemblage might be a recrystallized assemblage from a high T assemblage. There is no evidence that supports or contradicts this possibility.
Kelyphitic rims around M_{1A} garnets are indicative of decompression of 0.8 – 1.5 GPa. This is interpreted to correlate with period of continental rifting and possibly ocean opening. This period of rifting was probably a significant time after the refertilization as the M_{1A} assemblage is megacrystic. The opening of an ocean is invoked here because of the necessity to create a subduction zone near this peridotite. After the creation of a mantle wedge and concomitant oceanic crust the subduction of oceanic crust commences. During this period, Na and Eu enriched fluids percolated the mantle wedge, the M_2 foam like texture crystallized during fluid and deformation assisted recrystallization. In some samples this is more evident than others, causing the erratic Na and Eu concentrations. During this period of subduction the mantle wedge became deformed.
Subsequently continental material is subducted subjacent to lithospheric mantle and the peridotite is entrained in continental crust which correlates to M_2 metamorphism and F_2 deformation. Continental subduction continues, carrying the peridotite cargo to greater depths as is evident from the M_2 garnet overgrowths over M_{1B} kelyphite. This is likely coeval with the Sm-Nd age dating done on the dike *(~450 Ma, Brueckner et al., 2004)* and/or monazite age dating on the host rocks *(500 ± 50 Ma, Gademan et al., 2011).* The peridotite was then exhumed after slab-breakoff stopped the effects of slab pull. After slab pull terminates the buoyant continental crust can return to the surface. This process is called dunk tectonics *(Section 2.5; Brueckner & van Roermund, 2004).* During the exhumation the M_3-M_5 mineral parageneses formed.

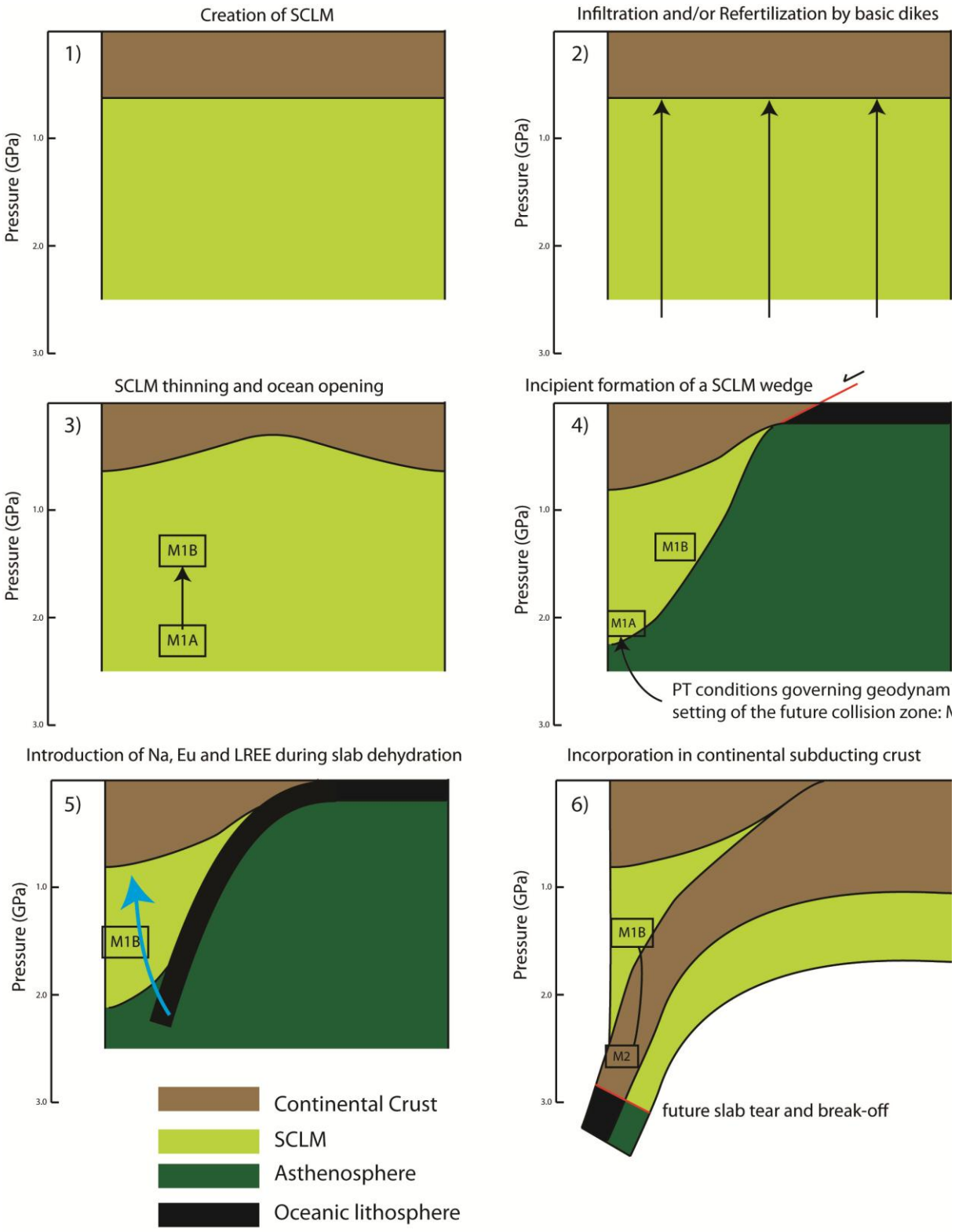

Figure 5.3.1; A geodynamic model showing 1) the creation of a SCLM, 2) infiltration/refertilization by basic dikes, 3) lithospheric thinning, 4) formation of a mantle wedge, 5) introduction of subduction zone fluids 6) The incorporation of the SCLM in continental subducting crust ± followed by infiltration of subduction zone fluids. The exhumation of the SCLM occurred in a 'dunk tectonic' style *(Section 2.6; Brueckner & van Roermund, 2004)*.

5.5 The proposed geodynamic model applied to the Scandinavian Caledonides

Gademan et al., (2011) dated the host rocks of the Friningen peridotite firmly as early Caledonian (500 ± 50 Ma). A collision between Baltica and a Virisen arc as proposed by *Stephens & Gee (1985)* cannot be responsible for the (U)HP metamorphism of the Seve Nappe Complex. As the lithosphere underneath such a colliding island arc is too shallow for olivine-garnet to be stable in the hanging wall of the colliding plate. A micro-continent continent collision must therefore be responsible for the HP metamorphism found in the SNC *(Brueckner & van Roermund, 2004)*. A very important question to be addressed is whether Baltica took part in this collision or not.

As *Corfu (2011)* pointed out, HP metamorphism of the Seve Nappe might have taken place anywhere in the Iapetus ocean *(Figure 5.5.1)*. If this occurred between two micro-continents both distal from Baltica, a composite terrane would later be wedged in between Baltica and Laurentia. The WGR is Baltic in affinity and would first have to underthrust this composite terrrane before it can subduct deep under Laurentia.

If Baltica was involved in the early Caledonian micro continent-continent collision, deep continental subduction, exhumation and emplacement of the SNC onto the Baltic margin is more likely. The Eastern and Central Belt were originally part of the outermost edge of Baltica, and the Western belt may be part of the microcontinent. The Eastern and Central Belt (Baltic margin) subduct beneath the Western Belt and are exhumed with eclogite and peridotite cargo. During the Scandina collision between Baltica and Laurentia the original thrust planes of the SNC are reactivated, sliding the nappes further over the continent and allowing for the subduction of WGR underneath Laurentia, resulting in the model of *Brueckner & van Roermund (2004)*.

Figure 5.5.1 shows a conceptual model of the early Caledonian (500 ± 50 Ma) collision as proposed by Corfu *(in review)* of the protolith positions. In this reconstruction, Corfu shows a composite terrane at 440 Ma where metamorphism had already taken place. In this model the early Caledonian collision did not include Baltica but instead another microcontinent that formed the composite terrane after collision. The SNC is then later squeezed in between Baltica and Laurentia as a result of large strike slip displacements. Early Caledonian HP metamorphosis might thus have occurred everywhere along the margin of Baltica. This creates the necessity of large strike slip translations between HP metamorphism and incorporation of the (U)HP metamorphic terrane on top of the Baltic margin. Considering this idea various authors have proposed the SNC (or the Kalak nappe) was derived from eastern Rodinia, Avalonia, Baltica and even Laurentia. The simplest interpretation is that translation should be placed prior to the early Caledonian metamorphism and occurred along the Baltoscandian margin.

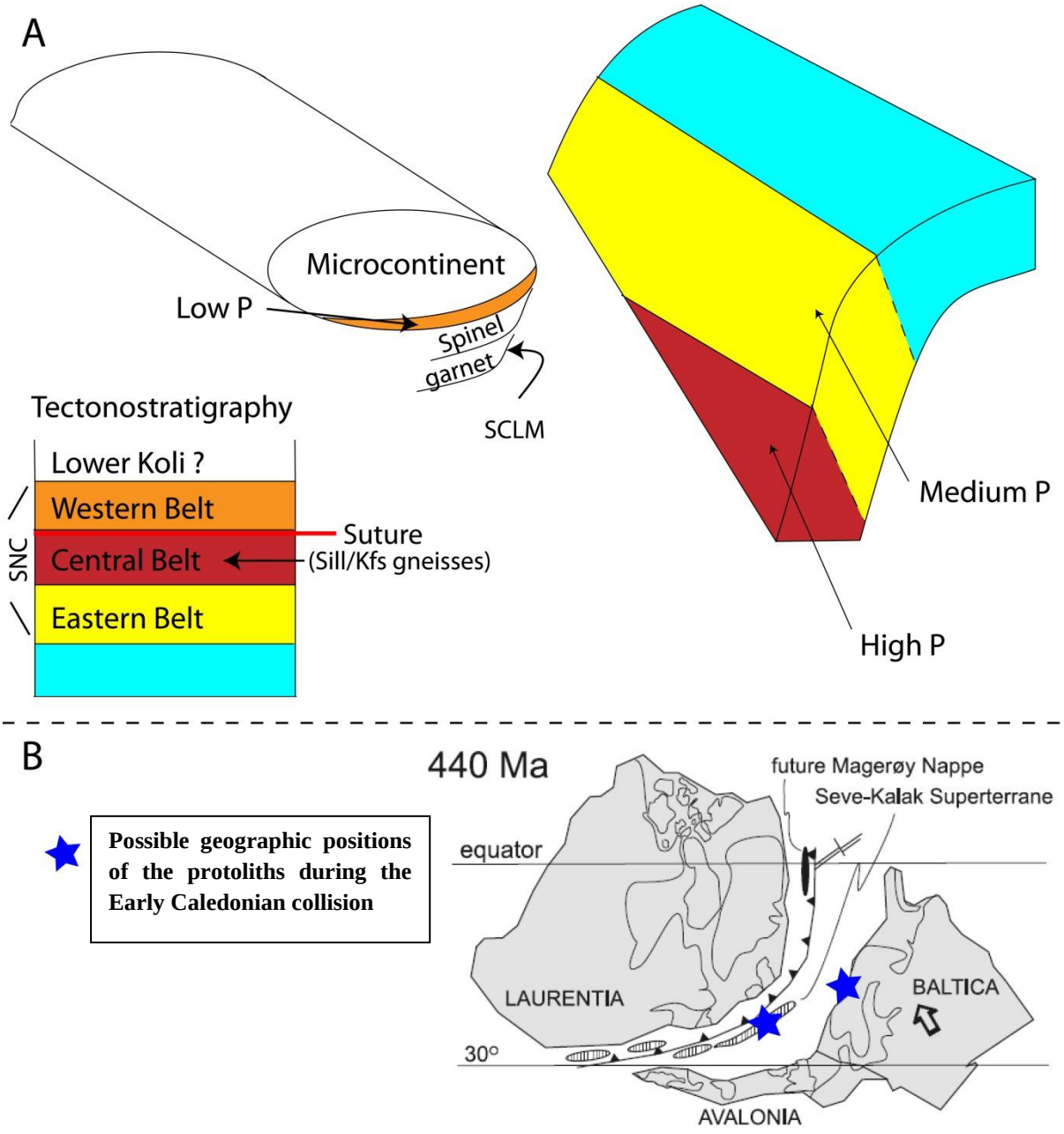

Figure 5.5.1, A) A cartoon illustrating the schematic collision at 500 ± 50 Ma between a microcontinent (left side) and an unknown continental fragment (right side) which collided and thus produced (U)HP metamorphism. The roles of the various Belts of the SNC in this collision are also illustrated *(edited after Gademan et al., 2011)*. B) The figure shows the configuration of Laurentia, Baltica and Avalonia at 440 Ma. The blue stars indicate possible locations for the 500 ± 50 Ma period of continental subduction. This might have taken place external to Baltica or along the Baltic margin. If it was Baltica, the blue part of figure A represents Baltic basement and/or nappes on top of it. If this period of early Caledonian continental subduction represents the joining of two microcontinents external to Baltica the blue part in figure A represents oceanic crust.

6 Conclusions

The Friningen garnet peridotite lens represents a SCLM mantle fragment which formed part of a type C mantle wedge. Its continental emplacement occurred during deep continental subduction of the Central Belt of the Seve Nappe Complex during continent-continent collision. A collision with the Virisen Arc is therefore rejected as a possible source for the early Caledonian metamorphism in the SNC.

The principle of least astonishment leads to the belief that the proposed strike slip translation of the external part of the SNC to the Baltic margin occurred prior to HP metamorphism. This implies the HP metamorphism is a result of the collision of an external terrane with the Baltic margin.

The main tectonostratigraphic units of the SNC should be subdivided in the Central and Eastern Belts which likely originated from the outermost Baltic margin. The Western belt represents part of the microcontinent. The paleo-plate interface or the paleo subduction zone is between the Central and Western Belt. Any detrital zircon record or provenancing study should recognize this and not confuse the different Belts.

On the basis of bulk rock chemistry or REE spider diagrams it is not possible to correlate dikes that truncate the garnet peridotite body with dikes that intruded the Baltoscandian margin during Proterozoic to Early Paleozoic times. This is a consequence of the varying chemistries and late alteration of the dikes. The only thing that would effectively be able to link these dikes to mafic material in the originally overlying crust is a solid U-Pb age dating of zircons. This study proved however that zircons cannot provide the outcome here due to the extreme low concentrations. Work in other HP lenses *(Root & Corfu, 2011)* of the central belt has demonstrated inheritance ages of 1700 Ma in a metagabbro. If the Friningen peridotite dike has a similar age, a correlation to the opening of the Iapetus ocean is impossible. Other methods should be attempted, as a solid intrusion age of this dike might serve as much needed paleogeographic constraint as well. The M_{1A} garnets in the peridotites might yield Lu-Hf or Sm-Nd ages provided M_1 can be separated from M_2 grains.

7 Future work

Research needs to be done in order to find out how much of the history of the Seve and Kalak nappes is shared. If the Kalak Nappes are indeed external to Baltica, they might correspond to the Eastern Belt of the SNC but not to the Central and Western Belt.

The Friningen garnet peridotite lens represents a mantle fragment that is extensively influenced by subduction zone fluids. It represents a perfect and beautiful example of SCLM which is not serpentinized extensively and still retains some of its primary features. Even better candidates for the study of the subduction zone fluids are the recrystallized M_2 assemblage formed during deformation and possibly fluid enhanced recrystallization that might host Eu, Na and other subduction zone elements. This provides a natural laboratory for the effect of subduction fluids on the formation of UHP mineral assemblages. The large advantage that this garnet peridotite has with respect to 'crustal' peridotites is that it was dry prior to the influx of subduction zone fluids. Laser ablation isotope studies on individual M_2 minerals can identify the role of subduction zone fluids during the crystallization of M_2 minerals.
The M_{1A} assemblage of the peridotite has not yet been recorded in such detail. A very useful and logical step would be to date the M_{1A} garnets to be able to conclude decisively that the M_{1A} UHP assemblage was coeval with the intrusion of the dike. This can be done either with Sm-Nd dating or Re-Os dating, provided that a complete separation between M_{1A} and M_2 grains is possible.

The diffusion of elements through the peridotite might be investigated by sampling every 5 cm, from the middle of one thick dike boudin to at least 1 m in the peridotite. Extensive geochemical analyses (bulk rock, REE) might yield information on how far different elements can travel through the rock. Different types of transportation of elements can also be observed, if travel paths differ in orders of magnitude.

8 Acknowledgements

First of all I would like like to thank Herman van Roermund, who showed me the way to some of the most interesting rocks on the globe. His views on the geology of Scandinavia and contributions to UHP metamorphism have been a great help. His guidance in the field was missed. Further I would like to thank my dear friend Jort Koopmans for his help in the field. Fieldwork was financially supported by a grant from the Molengraaff fund and this study would not have been possible without it. Support (and occasional distraction) from my parents, sisters and fellow students have helped me greatly in doing this research.

9 References

Andreasson, U.B., Larsson, L., Wikström, A. 1992 Mafic Dyke swarms of the Baltica Iapetus transition, Seve Nappe Complex of the Sarek Mts., Swedish Caledonides. *Geologiska Föreningens I Stockholm Förhandlingar, **114**, 31-45*

Andreasson, P.G. 1980. Metamorphism in extensive nappe terrains: A study of the Central Scandinavian Caledonides. *Geologiska Föreningens i Stockholm Förhandlingar, **102**, 335-357*

Andreásson, P.G., Svenningsen, O.M., Albrecht, L., 1998. Dawn of Phanerozoic orogeny in the North Atlantic tract: evidence from the Seve–Kalak superterrane, Scandinavian Caledonides. *Geol. Fören. Stockh. Förh. 120, 159–172.*

Arnbom, J.O. 1980. Metamorphism of the Seve Nappes at åreskutan, Swedish Caledonides. *Geologiska Föreningens i Stockholm Förhandlingar, **102,** 359-371*

Barnhoorn, A., Drury, M.R., van Roermund, H.L.M. Van, 2010. Evidence for low viscosity garnet-rich layers in the upper mantle. *Earth and planetary science letters **289**, 54-67*

Barth, M.G., Rudnick, R.L., Horn, I., McDonough, W.F., Spicuzza, M.J., Valley, J.W., Haggerty, S.E., 2001. Geochemistry of xenolithic eclogites from West Africa, Part I: a link between low MgO eclogites and Archean crust formation. *Geochimica Et Cosmochimica Acta **65 (**9), 1499–1527.*

Bassett, M.G. 1985: Silurian stratigraphy and facies development in Scandinavia. *In Gee, D.G. & Sturt, .A. (eds.) The Caledonide orogen – Scandinavia and related areas. John Wiley & Sons, Chichester, 83-292.*

Berman R.G., Brown T.H., Greenwood H.J. (1985): An internally consistent thermodynamic database for minerals in the system Na2O-K2O-CaO-MgO-FeO-Fe2O3-Al2O3-SiO2-TiO2- H2O-CO2. Includes unpublished solution models for WHITE MICA (L. Keller, 2004) (P. Hunziker 2003) SPIN, OPX, CHL4 *Atomic Energy of Canada Ltd. Technical Report 377,62p.*

Bertrand, P. & Merrier, J.-C.C. 1985. The mutual solubility of coexisting ortho- and clinopyroxene: toward an absolute geothermometer for the natural system? *Earth and Planetary Science Letters* **76,** *109-122.*

Bogdanove, S.V., Gorbatschev, R., Stephenson, R.A., 2001. Eurobridge: Paleoproterozoic accretion of Fennoscandia and Sarmatia. *Tectonophysics, **339,** vii-x*

Brey, G.P. & Koehler, T. 1990. Geothermobarometry in four-phase lherzolites II. New thermobarometers, and practical assessment of existing thermobarometers. *Journal of Petrology* **31**, *1353–1378.*

Brey, G.P., Bulatov, V.K., Girnis, A.V., 2008. Geobarometry for Peridotites: Experiments in Simple and Natural Systems from 6-10 Gpa. *Journal of petrology, **49**, 3-24*.

Brey, G.P., Köhler, T. and Nickel, K.G., 1990. Geothermobarometry in Four-phase Lherzolites I. Experimental Results from 10 to 60 kb. J. Petrol., 31, part 6, 1313-1352

Brey, G.P., Köhler, T; PTEXL is free software for thermobarometric calculations and PT estimates that can be downloaded at the site of the mineralogical department the university of Frankfurt, www.mineralogie.uni-frankfurt.de/petrologie.../brey/downloads/ptexl3.xls

Brueckner, H.K. & van Roermund, H.L.M., 2004. Dunk tectonics: a multiple subduction/eduction model for the evolution of the Scandinavian Caledonides. *Tectonics **23**; 1-20.*

Brueckner, H.K. & van Roermund, H.L.M., Pearson, N.J., 2004. An Archean (?) to Paleozoic Evolution for a Garnet Peridotite Lens with Sub-Baltic Shield Affinity within the Seve Nappe Complex of Jämtland, Sweden, Central Scandinavian Caledonides. *Journal of petrology, **45**, 415-437*

Brueckner, H.K. and Medaris, L.G., Jr. (2000) A general model for the intrusion and evolution of "mantle" peridotites in high-pressure and ultrahigh-pressure metamorphic terranes*: Jour. metamorphic Geol., v. 18, p. 123-133.*

Bucher, 1991. Mantle fragments in the Scandinavian Caledonides. *Tectonophysics **190**, 173-192*

Cocks, L. R. M. & Torsvik, T. H. 2006. European geography in a global context from the Vendian to the end of the Palaeozoic, *European Lithosphere Dynamics. Geological Society, London, Memoirs, **32,** 83–95.*

Cong, Z. van Roermund, H., Zhang, L., 2011; Orogenic garnet peridotites, tools to reconstruct the paleo geodynamical settings of fossil continental subduction zones, *in Ultra-High-Pressure metamorphism, 2011*

Corfu, F., Roberts, R.J., Torsvik, T.H., Ashwal, L.D., Ramsay, D.M., 2007. Peri-Gondwanan elements in the Caledonian nappes of Finnmark, Northern Norway: Implications for the paleogeographic framework of the Scandinavian Caledonides. *Am. Journal of Science, **307**, 434-458*

deCapitani, C. Petrakakis, K. The computation of equilibrium assemblage diagrams with Theriak/Domino software. *American Mineralogist, Volume 95, page 1006-1016, 2010*

F. Corfu, M. Gerber, T.B. Andersen, T.H. Torsvik, and L.D. Ashwal, Age and significance of Grenvillian and Silurian orogenic events in the Finnmarkian Caledonides, northern Norway, *Can. J. Earth Sci. Vol. 48, 2011*

Ellis, D.J. & Green, D.H. 1979. An experimental study of the effect of Ca upon garnet-clinopyroxene Fe-Mg exchange equilibria. *Contributions to Mineralogy and Petrology **71,** 13-22*

Gademan, M., Hogerwerf, M.A., Verbaas, J., van Roermund, H., 2011., Evidence for a Finnmarkian (~500 Ma) continental collision/subduction zone in the central belt of the Seve Nappe Complex, northern Jämtland-southern Västerbotten, Sweden; Constraints from chemical EMP monazite ages and orogenic mantle wedge garnet peridotite. *EGU meeting Vienna 2011, Subduction zone dynamics*

Gayer, R.A., Greiling, R.O., 1989. Caledonian nappe geometry in north-central Sweden and basin evolution on the Baltoscandian margin. *Geological Magazine **126,** 499–513.*

Gee, D.G., 1975. A tectonic model for the central part of the Scandinavian Caledonides. *Am. J. Sci. **275A,** 468– 515.*

Gee, D.G., Fossen, H., Henriksen, N. & Higgins, A.K. 2008: From the early Paleozoic platforms of Baltica nd Laurentia to the Caledonide orogen of Scandinavia and Greenland. *Episodes **31,** 44-51*.

Gerya, T.V., Perchuk, L.L., Burg, J.-P. 2007. Transient hot channnels: perpetrating and regurgitating ultrahigh-pressure, high-temperature crust-mantle associations in collision belts. *Lithos-01678*

Gonzaga, R.G., Lowry, D., Jacob, D.E., LeRoex, A., Schulze, D., Menzies, M.A., Eclogites and garnet pyroxenites, similarities and differences. *Journal of Volcanology and Geothermal Research, **190**, 235-247*

Greiling, R.O., Gayer, R.A., Stephens, M., 1993. A basement culmination in the Scandinavian Caledonides formed by antiformal stacking (B°angon°aive, northern Sweden). *Geological Magazine **130,** 471–82.*

Greiling, R.O., Stephens, M.B., Persson, P.-O., O. 2002. Crystalline basement rocks in the Lower and Middle Allochthons, V¨asterbotten, Sweden: Palaeoproterozoic U–Pb zircon ages from the north-central Swedish *C 834, 31–42.Caledonides. Sveriges Geologiska Undersökning Series*

Greiling, R.O. 1982. Precambrian Basement complexes in the north-central Scandinavian Caledonides and their Caledonian tectonic evolution. *Geologische Rundschau **71**, 85-93*

Greiling, R.O. 1989. The middle Allochton in Västerbotten, Northern Sweden. *In R.A. Gayer (ed): The Caledonide Geology of Scandinavia, 69-77. Graham & Trotman*

Greiling, R.O., Grimmer, J.C., De Wall, H. Björk, L., 2007. Mesoproterozoic dyke swarms in foreland and nappes of the Central Scandinavian Caledonides: structure, magnetic fabric and geochemistry. *Geol. Mag **144**, 525-546*

Griffin, W.L., O'Reilly, S.Y., 2007. Cratonic lithospheric mantle: is anything subducted? *Episodes **30** (1), 1–11.*

Harley, S.L. 1984. An experimental study of the partitioning of Fe and Mg between garnet and orthopyroxene. *Contributions to Mineralogy and Petrology **86**, 353–373.*

Jacob, D.E., 2004. Nature and origin of eclogite xenoliths from kimberlites. *Lithos 77 **(1–4),** 295–316.*

Jenkins, R., 1988, X-Ray fluorescence spectrometry. *Jogn Wiley and Sons inc. QD96 X2J47*

Johannson, L., Johannson, A., 1990. Isotope geochemistry and age relationships of mafic intrusions along the Protogine zone, Southern Sweden. *Precambrian research **48**, 395-414*

Kirkland, C.L., Bingen, B., Whitehouse, M.J., Beyer, E., Griffin, W.L., 2011. Neoproterozoic paleogeography in the North Atlantic Region: inferences from the Akkajaure and Seve Nappes of the Scandinavian Caledonides. *Precambrian Research, in press*

Krogh Ravna E. 2000 The garnet–clinopyroxene Fe^{2+}–Mg geothermometer: an updated calibration. *Journal of Metamorphic Geology **18, 211-219***

Krogh, E. J. 1988. The garnet-clinopyroxene Fe-Mg-geothermometer—a reinterpretation of existing experimental data. *Contributions to Mineralogy and Petrology **99,** 44-48.*

Liu Y. S., Gao S., Lee C.-T. A., Hu S. H., Liu X. M., and Yuan H. L. (2005) Melt-peridotite interactions: Links between garnet pyroxenite and high-Mg# signature of continental crust. *Earth Planet. Sci. Lett. **234**, 39-57.*

Lutro O. 1979 Lustarfjorden. Geological Map 1417 1:50000. Nor. geol. Unders..

MacGregor, I.D. 1974. The system MgO–Al2O3–SiO2: solubility of Al2O3 in enstatite for spinel and garnet peridotite compositions. *American Mineralogist **59,** 110–119.*

Majka, J. & Jának, M.; 2011; (U)HP Kyanite bearing eclogite from the Seve Nappe Complex, Jämtland, Swedish Caledonides, *9th international eclogite conference, Czech*

Manning, C. E., 2004, The chemistry of subduction-zone fluids. *Earth and Planetary Science Letters, v. **223,** p. 1-16.*

Medaris Jr., L.G., Carswell, D.A., 1990. Petrogenesis ofMg-Cr garnet peridotites in European metamorphic belts. *In: Carswell, D.A. (Ed.), Eclogite Facies Rocks. Chapman nd Hill, New York, pp. 260–290.*

Medaris, L.G. Jr., Jelínik, E. and Misar, Z. 1995 Czech eclogites: Terrane settings and implications for Variscan tectonic evolution of the Bohemian Massif: *Eur. Jour. Mineral., v. **7,** 7-28.*

Medaris, L.G., Jr., Beard, B.L., and Jelínek, E. 2006 Mantle-derived, UHP garnet pyroxenite and eclogite in the Moldanubian Gföhl Nappe, Bohemian Massif: A geochemical review, new P-T determinations, and tectonic interpretation: *International Geology Review, v. **48,** 765-777.*

Melezhik, V.A., Roberts, D., Gorokhov, I.M., Fallick, A.E., Zwaan, K.B., Kuznetsov, A.B., Pokrovsky, B.G., 2002. Isotopic evidence for a complex Neoproterozoic to Silurian rock assemblage in the north–central Norwegian Caledonides. *Precambrian Res. **114,** 55– 86.*

Montaser, A., 1998; Inductively coupled plasma mass spectrometry, *Wiley, vch.*

Mork, M.B.E; Kullerud, K.; Stabel, A.; 1988. Sm-Nd dating of Seve Eclogites Norrbotten, Sweden, evidence for early Caledonian (505 Ma) subduction. *Contributions to mineralogy and petrology. 99:344-351*

Nakamura, D. 2009. A new formulation of garnet-clinopyroxene geothermometer based on accumulation and statistical analysis of a large experimental dataset. *Jr. Of metamorphic Geology, **27-7**, 495-508*

Nickel, K.G. & Green, D.H. 1985. Empirical geothermobarometry for garnet peridotites and implications for the nature of the lithosphere, kimberlites and diamonds. *Earth Planetary Science Letters **73**, 158–170.*

Nimis, P. & Taylor, W.R. 2000 Single clinopyroxene thermobarometry for garnet peridotites. Part I. Calibration and testing of a Cr-in-Cpx barometer and an enstatite-in-Cpx thermometer. *Contributions to Mineralogy and Petrology**139,** 541-554*

Niu, Y.; O'Hara, M. J., 2009. MORB mantle hosts the missing Eu (Sr, Nb, Ta and Ti) in the continental crust: New perspectives on crustal growth, crust–mantle differentiation and chemical structure of oceanic upper mantle, *Lithos 112, 1-17*

O'Neill, H.St.C. & Wood, B.J. (1979). An experimental study of Fe–Mg-partitioning between garnet and olivine and its calibration as a geothermometer. *Contributions to Mineralogy and Petrology* **70**, 59–70.

Patchett, P.J., 1978. Rb/Sr ages of Precambrian dolerites and syenites in southern and central Sweden. *Sveriges Geologiska Undersökning C **747**, 1-63*

Powell, R. 1985. Regression diagnostics and robust regression in geothermometer/geobarometer calibration: the garnet-clinopyroxenc geothennometer revisited. *Journal of Metamorphic Geology* **3,** 231-43.

Prent, BSC thesis, 2011; A first attempt to apply the computer programs of the TheriakDomino suite to HP pyroxenite and peridotite bulk rock compositions.

Roberts, D. & Gee, D.G. 1985. An introduction to the structure of the Scandinavian Caledonides. In: *Gee, D.G. & Sturt, B.A. (eds) The Caledonide Orogen—Scandinavia and Related Areas. Wiley, Chichester, 55–68.*

Roberts, D., 1988. Geochemistry and Rb-Sr dating of the Muruvik rhyolite tuff, Trondheimsfjord, Cental Norway. *Nor. Geol. Unders. Bull. 412, 43– 53.*

Roberts, D., 2003. The Scandinavian Caledonides: event chronology, paleogeographic settings and likely modern analogues. *Tectonophysics **365**, 283-299*

Roberts, D., Heldal, T., Melezhik, V.M., 2001. Tectonic structural features of the Fauske conglomerates in the Løvgavlen quarry, Nordland, Norwegian Caledonides, and regional implications. *Nor. Geol. Tidsskr. 81, 245– 256.*

Roberts, D., Melezhik, V.M., Heldal, T., 2002. Carbonate formations and NW-directed thrusting in the highest allochthons of the Norwegian Caledonides: evidence of a Laurentian ancestry. *J. Geol. Soc. Lond. 159, 117–120.*

Roberts, R.J., Corfu, F., Torsvik, T.H., Hetherington, C.J., Ashwal, L.D. 2010. Age of alkaline rocks in the Seiland Igneous Province, Northern Norway. *Journal of the Geological Society, **167**, 71-81*

Root, D., Corfu, F., in review. U-Pb geochronology of two discrete Ordovician high-pressure metamorphic events in the Seve Nappe Complex, Scandinavian Caledonides. *Contributions to Mineralogy and Petrology*

Ryan, C. G., Griffin, W. L. & Pearson, N. J. 1996. Garnet geotherms: pressure–temperature data from Cr-pyrope garnet xenocrysts in volcanic rocks. *Journal of Geophysical Research **101,** 5611–5625.*

Söderlund, u., Isachsen, C.E., Bylund, G., Heaman, L.M., Patchett, P.J. Vervoort, J.D., Andersson, U.B., 2005. U–Pb baddeleyite ages and Hf, Nd isotope chemistry constraining repeated mafic magmatism in the Fennoscandian Shield from 1.6 to 0.9 Ga. *Contributions to Mineralogy and Petrology **150**, 174–94.*

Solyom, Z., Lindqvist, J.-E., Johannson, E., 1992. The geochemistry, genesis and geotectonic setting of Proterozoic mafic dyke swarms in southern and central Sweden. *Geologiska Föreningens I Stockholm Förhandlingar, **114**, 47-65*

Spengler, D. 2006, Origin and evolution of deep upper mantle rocks from western Norway, PhD thesis, *Geologica Ultraiectina, 266*

Stephens, M.B., Gee, D.G., 1985. A tectonic model for the evolution of the eugeoclinal terranes in the central Scandinavian Caledonides. *In: Gee, D.G., Sturt, B.A. (Eds.), The Caledonide Orogen—Scandinavia and Related Areas. Wiley, Chichester, pp. 953– 970.*

Sun S., and W. F. McDonough, 1989. Chemical and isotopic systematics of oceanic basalts: implications for mantle composition and processes, in *Magmatism in the Ocean Basins* edited by A. D. Saunders and M. J. Norry, *Geological Soc. Special Publ., 42, 313-345.*

Svenningsen, O.M., 2001. Onset of seafloor spreading in the Iapetus Ocean at 608 Ma: precise age of the Sarek Dyke Swarm, north Swedish Caledonides. *Precambrian Res. 110, 241– 254.*

Törnebohm, A.E., 1888, Om Fjällproblemet: *Geologiska Föreningens i Stockholm Förhandlingar, **10.** 328-336.*

Torsvik, T. H. & Cocks, L. R. M. 2005. Norway in space and time: a centennial cavalcade. *Norwegian Journal of Geology, **85,** 73–86.*

Torsvik, T.H. & Van der Voo, R., 2002. Refining Gondwana and Pangea Palaeogeography: Estimates of Phanerozoic (octupole) non-dipole fields. *Geophys. J. Intern., **151,** 771-794.*

Torsvik, T.H., Smethurst, M., Meert, J., Van der Voo, R., McKerrow, W.S., Brazier, M., Sturt, B.A., Walderhaug, H., 1996. Continental break-up and collision in the Neo-proterozoic and Palaeozoic—a tale of Baltica and Laurentia. *Earth-Sci. Rev. **40,** 229– 258.*

Torsvik, T.H., Smethurst, M.A., Van der Voo, R., Trench, A., Abrahamsen, N. & Halvorsen, E., 1992. BALTICA - A synopsis of Vendian-Permian palaeomagnetic data and their palaeotectonic implications. *Earth Science Reviews, **33,** 133-152.*

Trouw, R.A.J., 1973, Structural Geology of the Marsfjällen area Caledonides of Västerbotten Sweden, *Sveriges Geologiska Undersökning, årsbok **67** nr 7.*

Van Roermund, H.L.M, Bakker, E., 1984; Structure and metamorphism of the Tangen-Inviken area, Seve Nappes, Cenrtal Scandinavian Caledonides, *GFF 105; 301-309*

Van Roermund, H.L.M., 1985. Eclogites of the Seve Nappe, Scandinavian Caledonides. *In: Gee, D.G., Sturt, B.A. (Eds.), The Caledonide Orogen—Scandinavia and Related Areas. Wiley, Chichester P887-902*

Van Roermund, H. L. M. 1989, High-pressure ultramafic rocks from the allochthonous nappes of the Swedish Caledonides, *in The Caledonide Geology of Scandinavia, edited by R. A. Grayer, pp. 205 – 219, Graham and Trotman, Norwell, Mass.*

Van Roermund, H.L.M., Carswell, D.A., Drury, M.R. & Heijboer, T.C., 2002. Microdiamonds in a megacrystic garnet websterite pod from Bardane on the island of Fjortoft, western Norway: Evidence for diamond formation in mantle rocks during deep continental subduction. *Geology **30,** 959-962*

Van Roermund, H.L.M. 2009. Recent progress in Scandian ultrahigh pressure metamorphism in the northernmost domain of the Western Gneiss Complex, SW Norway: continental subduction down to 180-200 km depth. Journal Geological Soc. London 166: 739–751

Wells, P.R.A. 1977. Pyroxene thermometry in simple and complex systems. *Contributions to Mineralogy and Petrology **62,** 129-139.*

Zachrisson, E., 1969. Caledonian geology of Northern Jämtland-Southern Västerbotten. Köli stratigraphy and main tectonic outlines. *Sveriges Geologiska Undersöknung C 644, 1-33*

Zachrisson, E., 1973. Structural geology of the Marsfjallen area, Caledonides of Västerbotten, Sweden. *Sveriges Geol. Unders., C**689**, 1-115*

Zwart, H.J. 1974. Structure and metamorphism in the Seve–Köli Nappe Complex (Scandinavian Caledonides) and its implications concerning the formation of metamorphic nappes. *In: Bellière, J. & Duchesne, J.C. (eds) Géologie des Domains Cristallins. Centenaire de la Société Géologique de Belgique, Liège, 129–144.*